CONDENSATIONAL GROWTH OF ATMOSPHERIC AEROSOL PARTICLES IN AN EXPANDING WATER SATURATED AIR FLOW: NUMERICAL OPTIMISATION AND EXPERIMENT

Dissertation zur Erlangung des Grades
"Doktor der Naturwissenschaften"
am
Fachbereich Physik
der
Johannes Gutenberg-Universität Mainz

Jianliang Yang
Geboren in Jiangsu, VR China

Mainz 1999

Tag der mündlichen Prüfung: 19. Januar 2000

ABSTRACT

Aerosol particles and water vapour are two important constituents of the atmosphere. Their interaction, i.e. the condensation of water vapour on particles, brings about the formation of cloud, fog, and raindrops, causing the water cycle on the earth, and being responsible for climate changes. Understanding the roles of water vapour and aerosol particles in this interaction has become an essential part of understanding the atmosphere.

In this work, the heterogeneous nucleation on pre-existing aerosol particles by the condensation of water vapour in the flow of a capillary nozzle was investigated. Theoretical and numerical modelling as well as experiments on this condensation process were included. Based on reasonable results from the theoretical and numerical modelling, an idea of designing a new nozzle condensation nucleus counter (Nozzle-CNC), that is to utilise the capillary nozzle to create an expanding water saturated air flow, was then put forward and various experiments were carried out with this Nozzle-CNC under different experimental conditions.

Firstly, the air stream in the long capillary nozzle with inner diameter of 1.0 mm was modelled as a steady, compressible and heat-conducting turbulence flow by CFX-FLOW3D computational program. An adiabatic and isentropic cooling in the nozzle was found. A supersaturation in the nozzle can be created if the inlet flow is water saturated, and its value depends principally on flow velocity or flow rate through the nozzle.

Secondly, a particle condensational growth model in air stream was developed. An extended Mason's diffusion growth equation with size correction for particles beyond the continuum regime and with the correction for a certain particle Reynolds number in an accelerating state was given. The modelling results show the rapid condensational growth of aerosol particles, especially for fine size particles, in the nozzle stream, which, on the one hand, may induce evident 'oversizing' and 'over-numbering' effects in aerosol measurements as nozzle designs are widely employed for producing accelerating and focused aerosol beams in aerosol instruments like optical particle counter (OPC) and aerodynamical particle sizer (APS). It can, on the other hand, be applied in constructing the Nozzle-CNC.

Thirdly, based on the optimisation of theoretical and numerical results, the

new Nozzle-CNC was built. Under various experimental conditions such as flow rate, ambient temperature, and the fraction of aerosol in the total flow, experiments with this instrument were carried out. An interesting exponential relation between the saturation in the nozzle and the number concentration of atmospheric nuclei, including hygroscopic nuclei (HN), cloud condensation nuclei (CCN), and traditionally measured atmospheric condensation nuclei (CN), was found. This relation differs from the relation for the number concentration of CCN obtained by other researchers. The minimum detectable size of this Nozzle-CNC is 0.04 μm.

Although further improvements are still needed, this Nozzle-CNC, in comparison with other CNCs, has several advantages such as no condensation delay as particles larger than the critical size grow simultaneously, low diffusion losses of particles, little water condensation at the inner wall of the instrument, and adjustable saturation — therefore the wide counting region, as well as no calibration compared to non-water condensation substances.

ZUSAMMENFASSUNG

Aerosolpartikel und Wasserdampf sind zwei wichtige atmosphärische Bestandteile. Ihr Zusammenspiel, das ist die Kondensation des Wasserdampfes auf Aerosolpartikel, bringt die Entstehung von Wolken, Nebel, und Regentropfen zustande, ermöglicht deshalb den Wasserkreislauf auf der Erde, und ist für die Klimaveränderung verantwortlich. Das Verständnis ihrer Rollen in diesem Zusammenspiel ist ein wesentlicher Teil für das Verstehen der Atmosphäre.

In der vorliegenden Arbeit wurde heterogene Keimbildung von Wasserdampf auf Aerosolpartikel in der Strömung einer Kapillardüse untersucht. Eingeschlossen sind theoretische, numerische und experimentelle Untersuchungen. Als Ergebnisse aus dem Wachstum des atmosphärischen Aerosols mit Wasserdampf als Kondensationssubstanz wurde ein neuer Düsenkondensationkernzähler (Nozzle-CNC) aufgebaut, in dem die Abkühlung und Kondensation durch diese Düse erzeugt wird. Verschiedene Experimente wurden anschließend mit diesem Gerät durchgeführt.

Erstens: Strömung und Aerosoldynamik in der Düse mit innerem Durchmesser 1.0 mm wurden numerisch modelliert. Die Luft in der Düse wurde als ein turbulentes 3D-Medium mit dem Programm CFX-FLOW3D beschrieben. Die adiabatische und isentropische Abkühlung in dieser Düse ruft eine reproduzierbare Wasserdampfsättigung hervor, wenn man den Durchfluß ändert.

Zweitens: Ein Modell und ein Verfahren, mit dem das Wachstum der Partikel in der Strömung der Düse modelliert und bestimmt werden kann, wurde konstruiert. Dieses Modell dient der Bestimmung der Wachstumsraten des Aerosols und der Zeit, die gebraucht wird, um das Aerosol in der Düse bis zu der kleinsten meßbaren Größe für das nachgeordnete Nachweisgerät wachsen zu lassen. Schnelles Wachstum der Partikel und folglich große Verschiebung der Partikelverteilung in Düsen von Aerosolinstrumenten (wie OPC und APS), die großen Einfluß auf Messungsergebnisse haben, wurden gefunden.

Drittens: Als Beispiel für die Anwendung des Modells und des Verfahrens, wurde ein neuer Kondensationskernzähler mit Düse (Nozzle-CNC) nach diesem Prinzip aufgebaut. Experimente unter verschiedenen Zuständen, wie Durchfluß, Lufttemperatur, und Mischungsverhältnis des Aerosols, wurden mit diesem Kondensationskernzähler durchgefüht. Der Einfluß des Durchflusses auf die Bildungsraten atmosphärischer Aerosolpartikel wird ebenfalls vorgestellt. Die

Ergebnisse zeigen eine interessante Relation zwischen der Konzentration von atmosphärischen Kondensationskernen (CN), inklusive hygroskopische Kerne (HN), Wolkenkondensationskerne (CCN) und CN, und der in der Düse erzeugten Sättigung. Diese Relation unterscheidet sich von der Relation für CCN und Übersättigung. Die kleinste meßbaren Größe für diesen Kernzähler ist 0.04 μm in Radius.

Obwohl für diesen Düsen-CNC weitere Verbesserungen nötigt sind, hat er im Vergleich zu den anderen Kondensationkernzählern einige Vorteile, wie z.B. gleichzeitige Abkühlung, geringe Kondensation von Wasser auf der inneren Wand, vernachlässigbare Verluste von Partikeln durch Diffusion, einstellbare Sättigungen — daher ein breiter Einsatzbereich, und keine Kalibrierung, wie für Nicht-Wasser Kondensationssubstanzen.

List of Principal Symbols

The most important and most frequently used mathematical symbols are listed here for quick reference. Less frequently used ones are defined and explained at first use.

Nomenclature in Greek

Symbol	Unit	Definition
α		Constant
β		Correction factor for nucleus concentration
γ	$J\,cm^{-2}$	Surface tension of water
Γ		Turbulence diffusion coefficient
δ_d	cm	Thickness of diffusion boundary
ζ	cm	Condensation jump distance
ζ_T		Condensation jump distance for temperature
λ_g	μm	Mean free path of gas molecules
Λ		Source term of turbulence
Λ_p		Source term of particle
μ_g	$g\,cm^{-1}s^{-1}$	Viscosity of gas or fluid
ν		Number of ions for each molecule of salt when dissolved
ν_g	$cm^2\,s^{-1}$	Kinematic viscosity of gas (=μ_g / ρ_g)
ρ	$g\,cm^{-3}$	Density
ρ_E	$g\,cm^{-3}$	Density of saturated water vapour
ρ_g	$g\,cm^{-3}$	Density of gas
ρ_p	$g\,cm^{-3}$	Density of particle
ρ_w	$g\,cm^{-3}$	Density of water
σ		Geometric standard deviation
σ_s		Stress tensor
ς		Dimensionless deposition parameter
τ	s	Particle relaxation time
τ^+	s	Particle relaxation time with particle growth effect
τ_{St}	s	Particle relaxation time for Stokesian particle
Ψ_c, Ψ_h		Parameters in f_c and f_h

continue . . .

... *continue Symbol in Greek*		
Symbol	Unit	Definition
ϕ		fluctuating term of Φ
Φ		Any turbulent quantity
$\overline{\Phi}$		Averaged quantity of Φ
ψ		fluctuating term of Ψ
Ψ		Any turbulent quantity
$\overline{\Psi}$		Averaged quantity of Ψ

Nomenclature in Latin

Symbol	Unit	Definition
A	cm^2	Cross-sectional area of the nozzle
A_t		Thermal accommodation coefficient
A_w		Condensation coefficient
B	$N\,m^{-3}$	Body force
C		Constant
C_c		Cunningham correction factor
C_g	$J\,g^{-1}K^{-1}$	Specific heat of gas
C_p	$J\,g^{-1}K^{-1}$	Specific heat of particle
C_D		Drag factor
D	cm	Diameter of the nozzle
D_p	cm^2s^{-1}	Diffusion coefficient of particle
D_v	cm^2s^{-1}	Diffusion coefficient of vapour
e	hPa	Vapour pressure
$E(T)$	hPa	Saturated water vapour pressure at temperature T
E_s	hPa	Equilibrium pressure over particle surface
$E_{s,s}$	hPa	Equilibrium pressure over particle surface with soluble salt effect
E_∞	hPa	Equilibrium pressure over plane surface
$E_{\infty,0}$	hPa	Equilibrium pressure over plane surface without salt effect
f_c, f_h		Correction factor for non-continuum effect
F	N	Force on particle
F_a	cm^3s^{-1}	Flow rate of aerosol
F_A	N	Added mass force on particle
F_B	N	Buoyancy force on particle
F_c	cm^3s^{-1}	Flow rate of saturated clean air
	continue ...	

... *continue Symbol in Latin*

Symbol	Unit	Definition
F_D	N	Drag force on particle
F_p	N	Pressure gradient force on particle
g	$m\,s^{-2}$	Gravitational acceleration
h	W	Static enthalpy
H	W	Total enthalpy
I_r	$\mu m\,s^{-1}$	Radius condensational growth rate
J	$cm^{-2}\,s^{-1}$	Flow rate of vapour molecules
J_-	$cm^{-2}\,s^{-1}$	Flow rate of vapour molecules leaving from particle
J_+	$cm^{-2}\,s^{-1}$	Flow rate of vapour molecules towards particle
k	$g\,cm^2 s^{-2} K^{-1}$	Boltzmann constant
K_g	$cal\,cm^{-1} s^{-1} K^{-1}$	Thermal conductivity of gas
Kn		Knudsen number
L	cm	Length of nozzle
L_v	$cal\,g^{-1}$	Latent heat of vaporisation
$\dot{m}$	$g\,s^{-1}$	Mass condensational growth rate
m_g	g	Mass of single molecule of background gas (air)
m_p	g	Mass of particle
m_s	g	Mass of dissolved salt
m_v	g	Mass of single molecule of vapour
M_g	$g\,mol^{-1}$	Molecular weight of gas
M_s	$g\,mol^{-1}$	Molecular weight of salt
M_v	$g\,mol^{-1}$	Molecular weight of water vapour
M_w	$g\,mol^{-1}$	Molecular weight of water
n		Particle size distribution function
N	cm^{-3}	Particle number concentration
Nu		Nusselt number
p	hPa	Pressure
p_∞	hPa	Background pressure
Pr		Prandtl number
q	cal	Heat
$\dot{q}$	$cal\,s^{-1}$	Heat release rate
$\dot{q}_c$	$cal\,s^{-1}$	Heat flow rate associated with convection
$\dot{q}_m$	$cal\,s^{-1}$	Heat flow rate associated with mass transfer
Q	$l\,h^{-1}$	Volume flow rate

continue ...

... *continue Symbol in Latin*		
Symbol	Unit	Definition
r	μm	Radius
r^*	μm	Kelvin radius
r_g	μm	Geometric mean radius
r_k	μm	Critical particle radius
r_m	μm	Minimum detectable radius
r_p	μm	Particle radius
R	$J\,mol^{-1}K^{-1}$	Universal gas constant
R_w	$J\,g^{-1}K^{-1}$	Gas constant for water vapour
Re		Fluid Reynolds number
Re_p		Particle Reynolds number
S		Saturation
S_a		Saturation of aerosol flow
S_c		Saturation of clean air
S_s		Supersaturation
Sc		Schmidt number
Sh		Sherwood number
t	s or ^oC	Time or temperature in Celsius
T	K	Absolute temperature
u	$m\,s^{-1}$	Velocity
u_g	$m\,s^{-1}$	Velocity of gas
u_p	$m\,s^{-1}$	Velocity of particle
u_r	$m\,s^{-1}$	Relative velocity
$\overline{U}$	$m\,s^{-1}$	Mean velocity of gas flow
$\overline{v}$	$m\,s^{-1}$	Mean speed of molecule
V_{dep}	$m\,s^{-1}$	Deposition velocity of particle
x	cm	Instantaneous location of particle
z	cm^{-3}	Molecular number density

Subscripts and Superscripts

Symbol	Definition
g	Pertaining to gas or air
p	Pertaining to particle
s	On particle surface
	continue ...

... *continue Sub- and Superscripts*	
Symbol	Definition
v	Pertaining to water vapour
w	Pertaining to liquid water
∞	Infinity

Abbreviations

Abbreviation	Definition
AP	Atmospheric Aerosol Particle
APS	Aerodynamic Particle Sizer spectrometer
CCN	Cloud Condensation Nuclei
CCN-CN	Nuclei between CCN and CN
CN	Atmospheric Condensation Nuclei
CNC	Condensation Nucleus Counter
CNC 3020	Condensation Nucleus Counter – TSI Model 3020
HN	Hygroscopic Nuclei
LPC	Laser Particle Counter
Nozzle-CNC	Nozzle Condensation Nucleus Counter
OPC	Optical Particle Counter
TDMA	Tandem Differential Mobility Analyser

x

Contents

List of Figures

List of Tables

Chapter 1

INTRODUCTION

1.1 Atmospheric Aerosol Particles

Atmospheric air contains not only air molecules such as N_2, O_2, CO_2, H_2O and others, which approximately amount to $2.0 \cdot 10^{19}$ per cubic centimetre, but also ions and a substantial amount of suspended particles. They interact with each other and form a complex and dynamic three-phase mixture (see Fig. 1.1). This mixture system is named atmospheric aerosol. The particulate matter in this system is usually known as aerosol particles.

Atmospheric aerosol particles have sizes ranging from several Angströms to several micrometer (up to more than 50 μm), with number concentrations from 1 cm^{-3} in clean background to over $2.0 \cdot 10^5$ cm^{-3} in polluted city air. They origin from a number of natural sources such as sea salt from ocean spray, botanical debris, soil and desert dust, volcanic dust, gas-to-particle conversion, atmospheric clouds of water droplets or ice particles (Jaenicke, 1993), and human activities such as the emission of smoke and pollutants.

The research of the atmospheric aerosol includes the study of the physical properties, atmospheric behaviours, and the chemical contents. The result of this research has triggered global concerns. Aerosol particles play important roles with relation to human health and many atmospheric phenomena. Particles less than 1.0 micrometer can easily enter the human lung, either deposit in the respiratory tract (Heyder, 1986) or enter the human blood cycle, and therefore are potentially harmful to human health. In the atmosphere, aerosol particles serve as nuclei for condensation of water vapour, and they play a pivotal role in the

formation of cloud droplets and then raindrops. Without these nuclei, there will be no clouds, no rain, no hydrological cycle and no complex weather system on the earth. Aerosol particles suspended in the atmosphere absorb and scatter solar radiation and therefore modify the radiation balance of the earth system. Studies show that the radiative and climate perturbation of the sulphate aerosol may offset the greenhouse effect over large portions of the northern hemisphere (Charlson *et al.*, 1992). Aerosol particles are also responsible for the deterioration of air quality in spatial scales, and can cause a widespread visibility reduction as well as the formation of Arctic Haze (Rahn *et al.*, 1981; Dreiling *et al.*, 1997). Because of their long-range transport with the circulation of the atmosphere, they can redistribute solid pollution substances in the atmosphere. For desert aerosol particles, such long distance transport is responsible for the redistribution of nutrient soils in a large scale on the earth (Duce *et al.*, 1980; Iwasaka *et al.*, 1988). Aerosol particles interact with atmospheric gases, for example SO_2, NO_x, O_3, and H_2O_2, and serve not only as major supplies in chemical reactions, but also as important surfaces, on which catalytic chemical reactions can take place. It is assumed that stratospheric particles may play a key role in ozone depletion because of their catalytic function in reactions with chlorine compounds, such as anthropogenic chlorofluorocarbons (CFCs) (Hofmann and Solomon, 1989; Prather, 1992; Johnston *et al.*, 1992; Mills *et al.*, 1993).

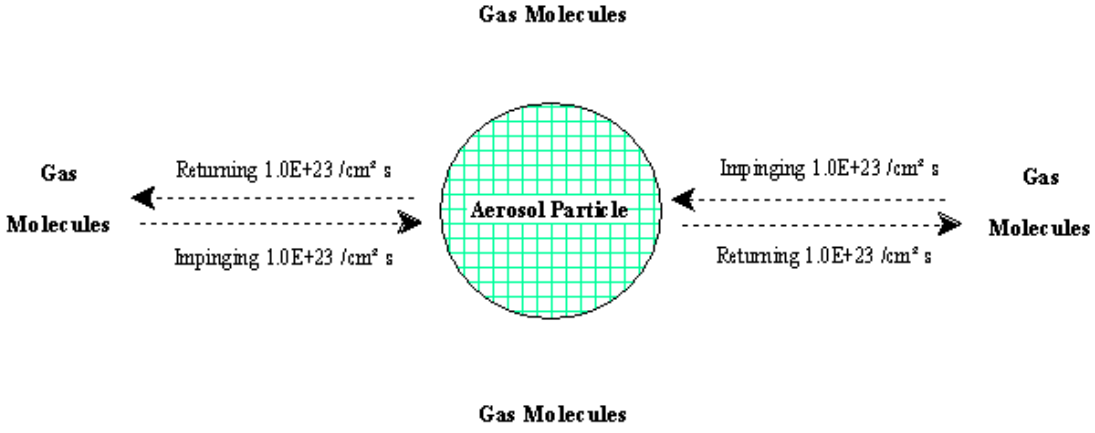

Figure 1.1: Interaction in the atmospheric aerosol system

Studying and understanding basic properties as well as physical and chemical principles of aerosols and then applying these knowledges in measurements and controls have doubtless practical values. This is a main purpose of basic aerosol study, and such practical employment of aerosol knowledges is called as aerosol technology. Aerosol technology today has found numerous scientific and engineering applications. Examples are commercial uses in numerous aerosol instrument designs, in the manufacturing of spray-dried products, and in the area of pesticides in agriculture or forestology. In medical treatment, therapeutic aerosols are commonly used for the treatment of respiratory diseases.

There is a tight relation between the aerosol research and aerosol technology. Aerosol research provides new knowledges and new methods for the development of aerosol technology, and in return the new aerosol technology can provide us with new tools for the aerosol study. In this work, the behaviour of aerosol particles by the condensation of water vapour in a saturated air flow will be studied. The results will then be applied for an aerosol measurement design, that is the construction of a new continuous flow nozzle condensation nucleus counter (Nozzle-CNC).

1.2 Size Distribution of Aerosol Particles

The basic behaviours of aerosol particles such as deposition, transport, lifetime, and optical influence, depend strongly on their size, their chemical composition, and on the nature of the carrier gas. The size of aerosol particles may vary from a few Angströms to several micrometers. Aerosol particles in atmospheric air are not monodisperse, but polydisperse. Since all particle sizes are present and the behaviours of atmospheric aerosols are always related to their integral action, it is more useful applying size-dependent function than characterising the size property of a single-particle.

In the early 1950's, Junge found in measurements that atmospheric aerosol particles have the interesting property that the mass was almost uniformly distributed in equal geometric intervals. Then he derived the Junge distribution (Junge, 1963):

$$n = \frac{\mathrm{d}\,N}{\mathrm{d}\log r} = C\,r^{-\alpha}, \tag{1.1}$$

where N is the number concentration, C is a constant, r is the particle radius, and α is an adjustable constant in the range from 2.2 to 4.0. The Junge distribution was proved to be very good, especially for aerosol particles with radii r_p>0.1 μm. However because of the limitation of the development of aerosol technology to measure particles with sizes smaller than 0.1 μm in 1950's, Junge didn't find a suitable size distribution for describing fine size particles. Usually particles in fine size region have bimodal and other distribution shapes because of the strong interactions among them such as coagulation and diffusion collision.

One type of aerosol size distribution that is used widely in atmospheric studies, such as in aerosol radiation models (D'Almeida $et\ al.$, 1991), is the log-normal distribution:

$$n = \frac{\mathrm{d}N}{\mathrm{d}\log r} = \frac{N}{\sqrt{2\pi}\log\sigma}\exp[-\frac{1}{2}\cdot(\frac{\log(r/r_g)}{\log\sigma})^2], \tag{1.2}$$

where r_g is the geometric mean radius, and σ is the geometric standard deviation. There are other types of aerosol size distributions such as the Gamma distribution, but they are not so widely used as the log-normal distribution. One advantage of the log-normal distribution is that it can be superimposed to form a new size distribution describing specific atmospheric aerosol modes. Jaenicke (1988, 1993) gave a series of these aerosol modes which can quite well describe size distributions of the aerosols in urban, rural, polar, desert, and oceanic regions by superimposing 3 log-normal distributions:

$$n = \sum_{i=1}^{3}\frac{N_i}{\sqrt{2\pi}\log\sigma_i}\exp[-\frac{1}{2}\cdot(\frac{\log(r/r_{gi})}{\log\sigma_i})^2]. \tag{1.3}$$

The parameters for various aerosol modes are tabulated in Table 1.1. Figure 1.2 shows aerosol size distribution of 7 modes parameterised as in Tab. 1.1. In this work, the log-normal distribution is adopted to characterise the atmospheric aerosol particles. The evolution and analysis in this work are based on this type of distribution.

1.3 Composition of Aerosol Particles

The composition of aerosol particles determines mainly their physico-chemical properties, such as the hygroscopic properties of aerosol particles, their nucle-

Table 1.1: Parameters for aerosol modes composed of 3 log-normal distributions in various geographical regions (Jaenicke, 1988)

Mode	N_1 cm^{-3}	r_{g1} μm	σ_1	N_2 cm^{-3}	r_{g2} μm	σ_2	N_3 cm^{-3}	r_{g3} μm	σ_3
rural	6.65E+3	7.39E-3	1.68	1.47E+2	2.69E-2	3.61	1.99E+3	4.19E-2	1.85
urban	9.93E+4	6.51E-3	1.76	1.11E+3	7.14E-3	4.63	3.64E+4	2.48E-2	2.17
continental	9.97E+2	1.00E-3	2.13	8.42E+2	2.18E-2	3.20	7.14E-4	6.24E-0	1.89
desert dust	7.26E+2	1.00E-3	1.77	1.14E+3	1.88E-2	5.89	1.78E-1	1.08E-3	2.74
maritime	1.33E+2	3.90E-3	2.13	6.66E+1	1.33E-1	1.62	3.06E+2	2.90E-1	2.49
polar	2.17E+1	6.89E-2	1.76	1.86E-1	3.75E-1	2.00	3.04E-0	4.29E-0	1.95
background	1.29E+1	3.60E-3	4.42	5.97E+1	1.27E-1	1.79	6.35E-1	2.59E-1	2.66
stratosphere				4.49E+0	2.17E-1	1.77			

ation activities, their absorption and scattering coefficients, and their chemical behaviours with other atmospheric species. Aerosol particles contain numerous chemical and mineral species depending on their sources. Biological particles have also been found to be an important source type of the atmospheric aerosol, from taking about 15% in maritime aerosol to about 20% in continental aerosol (Gruber $et\ al.$, 1998). The chemical composition and the solubility of fine and coarse particles differ from each other as they origin from totally different sources.

Coarse particles (larger than 2.0 μm) are generally from mechanical processes, and are rich in crustal elements like Ca, Al, Si, Ti, and other constituents of earth. Fine particles, as they are generally derived from chemical processes such as 'gas-to-particle' conversion and combustion, are acidic and rich in sulphate, ammonium, nitrate, hydrocarbon, elemental carbon (soot), toxic metals, and water (whitby, 1978). Usually, fine particles are more water dissolvable than coarse particles.

The study of urban aerosol shows that sulphate, nitrate and ammonium have two modes in the 0.1 to 1.0 μm size range (see Fig. 1.3). They are condensation mode and droplet mode (John $et\ al.$, 1987). The condensation mode has a mean size of about 0.2 μm, which results from the condensation of secondary aerosol components from gas phases. The droplet mode is at a size of about 0.7 μm. Its formation mechanism is the heterogeneous aqueous-phase reactions in droplets.

The comparison of the chemical compositions for fine and coarse particles is listed in table 1.2. As fine size particles have larger number concentrations, and are more dissolvable than coarse particles, they play a major role in many aspects

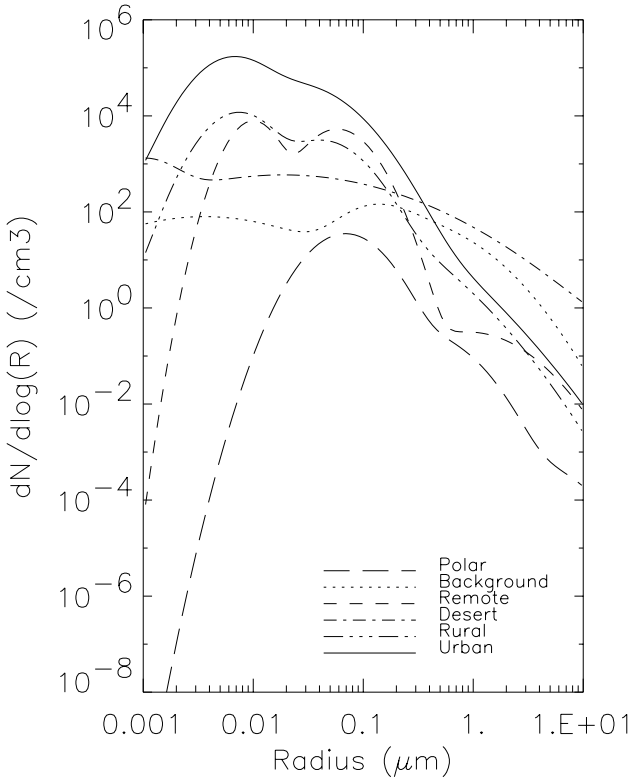

Figure 1.2: Model aerosol size distributions in various geographical regions

such as radiative scattering and absorbing, serving as condensation nuclei, and causing chemical reactions in the atmosphere.

1.4 Aerosol-Cloud Interaction

Aerosol particles can be activated at a given supersaturation and grow. As being discussed in the section 1 of the next chapter, for a given aerosol size distribution, if a supersaturation is reached for the condensation on a certain particle radius (the critical particle radius r_k), then condensation can take place on all particles larger than r_k. If the supersaturation is high enough, for example $\geq 400\%$, all aerosol particles can form water droplets. Therefore this is used for the definition of atmospheric condensation nuclei (CN). In a natural cloud, supersaturation remains usually below 5% and typically below 2%. So only a part of CN can be activated. These particles, which are capable of initiating droplet formation at

Table 1.2: Comparison of chemical composition in fine and coarse size particles

*	Fine Particles	Coarse Particles
Composition	Sulphate	Wind-blown dust
	Nitrate	Coal and fly ash
	Hydrogen ion	Crustal element (Si, Al, Ti) oxides
	Ammonium	$CaCO_3$, NaCl
	Elemental carbon	Biological particles such as pollen, spores
	Metal Fe, Zn, Mn, Pb, etc.	Plant, debris
	Organic compounds	
Solubility	Quite soluble and hygroscopic	Only partly soluble and non-hygroscopic

low supersaturations as observed in clouds are called 'cloud condensation nuclei' (CCN). The role of aerosol particles as serving nuclei for cloud formation is not the only connection between aerosol and clouds. In fact, they interact with each other, and have a very close relation. Studying their interaction has become one of the most important topics in current atmospheric aerosol and atmospheric studies. It is very helpful for us to understand the hygroscopic property and transformation between aerosol particles and water droplets in this work .

This aerosol-cloud interaction is schematically shown in Fig. 1.4. In cloud formation, aerosol particles serve as CCN. For aerosol particles, this is an important removal process, usually called nucleation scavenging of particles in clouds. Besides that other removal processes exist: the collision of aerosol particles with cloud droplets and the capturing of the particles. This nucleation process determines the initial composition of the cloud droplets. After the droplet formation, soluble gases such as sulphur dioxide, ammonia, nitric acid and atmospheric radicals such as HO and H_2O_2 dissolve into the droplet. The cloud droplet serves as reaction medium for aqueous phase reactions, in which a series of chemical reactions can take place – for example, most S(IV) can be oxidised to S(VI) and other dissolved species can react with sulphuric or nitric acid. When supersaturation disappears, the cloud droplet evaporates and returns to aerosol particle. The non-volatile species such as sulphate remain in the aerosol particle. By this way, a totally new aerosol particle is produced because of its new size, shape, and chemical composition. Jaenicke (1993) once proposed that the cloud evaporation

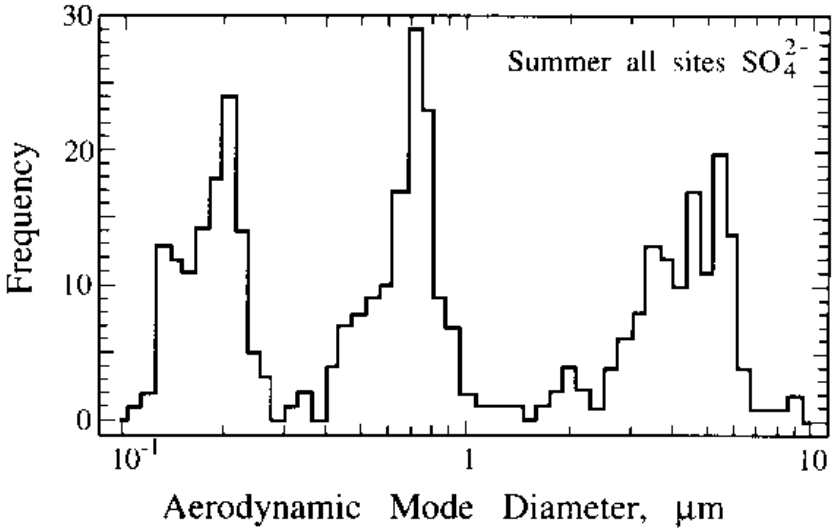

Figure 1.3: Frequency of observed occurrence of sulphate modes (John *et al.*, 1987)

is the largest natural source of aerosol particles, by producing new particles of about 3000 Tg / yr, larger than world deserts by producing a total particle mass of 2000 Tg / yr.

The changes of the distribution of atmospheric aerosol particles can also result in the modification of the cloud droplet sizes, and therefore the changes of cloud lifetime and albedo, which can induce the indirect effect of aerosol in the radiation balance of the earth climate system.

1.5 Atmospheric Condensation Nuclei – Measurement and CNC

According to the physical property of water condensation on aerosol particles in supersaturation, an instrument to measure the number concentration of CN named 'condensation nucleus counter' (CNC) can be constructed. The main principle of a CNC is to create a temperature decrease for forming a supersaturation by adiabatic expansion in an expansion vessel. This causes water to condense by heterogeneous condensation on particles, and these particles, in spite of variations in the sizes of the original nuclei, then grow into larger water droplets of uniform size. These droplets can be counted and photographed, or be detected with electronic devices by scattering a detectable amount of light when

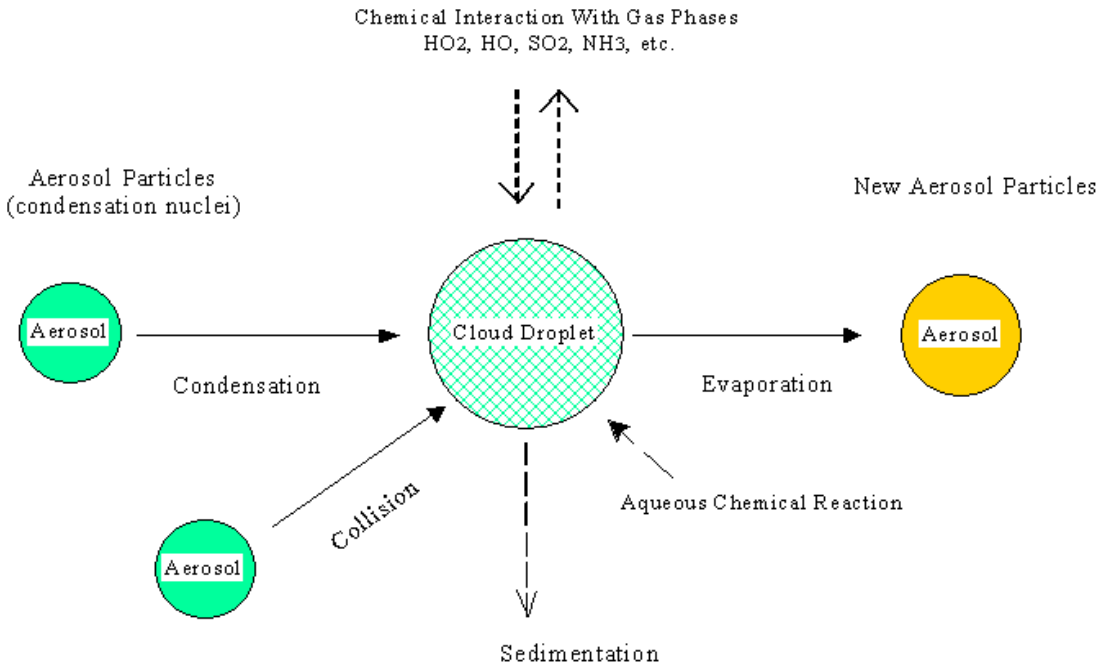

Figure 1.4: Schematic diagram of aerosol-cloud interaction

they pass through a light beam. By this way the number concentration of submicron aerosol particles may be directly or indirectly measured by counting the number concentration of these water droplets. However, the measured droplet size is nearly independent of the size of the original particle over a wide range of particle sizes, so the detected concentration is the number concentration for particles larger than r_k only, with no relation to their initial size distribution. Despite this inability of CNCs to give size discrimination, CNCs have enjoyed great value in their wide applications in the study of air pollution, cloud physics, and in general atmospheric aerosol researches.

The first CNC construction was attributed to Aitken (1888a, 1888b, 1891). His counter was a simple, manually operated mechanical device, requiring direct counting by visually inspecting the individual droplets formed after adiabatic expansion. Following his initial work, numerous CNCs with various designs have been developed. The development of CNCs, just as many modern technologies, is towards the designs for more accurate and more reliable measurements, and also more convenient automatic operations. It includes mainly two aspects — the im-

provement of the expansion way and the improvement of the counting method.

Based on the Aitken's preliminary instrument, Scholz (1932) improved this counter. Several disadvantages of this counter, such as the problem of air leakage, were eliminated. Scholz also provided a means to change the dilution for using at different concentration levels. The same expansion principle could be found in the design of the famous Wilson cloud chamber which was used to observe the ion tracks associated with radioactive decay in a high saturation ratio.

The adiabatic expansion can not only be achieved by volume expansion, but also pressure expansion. The example of pressure expansion can be found in the Nolan-Pollak (N-P) counter (Nolan and Pollak, 1946) in which an overpressure system with a free expansion rather than a piston operated volumetric expansion was used. Similar adiabatic expansion was also used in the studies of Liu $et\ al.$ (1975), Miller and Bodhaine (1982), and Schmidt $et\ al.$ (1982). The UMR Absolute Aitken Nucleus Counters (UMP-AANC; Kassner $et\ al.$,1968) consists basically of a large Wilson expansion chamber with piston under water surface. It can be operated automatically at supersaturation ranging from 24% to 380%.

The preliminary used counting method is direct visual inspection as in Aitken (Aitken, 1988) and Scholz (1932) counters. Similar direct counting also includes direct photography of droplets and the use of the 'out-of-focus method' for the evaluation of the photographs too, employed in those such as Kanter counter (Kanter and Junge, 1971), and Jaenicke-Kanter counter (Jaenicke and Kanter, 1976). The UMR Absolute Aitken Nucleus Counter (UMP-AANC; Kassner $et\ al.$,1968) is a semi-automatic photographic counter. The direct counting counter is also termed as 'absolute counter' as suggested by Pollak (1959).

As direct counting is tedious, time consuming and not continuous, it was gradually replaced by indirect counting. That is the measurement of light extinction produced by the droplet population so that a concentration can be inferred from this measurement. As this counting method is less direct, the counter employed this counting is given the name 'relative' counter. Nolan and Pollak (1946) constructed the first photoelectric condensation nucleus counter. Systematic and careful experiments were made with the N-P counter and this counter was selected by many investigators as a standard instrument despite its indirect measurement. The principle of relative counting in N-P counters was used in Gardner counter, Verzar (1953) counter, General Electric (GE) counter [1] and other coun-

[1]General Electric Co., 100 Plastics Ave., Pittsfield, MA 01201, U.S.A.

ters. The particle information can not only be inferred from light attenuation, but also from angular scattering. Wagner (1974) once described a more sophisticated counting and measuring method for recording particle growth in his counter.

Recently the cooling to produce supersaturation is achieved by thermal diffusion. The aerosol stream warmed and saturated with a working fluid, is cooled in a condensation tube that is kept at a lower temperature. Because of the lower temperature at the wall of the condensation tube, aerosol flow is cooled by heat conduction and convection. This type of CNCs was reported by some researchers such as Rosen *et al.* (1974, 1978), Hoppel *et al.* (1979), Bricard *et al.* (1976), Sinclair (1975, 1982), Agarwal and Sem (1980), and Keady *et al.* (1983). In these CNCs, working vapours of organic liquids such as ethanol, glycol and butanol other than water were used. As organic molecules have larger molecular weight and smaller mobility than water molecules, they are easier, compared to water vapour, to condensate on aerosol particles. So these CNCs can measure very low concentrations of CN. However, it is a question if the water condensation and non-water condensation on particles are the identical. It would be necessary to calibrate such counters by using a great variety of nuclei and a wide range of nucleus concentration before converting the number of measured nuclei in this manner into “absolute” atmospheric CN concentration.

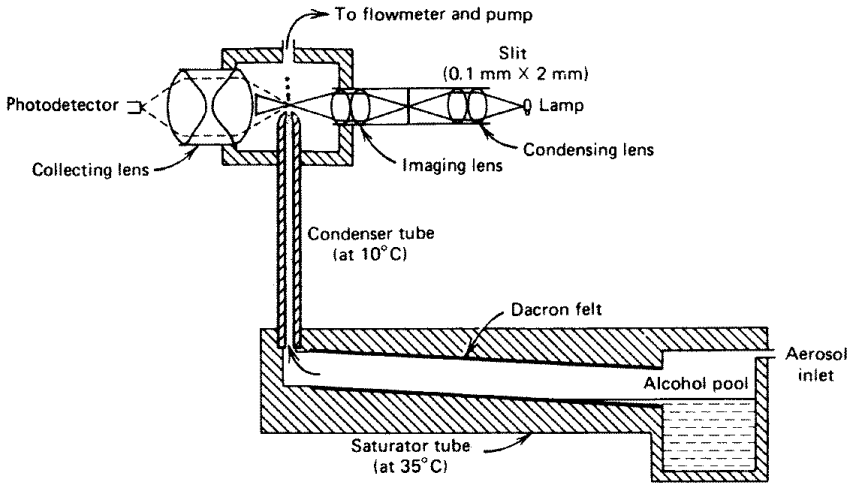

Figure 1.5: Schematic diagram of the continuous flow condensation nucleus counter Model 3020 (TSI)

The TSI[2] continuous flow condensation nucleus counter (TSI CNC Model

[2]TSI - Thermo Systems Inc., St. Paul, MN 55164, U.S.A.

3020), as shown in Fig. 1.5, is widely used today in atmospheric aerosol studies. It was designed by Bricard $et\ al.$ (1976), and then was developed for commercial use by TSI company. It does not make use of an expansion to produce a supersaturation vapour. First the aerosol sample is introduced to pass through a saturation pool where the condensation liquid (alcohol) is warmed and maintained at a temperature of 35^oC. Here the aerosol sample is saturated with alcohol. Then the flow is led to a condensation tube where the temperature is maintained at a lower temperature of around 10^oC. In this tube the vapour of alcohol becomes supersaturated and condenses on the particles.

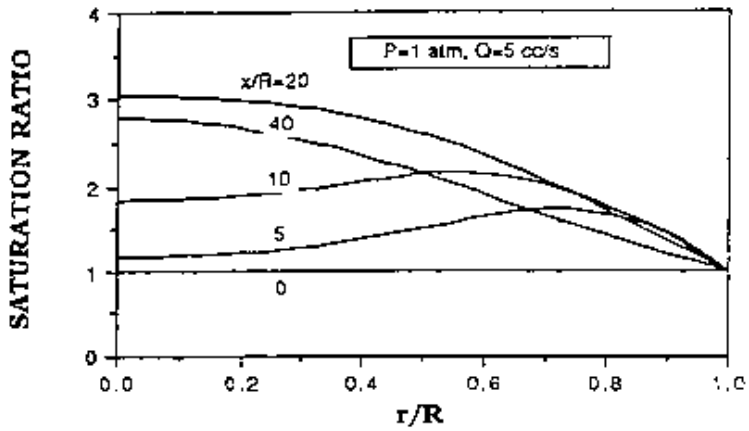

Figure 1.6: Calculated saturation in the condensation tube of the CNC Model 3020 between axis and wall as well as along the length (x) of the tube (Zhang and Liu, 1990). R is the radius of the tube, and r is the radial distance from the axis.

However as the cooling is achieved by thermal diffusion from the tube outside to inside, time for heat transport is needed. Therefore one has a reason to believe that the sampled air is not cooled isentropically and simultaneously, which can result in an uneven saturation distribution in the tube. Zhang and Liu (1990) studied the saturation profile in the tube of the CNC Model 3020. Great differences of saturation between the axis of condensation tube and tube wall as well as along the length of the tube, as shown in Fig. 1.6, were found. Furthermore, particle behaviour in the vapour of alcohol is obviously not the same as in water vapour, as the chemical and physical equilibrium between the vapour of alcohol and particle surface is different from that between water vapour and particle surface. So it should be suspected if the measured particle number concentration stands for the actual concentration of atmospheric condensation nuclei.

1.6 Motivation of this Work

By studying condensation nucleus particles, various designs of condensation nucleus counters (CNC) were invented. A commercial counter with alcohol as the condensation substance is used widely in aerosol measurements. However, doubts arise whether the particles in the alcohol vapour are activated in the same way as in the water vapour, and whether the measured number of the atmospheric nuclei can stand for the “absolute” number of nuclei in the natural atmosphere. Water cannot be used in the same way as alcohol, as water would condense at the inner wall of the instrument. The use of single-particle continuous counters is especially valuable, does it permit tandem operation, like in the tandem differential mobility analyser (TDMA).

The study of the condensational growth of aerosol particles in an expanding nozzle flow saturated with water vapour opens an alternative. As being discussed later by theoretical and numerical modelling, expansion by nozzle flow is a good method to produce air cooling as it can give fast, nearly adiabatic and isentropic cooling due to the continuous expansion. When an air sample saturated with water vapour is introduced into the nozzle, then the condensation process will be initiated. Based on this, a new idea for constructing a continuous flow nucleus counter has been put forward, and experiments were carried out for studying this new counter. This method differs greatly from other expansion methods used in other CNCs before.

Chapter 2

BASIC THEORIES

In order to study the particle growth in air flow, it is necessary to introduce these theories:

- surface equilibrium theory on particle surface;
- particle properties depending on size range;
- particle behaviour in the air flow; and
- mass and heat transfer between particles and gas.

2.1 Equilibrium Behaviour of Aerosol Particles

Köhler Effect

Aerosol particles, existing in a gas medium, have interactions with gas molecules. There are 10^{23} gas molecules per square centimetre impinging on a suspended particle per second, and in equilibrium, a current of the same magnitude returning back from the particle's surface to the ambient gas (see Fig.1.1).

On a flat liquid surface, saturation vapour pressure (at 100%) is the equilibrium partial pressure required for the balance, at which the rate of vapour molecules leaving from the surface is the same as that impinging on the surface. If the liquid surface is sharply curved, like a particle surface, the partial pressure (E_s) required to maintain equilibrium is greater than that for a flat surface (E_∞). This

is because the curvature of the surface decreases the attractive forces between surface molecules, which results in an easier leaving for molecules from the surface. So in order to maintain balance, the partial pressure of vapour in surroundings should be greater than that for flat surface.

The relationship between the saturation ratio E_s/E_∞ and the droplet size for pure liquids, for example water, can be expressed by the Kelvin or Thomson-Gibbs equation (Pruppacher and Klett, 1997)

$$\ln \frac{E_s}{E_\infty} = \frac{2\gamma M_w}{\rho_w \mathrm{R} T r^*}, \tag{2.1}$$

where γ is the surface tension of the water-vapour interface; M_w is the molecular weight of water; ρ_w is the difference between the densities of water and the vapour; R is the universal gas constant; r^* is the Kelvin radius at which the particle will neither grow nor evaporate at the saturation ratio E_s/E_∞.

According to this Kelvin equation, the equilibrium particle radius can be calculated at a given saturation ratio. Only particles with radius r^* are stable. Smaller ones evaporate and larger ones grow. The Kelvin effect causes an increase of the equilibrium vapour pressure as particle size decreases.

Usually the liquid is not ideally pure. The dissolved chemical composition in liquid changes the equilibrium vapour pressure too. The relationship between the saturation ratio and particle size for droplets containing dissolved materials is given as (Pruppacher and Klett, 1997)

$$\frac{E_{s,s}}{E_{\infty,0}} = \left(1 + \frac{3\nu m_s M_w}{4 M_s \rho_w \pi r^{*3}}\right)^{-1} \exp\left(\frac{2\gamma M_w}{\rho_w \mathrm{R} T r^*}\right), \tag{2.2}$$

where m_s is the mass of the dissolved salt having a molecular weight M_s; ν is the number of ions for each molecule of salt when it dissolves. For salt NaCl, the value is 2.

The first term in Eq. (2.2) is due to the effect of the dissolved salt, and the exponential term is the Kelvin effect. Equation (2.2) is widely used for studying the effects of curvature as well as dissolved salt on the equilibrium pressure on particle surfaces, which is named as Köhler effect. An example presentation of the Köhler effect for particles containing soluble salt NaCl is shown in Fig. 2.1.

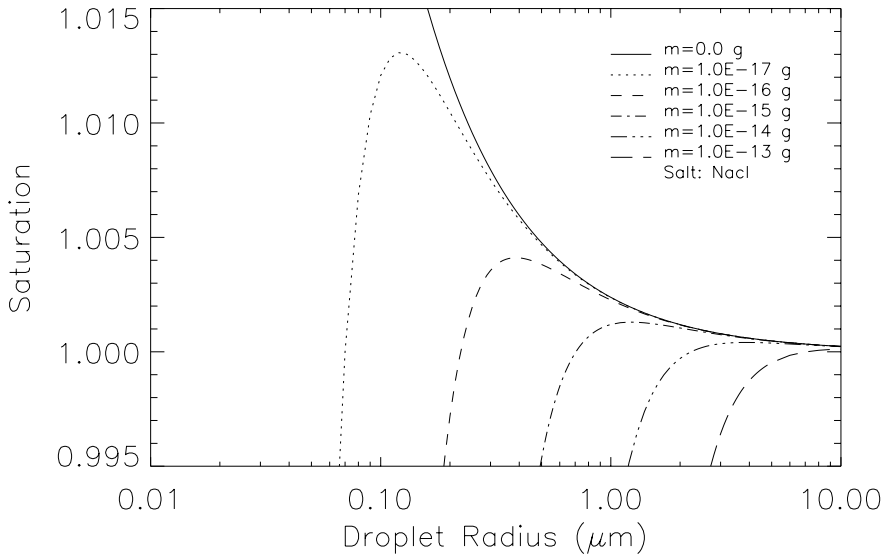

Figure 2.1: Köhler effect on the equilibrium vapour pressure over droplet containing salt NaCl

2.2 Particle Properties with Size Regimes

One set of mathematical equations cannot usually be used to predict particle dynamics for all sizes of particles. When a particle size is much larger than the mean free path λ_g of gas molecules, the gas acts as a viscous fluid and the dynamics of particles can be described by continuum theory. On the contrary, the continuum theory couldn't be applied and should be corrected for very tiny particles. The Knudsen number is often used as a measure characterising different particle size regimes. It is defined as

$$\mathrm{Kn} = \frac{\lambda_g}{r_p}. \tag{2.3}$$

For air under standard conditions (1013 hPa and 20 ^{o}C), the mean free path of air molecules is about 0.066 μm. Values of Kn, as tabulated in Table 2.1, are larger than 10 in the free molecule regime, 0.3 to 10 in transition regime, smaller than 0.3 in the slip flow regime, and very small in the continuum regime.

As particles with sizes smaller than 0.65 μm are of main concern in this study, the continuum theory for large particles should therefore be corrected.

Table 2.1: Particle size regime and Knudsen number (1013 hPa, 20^0C)

Size Regime	Free Molecule	Transition	Slip Flow	Continuum (Stokes)
Kn	>10	10 - 0.3	0.3 - 0.1	$<$0.1
Radius r_p (μm)	<0.005	0.005 - 0.2	0.2 - 0.65	$>$0.65

2.3 Particle Response to Flow Fields

Particles in air flow can, depending on their sizes, obtain different accelerations because of their different inertias. This property is often used in aerosol sizing devices such as multi-stage cascade impactors and many aerosol sizing devices such as Aerodynamic Particle Sizer spectrometer (for example TSI APS Model 3320, see Fig. A.1). The particle's response to the flow can generally be characterised by the particle relaxation time. Large particles have a longer 'residence' time in an accelerating flow than small particles and air molecules.

A general expression for the drag force $\mathbf{F}_D$ on a spherical particle in a gas of constant velocity can be written as follows:

$$\mathbf{F}_D = \frac{1}{2}\pi {r_p}^2 \rho_g |\mathbf{u_r}| \mathbf{u_r} \frac{C_D}{C_c}, \tag{2.4}$$

where r_p is the particle radius, $\mathbf{u_r} = \mathbf{u_p} - \mathbf{u_g}$ the relative velocity of the two phases. C_D is the drag factor (Seinfeld, 1986), and C_c is Cunningham non-continuum correction (Cunningham, 1910).

The above equation can be rewritten as

$$\mathbf{F}_D = \frac{C_D \mathrm{Re}_p}{24 C_c}(6\pi\mu_g r_p \mathbf{u_r}) \tag{2.5}$$

with μ_g the viscosity of the gas. Re_p is the particle Reynolds number defined as

$$\mathrm{Re}_p = \frac{2\rho_g |\mathbf{u_r}| r_p}{\mu_g} = \frac{2|\mathbf{u_r}| r_p}{\nu_g} \tag{2.6}$$

with ν_g the kinematic viscosity of the gas.

When the particle Reynolds number is very small ($\mathrm{Re}_p \ll 1$), then

$$C_D = \frac{24}{\mathrm{Re}_p}. \tag{2.7}$$

Therefore Eq. (2.5) can be written as

$$\mathbf{F}_D = 6\pi\mu_g r_p \mathbf{u_r}. \tag{2.8}$$

This state ($\mathrm{Re}_p \ll 1$) is generally called Stokes Law.

For high velocity flows, the Reynolds number for particles may be too large for the Stokes law approximation to hold. Depending on the Reynolds number for particles, as shown in Fig. 2.2, the drag factor C_D can be approximated as (Seinfeld, 1986) :

$$C_D = 24/\mathrm{Re}_p \qquad \mathrm{Re}_p < 0.1$$

$$C_D = (24/\mathrm{Re}_p)[1 + \frac{3\mathrm{Re}_p}{16} + \frac{9\mathrm{Re}_p{}^2}{160}\ln(2\mathrm{Re}_p)] \qquad 0.1 < \mathrm{Re}_p < 2$$

$$C_D = (24/\mathrm{Re}_p)[1 + 0.15\mathrm{Re}_p{}^{0.687}] \qquad 2 < \mathrm{Re}_p < 500$$

$$C_D = 0.44 \qquad 500 < \mathrm{Re}_p < 2 \cdot 10^5$$

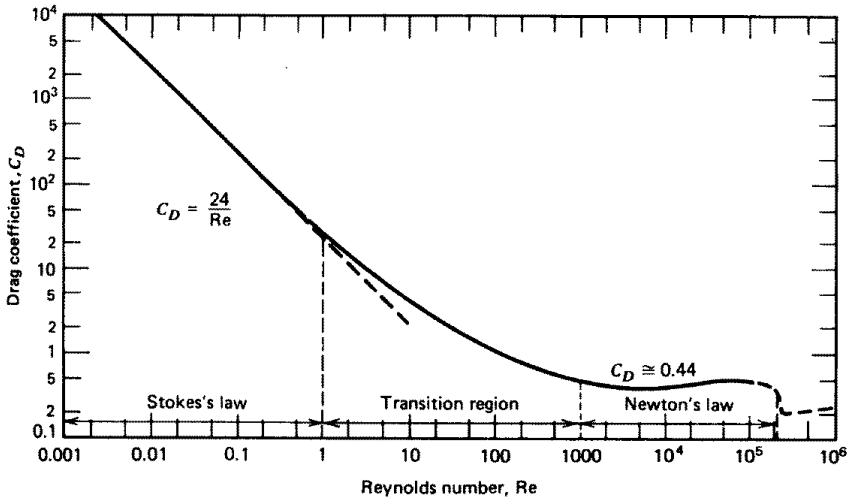

Figure 2.2: Drag coefficient versus Reynolds number for a sphere

The Cunningham correction C_c has been found important when the particle size has the same and smaller order of magnitude than the mean free path of air molecules. It can be expressed as (Seinfeld, 1986)

$$C_c = 1 + \frac{\lambda_g}{r_p}[1.257 + 0.4\exp(-1.1 r_p/\lambda_g)]. \tag{2.9}$$

There are additional forces on the particle, which may be included in the calculation. These are:

- Pressure gradient force

$$\mathbf{F}_P = -2\pi r_p{}^3 \nabla p, \tag{2.10}$$

where p is the pressure in the continuous phase;

❍ Buoyancy force

$$\mathbf{F}_B = \frac{4}{3}\pi {r_p}^3(\rho_p - \rho_g)\mathbf{g}, \tag{2.11}$$

where ρ_p is the density of the particle and g is the gravitational acceleration;

❍ Added mass force

$$\mathbf{F}_A = \frac{4}{3}\pi {r_p}^3\rho_g\frac{\mathrm{d}\mathbf{u}_r}{\mathrm{d}t}. \tag{2.12}$$

The pressure gradient force is small for particles with much higher density than the continuum fluid and need not be included in the modelling of particle movement.

Fuchs (1964) once gave the drag force at low Reynolds numbers for an accelerating sphere moving in a straight line through a fluid at rest as

$$\mathbf{F}'_D = 6\pi\mu_g r_p\mathbf{u_r} + \frac{4}{3}\pi\rho_g {r_p}^3\frac{\mathrm{d}\mathbf{u_r}}{\mathrm{d}t} + 6\pi\rho_g {r_p}^2(\frac{\nu_g}{\pi})^{1/2}\int_{-\infty}^{t}\frac{\mathrm{d}\mathbf{u_r}}{\mathrm{d}t'}\frac{\mathrm{d}t'}{(t-t')^{1/2}}. \tag{2.13}$$

The first term on the right-hand side is equivalent to the Stokes drag. The second and third terms arise from added mass and the particle acceleration, respectively. They are usually neglected under normal circumstances for spheres of unit density in air.

The motion equation of particles can be generally expressed as

$$m_p\frac{\mathrm{d}\mathbf{u_p}}{\mathrm{d}t} = -\mathbf{F}_D - \mathbf{F}_p - \mathbf{F}_B - \mathbf{F}_A. \tag{2.14}$$

Usually the drag force $\mathbf{F}_D$ can be considered as the only external force acting on particles passing through the nozzle. Then particles have the motion equation

$$m_p\frac{\mathrm{d}\mathbf{u_p}}{\mathrm{d}t} = -\mathbf{F}_D = -\frac{C_D\mathrm{Re}_p}{24C_c}(6\pi\mu_g r_p(\mathbf{u_p} - \mathbf{u_g})). \tag{2.15}$$

Here m_p is the mass of the particle. This equation can be rewritten as

$$\tau\frac{\mathrm{d}\mathbf{u_p}(x)}{\mathrm{d}t} + \mathbf{u_p}(x) = \mathbf{u_g}(x), \tag{2.16}$$

where x is the instantaneous location of the particle, τ is the particle relaxation time given by

$$\tau = \frac{2r_p^2\rho_p}{9\mu_g}\frac{24C_c}{C_D\mathrm{Re}_p}. \tag{2.17}$$

When particle growth is taken into consideration, the particle relaxation time is τ^+ (Dahneke and Padliya, 1977)

$$\tau^+ = \frac{\tau}{1 + \tau \frac{\mathrm{d} \ln m_p}{\mathrm{d}t}}, \tag{2.18}$$

where $\mathrm{d}(\ln m_p)/\mathrm{d}t$ is the particle mass growth rate, m_p is the mass and τ is the relaxation time in the absence of particle growth. With the expression for C_D, τ can be expressed as (Seinfeld, 1986; Mallina *et al.*, 1997)

$$\begin{aligned}
&\tau = \tau_{St} && \mathrm{Re}_p < 0.1 \\
&\tau = \tau_{St}/[1 + \frac{3}{16}\mathrm{Re}_p + \frac{9}{160}{\mathrm{Re}_p}^2 ln(2\mathrm{Re}_p)] && 0.1 < \mathrm{Re}_p < 2 \\
&\tau = \tau_{St}/[1 + 0.15{\mathrm{Re}_p}^{0.687}] && 2 < \mathrm{Re}_p < 500
\end{aligned}$$

with

$$\tau_{St} = \frac{2{r_p}^2 \rho_p C_c}{9\mu_g}, \tag{2.19}$$

τ_{St} is the relaxation time associated with the application of linear Stokes drag law. Under atmospheric conditions, $\tau_{St} < 3 \cdot 10^{-4}$ for particles of 10 μm in radius or smaller.

2.4 Mass and Heat Transfer between Particles and Gas

The basic equations for mass and heat transfer can be considered separately before forming combining equations.

Mass Transfer

The mass transfer rate between the particle and the air medium can be expressed by the mass increase or decrease rate on the particles (condensation or evaporation rate):

$$\dot{m} = 4\pi r_p^2 m_v (J_+ - J_-), \tag{2.20}$$

where J_+ is the flow rate of vapour molecules directed towards the particle and J_- is the outward flow rate from the particle surface; m_v is the mass of a single molecule of vapour. This equation has different solutions depending on the Knudsen number Kn as tabulated in Table 2.1. For Kn $\gg 1$, the incident molecular distribution follows the Maxwellian law. J_+ and J_- can be expressed as

$$J_+ = \frac{z_\infty \overline{v}}{4}, \qquad J_- = \frac{z_s \overline{v}}{4}, \qquad \overline{v} = \sqrt{\frac{8kT}{\pi m_v}}, \tag{2.21}$$

where z_s and z_∞ are molecule number densities close to the particle surface and in background gas, respectively. $\overline{v}$ is the mean speed of vapour molecules. As $\rho = m_v z$, so the free molecular condensation rate is

$$\dot{m}_{free} = \pi r_p^2 (\rho_\infty - \rho_s) \sqrt{\frac{8kT}{\pi m_v}}. \tag{2.22}$$

In the continuum region (Kn $\ll 1$), the net molecule flow rate $J = J_+ - J_-$ obeys Fick's law:

$$J = -D_v \frac{\mathrm{d}z}{\mathrm{d}r}, \tag{2.23}$$

where D_v is the molecular diffusivity of vapour in a fluid or media. With boundary conditions $z(r) = z_s$ at $r = r_p$ and $z = z_\infty$ at $r = \infty$, we obtain the solution

$$\dot{m}_{cont} = 4\pi D_v r_p (\rho_\infty - \rho_s), \tag{2.24}$$

For other intermediate Kn, the Boltzmann equation should be solved to obtain $\dot{m}$. The molecular velocity distribution is discontinuous in this region. By introducing the concept of the "jump distance", as discussed by Loyalka (1982) and Loyalka *et al.* (1989), the condensation rate Eq. (2.24) can be modified for this region as

$$\dot{m}_{jump} = 4\pi D_v r_p (\rho_\infty - \rho_s)(1 - \frac{\tilde{\zeta}}{r_p}), \tag{2.25}$$

where $\tilde{\zeta}$ is the "jump coefficient". It has length unit, and can also be called "jump distance".

For particles moving in an air flow, the moving flow around particles can cause an increase of mass transfer because of the 'forced' convection besides the 'free' diffusion convection. For particles in the continuum regime Eq. (2.24)

should be developed for the consideration of relative movement between particles and gas medium. It can then be written as

$$\dot{m} = 2\pi r_p D_v \mathrm{Sh}(\rho_\infty - \rho_s). \tag{2.26}$$

Sh is the Sherwood number given by (Bird $et\ al.$, 1960; Hughmark, 1967; Williams and Loyalka, 1991)

$$\mathrm{Sh} = 2.0 + 0.6\mathrm{Re}_p{}^{0.5}(\mathrm{Sc})^{\frac{1}{3}}. \tag{2.27}$$

Here $\mathrm{Sc} = \frac{\nu_g}{D_v}$ is the Schmidt number, $\nu_g = \mu_g/\rho_g$. It is clear that if there is no relative velocity between the particle and the gas medium (u_r=0), therefore $\mathrm{Re}_p = 0$ in Eq. (2.6), so Sh=2.0. Based on experimental data, a new modified expression for the particle Sherwood number was recently presented (Kulmala $et\ al.$, 1995):

$$\mathrm{Sh} = 2.009 + 0.514\mathrm{Re}_p{}^{1/2}\mathrm{Sc}^{1/3}. \tag{2.28}$$

Heat Transfer

Similar to the derivation of the mass transfer rate, the heat transfer rate by heat convection can be given as:

$$\dot{q}_{free} = 2\pi r_p^2 p_\infty \frac{T_\infty - T_s}{T_\infty}\sqrt{\frac{8kT_\infty}{\pi m_g}}, \tag{2.29}$$

$$\dot{q}_{cont} = 4\pi K_g r_p (T_\infty - T_s), \tag{2.30}$$

$$\dot{q}_{jump} = \dot{q}_{cont}(1 - \mathrm{Kn}\,\zeta_T), \tag{2.31}$$

where m_g is the mass of a single molecule of the background gas (air); p_∞ is the background pressure; T_s and T_∞ are the temperatures on particle surface and of the ambient gas, respectively; K_g is the thermal conductivity of the medium gas; ζ_T is the temperature jump distance (Loyalka, 1989).

Like the mass transfer rate of Eq. (2.26), the convection heat transferred between the air medium and the particles in the continuum regime moving in an air flow, satisfies the equation:

$$\dot{q} = 2\pi r_p K_g \mathrm{Nu}(T_\infty - T_s), \tag{2.32}$$

where Nu is the Nusselt number given by

$$\mathrm{Nu} = 2.0 + 0.6\mathrm{Re}_p^{0.5}\mathrm{Pr}^{\frac{1}{3}}, \tag{2.33}$$

$$\mathrm{Pr} = \frac{\nu_g}{K_g} = \mu_g \frac{C_g}{K_g}, \tag{2.34}$$

where Pr is the Prandtl number, C_g is the specific heat of the gas. For air at standard conditions, C_g=$1.004 \cdot 10^6\ cm^2 s^{-2} K^{-1}$.

The heat transfer rate $\dot{q}_m$ associated with the mass transfer rate of several participating constituents is given by the relation:

$$\dot{q}_m = \sum_i \frac{\mathrm{d}m_i}{\mathrm{d}t} L_{vi}, \tag{2.35}$$

where L_v is the latent heat of vaporisation of participating substances. The temperature for the particles is then determined by:

$$C_p m_p \cdot \frac{\mathrm{d}T}{\mathrm{d}t} = \dot{q}_c + \dot{q}_m, \tag{2.36}$$

where m_p is the mass of all components of the particles including those not affected by mass transfer; C_p is the specific heat of particle; and q_c is the convective heat transfer.

Chapter 3

AIR FLOW IN NOZZLES

The air flow in a Laval nozzle was once widely studied (Wegener, 1954; Courant and Friedrichs, 1963). As supersonic and transonic nozzles produce strong cooling which may cause homogeneous nucleation, a subsonic 'standard' nozzle (capillary nozzle) was employed here because the condensation on pre-existing particles is our main concern.

3.1 Mathematical Model

3.1.1 Governing Equations

The basic set of governing equations to solve air flows in nozzles comprises equations for conservation of mass, momentum, and energy. They are usually called the Navier Stokes equations. These equations are the continuity equation

$$\frac{\partial \rho}{\partial t} + \nabla \cdot (\rho \mathbf{U}) = 0, \tag{3.1}$$

the momentum equation

$$\frac{\partial \rho \mathbf{U}}{\partial t} + \nabla \cdot (\rho \mathbf{U} \otimes \mathbf{U}) = \mathbf{B} + \nabla \cdot \sigma_{\mathbf{s}}, \tag{3.2}$$

and the energy equation

$$\frac{\partial \rho H}{\partial t} + \nabla \cdot (\rho \mathbf{U} H) - \nabla \cdot (K_g \nabla T) = \frac{\partial p}{\partial t}, \tag{3.3}$$

where ρ is the fluid density, $\mathbf{U} = (u, v, w)$ the fluid velocity, p the pressure, T the temperature, $\mathbf{B}$ the body force, σ_s the stress tensor, and K_g the thermal conductivity of the fluid. H is the total enthalpy, given in terms of the static enthalpy h by

$$H = h + \frac{1}{2}\mathbf{U}^2. \tag{3.4}$$

In addition, the air flow is treated for a compressible ideal gas:

$$\rho = \frac{pM_g}{\mathrm{R}T}, \tag{3.5}$$

where M_g is the molecular weight, and R is the universal gas constant.

In fluid calculations, laminar flow can usually be regarded as one state of turbulent flows with small fluid Reynolds number. As the fluid Reynolds number in the main nozzle part is usually larger than 2000, the flow in the nozzle is treated as turbulent flow.

For turbulence quantities, a Reynolds-averaged model was used:

$$\overline{\Phi}(t) = \frac{1}{2\delta t}\int_{t-\delta t}^{t+\delta t} \Phi(\tau)\mathrm{d}\tau, \tag{3.6}$$

where δt is a time scale which is large relative to the time scale of turbulent fluctuations, and small relative to the time scale which we wish to resolve. We can split the fields into their mean and fluctuating parts

$$\Phi = \overline{\Phi} + \phi, \qquad \Psi = \overline{\Psi} + \psi. \tag{3.7}$$

It is obvious that Reynolds averaging quantities have the properties:

- $\overline{\Phi} = \overline{\Phi}, \qquad \overline{\phi} = 0$;
- $\overline{a\Phi + b\Psi} = a\overline{\Phi} + b\overline{\Psi}, \qquad$ a, b constant ;
- $\overline{\Phi\Psi} = \overline{\Phi}\,\overline{\Psi} + \overline{\phi\psi}$;
- $\frac{\overline{\partial\Phi}}{\partial t} = \frac{\partial\overline{\Phi}}{\partial t}, \qquad \frac{\overline{\partial\Phi}}{\partial x^i} = \frac{\partial\overline{\Phi}}{\partial x^i}$.

By applying the Reynolds averaging model in the governing equations such as the continuity equation, the momentum equation, transport equation, and energy equation, we obtain:

$$\frac{\partial\rho}{\partial t} + \nabla\cdot(\rho\mathbf{U}) = 0, \tag{3.8}$$

$$\frac{\partial \rho \mathbf{U}}{\partial t} + \nabla \cdot (\rho \mathbf{U} \otimes \mathbf{U}) = \mathbf{B} + \nabla \cdot (\sigma_{\mathbf{s}} - \rho \overline{\mathbf{u} \otimes \mathbf{u}}), \tag{3.9}$$

$$\frac{\partial \rho \Phi}{\partial t} + \nabla \cdot (\rho \mathbf{U} \Phi) = \nabla \cdot (\Gamma \nabla \Phi - \rho \overline{\mathbf{u} \phi}) + \Lambda, \tag{3.10}$$

$$\frac{\partial \rho H}{\partial t} + \nabla \cdot (\rho \mathbf{U} H + \rho \overline{\mathbf{u} h} - K_g \nabla T) = \frac{\partial p}{\partial t}, \tag{3.11}$$

where Γ is the turbulence diffusion coefficient, and Λ is a source or sink term representing creation and destruction of Φ. The mean total enthalpy can be expressed as:

$$H = h + \frac{1}{2}\mathbf{U}^2 + \kappa, \qquad \kappa = \frac{1}{2}\overline{\mathbf{u}^2}. \tag{3.12}$$

The above governing equations contain turbulent flux terms reflecting that convective transport due to turbulent velocity fluctuations exists besides the molecular diffusive fluxes. The turbulent flux terms are:

$$\rho \overline{\mathbf{u} \otimes \mathbf{u}} = \text{ Reynolds stress}, \tag{3.13}$$

$$\rho \overline{\mathbf{u} \phi} = \text{Reynolds flux} . \tag{3.14}$$

By using turbulence model to treat Reynolds stress and Reynolds flux, the above turbulence equations can be solved. In this computation, the low Reynolds number "$k - \varepsilon$ model" in which the Reynolds stresses are treated to be linearly related to the mean velocity gradients, and the turbulence dissipation rate ε is set to zero at walls, was used. The "$k - \varepsilon$ model" is suitable for calculating turbulent flow at low Reynolds number, especially for flow with the Reynolds number smaller than 30,000 (Launder and Sharma, 1974). The flow Reynolds numbers in the nozzle in our cases are in this range.

3.1.2 Boundary Conditions

The inlet and outlet boundaries were set to pressure constant conditions. At the inlet the pressure was set equal to the ambient air pressure, and the temperature was set to the measured temperature at the entry of the nozzle. Near-wall velocity was set to be a quadratic profile. This profile meets the low Reynolds number

turbulence "$k-\varepsilon$ model" which sets the turbulence dissipation rate ε to zero at the walls (Launder and Sharma, 1974). Heat conduction between the nozzle wall and the flow inside the nozzle was allowed. The nozzle wall temperature was set equal to the air ambient temperature.

Air flow in the nozzle was assumed to be steady, compressible and heat-conducting. The nozzle was divided into 20×150 grids in the modelling. The CFX-FLOW3D (AEA, 1997) algorithm was used for simulating the turbulent air flow in the nozzle. This calculation algorithm uses a structured mesh solver with many different models from AEA Technology. It contains a general purpose package which can be applied to simulate a wide range of fluid flows and heat transfer processes, including modelling laminar and turbulent flows, modelling stable and transient flows, and subsonic, transonic and supersonic flows. The programs are based on the finite volume method in which the equations are solved in their conservations for final solutions.

All calculations are madefor a certain nozzle (shown in Fig. 3.1). This nozzle was selected after several trials as it results in the conditions best for our purpose.

3.2 Saturation in the Nozzle

The particle number concentration was assumed to be low enough, so that lack of water for condensation and the effect of heat release on the flow can be neglected. This assumption is close to reality, as particle loaded air in an optical particle counter (OPC) is diluted before being measured if the particle concentration is very high (Willeke and Liu, 1976), in order to reduce the occurrence of cross-sensitivity and coincidence effects (Jaenicke, 1972). The same is true in continuous flow CNC.

For particle condensational growth, one of the most important factors is the vapour pressure, i.e. water vapour saturation (S). According to the mass balance equation, we have

$$\rho_{v_1} A_1 U_1 = \rho_{v_2} A_2 U_2, \tag{3.15}$$

$$\rho_{g_1} A_1 U_1 = \rho_{g_2} A_2 U_2, \tag{3.16}$$

where ρ_v is the density for water vapour and ρ_g for air. A is the cross-sectional area of the nozzle and U the velocity of flow. The subscripts '1' and '2' stand for initial and end states, respectively. Therefore,

$$\rho_{v_2} = \frac{\rho_{g_2}}{\rho_{g_1}} \rho_{v_1} . \tag{3.17}$$

It can be transformed, according to the ideal gas law, to

$$\rho_{v_2} = \frac{T_{g_1}}{p_{g_1}} \frac{p_{g_2}}{T_{g_2}} \rho_{v_1} , \tag{3.18}$$

where p_g and T_g are the pressure and temperature of air, respectively. The saturation S at any 3D location can be expressed as

$$S = \frac{\rho_v}{\rho_E(T_g)}, \tag{3.19}$$

where $\rho_E(T_g)$ is the saturated water vapour density at air temperature T_g. If the saturation at state '1' is S_1, then $\rho_{v_1} = \rho_E(T_{g_1})S_1$, so

$$S_2 = \frac{T_{g_1}}{p_{g_1}} \frac{p_{g_2}}{T_{g_2}} \frac{\rho_E(T_{g_1})}{\rho_E(T_{g_2})} S_1 = \frac{p_{g_2}}{p_{g_1}} \frac{E_1(T_{g_1})}{E_2(T_{g_2})} S_1 . \tag{3.20}$$

Fig. 4.14 shows an example for the saturation along the centreline of the nozzle. The relative humidity at the inlet was set to 70%. The increase of saturation to about 2.1 in the nozzle is clearly shown in the figure.

3.3 Flow in the Capillary

The nozzle configuration is shown in Fig. 3.1. The main nozzle capillary has an inner diameter of 1.0 mm. The inlet is assumed to be 12 mm in diameter, leading in a tapering nozzle with a length of 20 mm connected to the main nozzle capillary with a length of 120 mm. The origin of the x-coordinate is the modelling starting point. The whole nozzle is assumed to have a rotational symmetry.

By setting a sufficient high convergence criterion in the CFX-FLOW3D algorithm, flow fields in the nozzle with the configuration as in Fig. 3.1 can be modelled to a sufficient precision.

Fig. 3.2, 3.3, 3.4 and Fig. 3.5 show the modelling results of the changes of velocity, pressure, air density and temperature respectively along the nozzle centreline

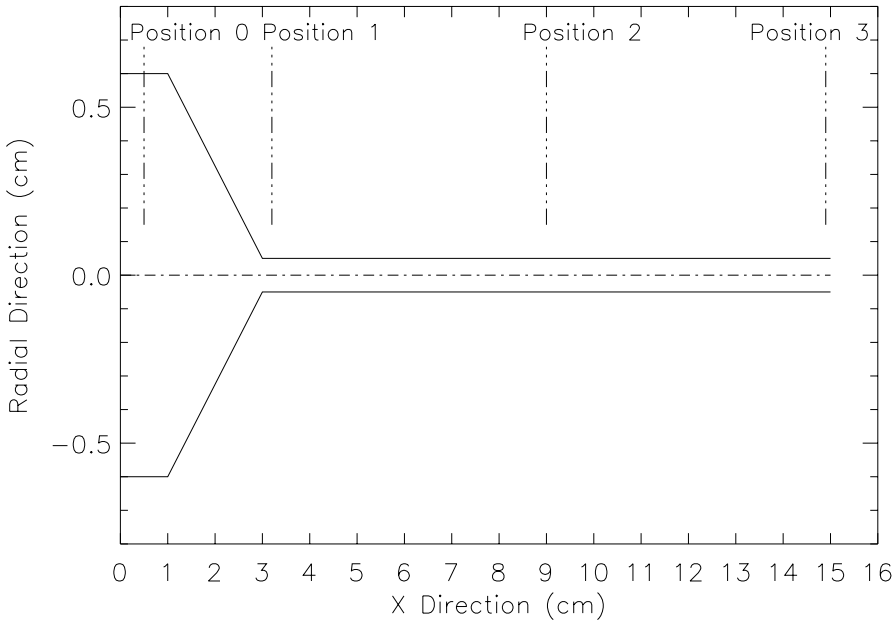

Figure 3.1: The shape of the capillary (the flow is from left to right). The capillary extends to 12 cm to the right. Positions '0', '1', '2' and '3' are marked here, which will be referred to later.

in three cases. The inlet condition is the same with a temperature of 301.35 K and a pressure of 1000 hPa. The outlet pressures are set to 925 hPa, 820 hPa and 700 hPa, respectively, which produce the flow rates of 42.0 l/h, 126.0 l/h and 228.2 l/h, through the nozzle. The flow Reynolds numbers in these three cases are 2618.6 for flow rate 42.0 l/h, 5685.2 for 126.0 l/h, and 8156.2 for 228.2 l/h, respectively. They can be regarded as turbulent flow as their Reynolds numbers are greater than 2000.

The expansion of the air flow in the nozzle is obvious to see by the density decrease as in Fig. 3.4. Because of the expansion, the flow gets accelerating velocity, which results in the temperature decrease as the inner energy of air molecules converts to the dynamical energy as expressed in Eq. (3.12). Larger flow velocity produces larger expansion and hence larger temperature decrease. The change of the saturation calculated by Eq. (3.20) along the centreline of the nozzle is shown in Fig. 3.6.

At the entrance of the nozzle (position 1), the flow is suddenly accelerated. It is similar to a discontinuous adiabatic pressure expansion, which is the principle

of pressure expansion CNCs, e.g. N-P counter. An “abrupt” pressure and temperature decrease, and therefore a sudden saturation increase can be seen here. But they turn smooth quickly.

The heat conduction between the nozzle wall and the air flow can result in a temperature profile that is shown in Fig. 3.7. Because of the treatment of the near-wall boundary condition for the velocity in the nozzle, the velocity has a cross-profile as shown in Fig. 3.8. The flow rate near the centreline carries a major fraction of air volume through the nozzle.

Table 3.1 is the modelling result for different lengths of the nozzle with the same inlet and outlet boundary conditions. From this table, we can see that the temperature drop is larger in the shorter nozzle than that in the longer nozzle.

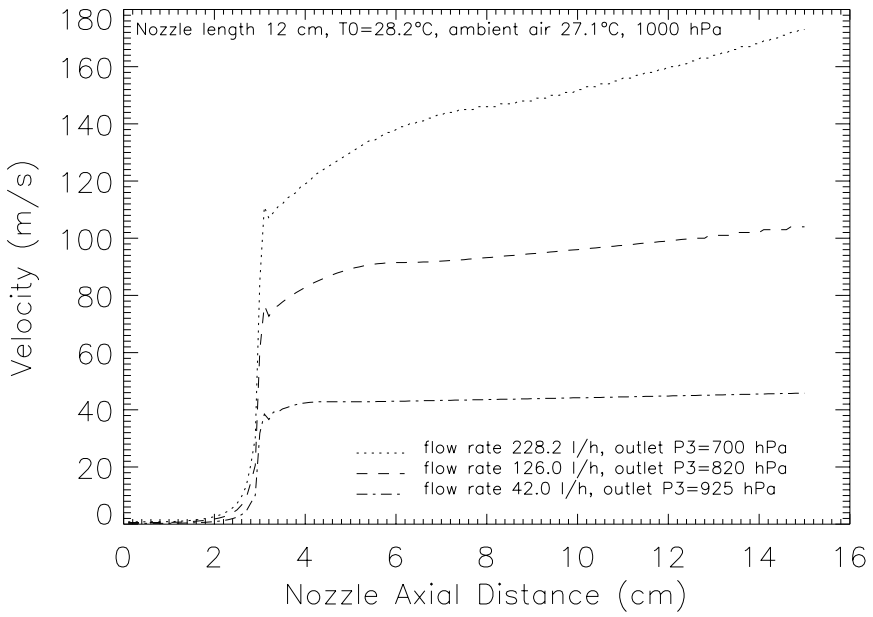

Figure 3.2: Velocity changes along the axis in the nozzle. The flow with velocities up to 80.0 m / s is weakly compressible.

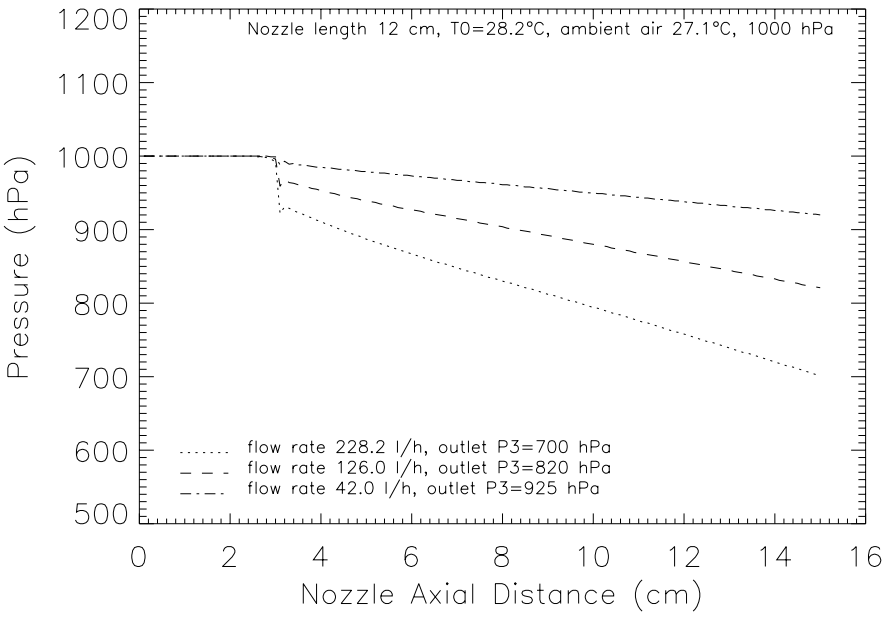

Figure 3.3: Pressure changes along the axis in the nozzle

3.4 Conclusions of Air Flow Modelling

After modelling flow fields in nozzles with various flow rates and different nozzle lengths, we conclude the followings:

① There is an adiabatic and isentropic cooling that can occur in the subsonic air flow in the nozzle.

② A larger flow rate will cause a larger expansion ratio and a larger temperature drop, and therefore a larger saturation can be created in the nozzle.

③ An expected saturation can be achieved by adjusting the flow rate through the nozzle.

④ For unchanged boundary conditions at both sides, there is a larger temperature drop in a short nozzle than that in a long nozzle.

⑤ Heat conduction between the nozzle wall and the inside air flow can increase the air temperature near the nozzle wall, but it has small influence on the flow near the centreline of the nozzle. The flow rate near the centreline carries a major fraction of air volume through the nozzle.

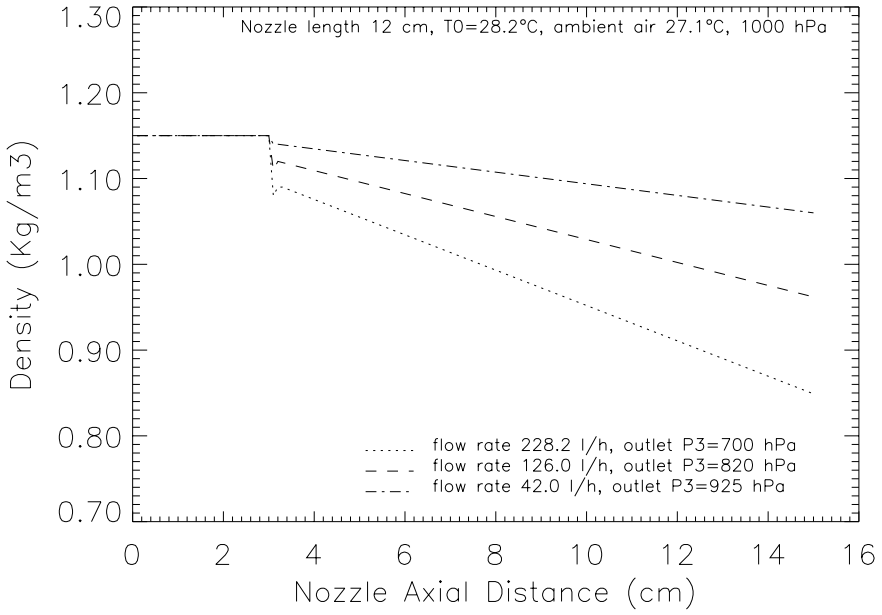

Figure 3.4: Density changes along the axis in the nozzle

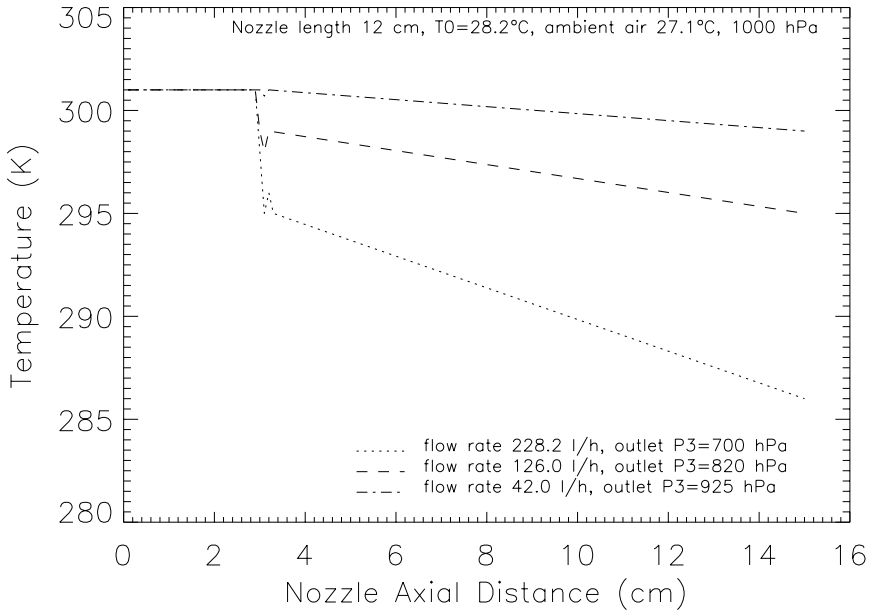

Figure 3.5: Temperature changes along the axis in the nozzle

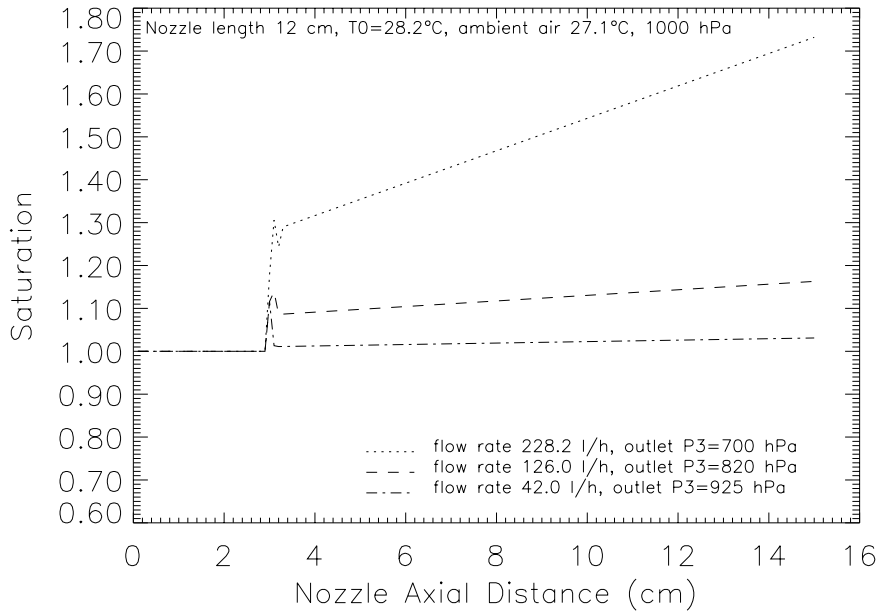

Figure 3.6: Saturation changes along the axis in the nozzle

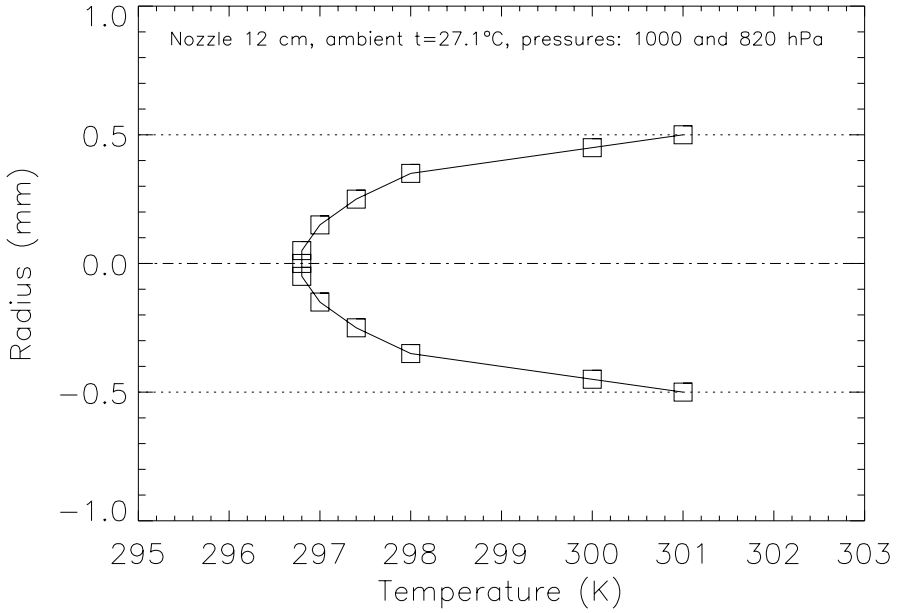

Figure 3.7: Temperature profile in the nozzle (nozzle length 12 cm plus 3 cm conical part, inner diameter 1.0 mm, wall temperature t=27.1^{o}C, pressure 1000 hPa and 820 hPa at both sides)

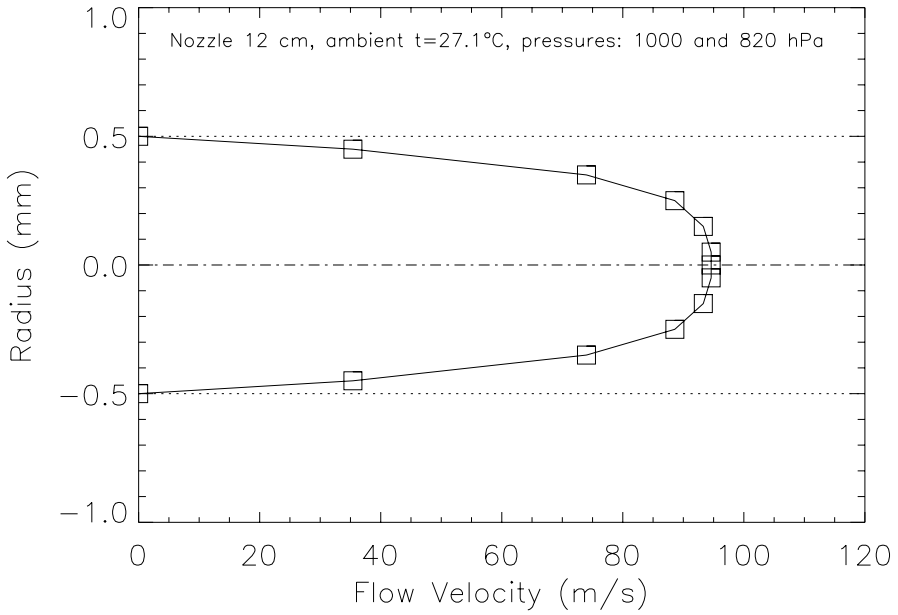

Figure 3.8: Velocity profile in the nozzle (nozzle length 12 cm plus 3 cm conical part, inner diameter 1.0 mm, wall temperature t=27.1^{o}C, pressure 1000 hPa and 820 hPa at both sides)

Table 3.1: The flow fields in nozzles with various length from modelling results
(nozzle shape as in Fig. 3.1 but with various lengths, no slip at wall, two pressure boundaries. Subscriptions '0', '1', '2' and '3' refer to the four positions as marked in Fig. 3.1)

No.	1	2	3	4	5
Nozzle length (cm)	1 cm	3 cm	6 cm	12 cm	20 cm
p_0 (hPa)	1000	1000	1000	1000	1000
p_1 (hPa)	800	837	871	922	958
p_2 (hPa)	736	765	781	812	835
p_3 (hPa)	700	700	700	700	700
T on the wall (K)	300	300	300	300	300
T_0 (K)	301	301	301	301	301
T_1 (K)	282	286	290	295	298
T_2 (K)	278	280	282	290	296
T_3 (K)	274	274	275	286	293
U_0 (m / s)	1.47	1.29	1.12	0.82	0.57
U_1 (m / s)	195	172	149	111	78
U_2 (m / s)	217	205	194	148	103
U_3 (m / s)	233	235	226	173	125
ρ_0 (Kg / m^3)	1.15	1.15	1.15	1.15	1.15
ρ_1 (Kg / m^3)	0.98	1.01	1.04	1.08	1.11
ρ_2 (Kg / m^3)	0.92	0.95	0.96	0.97	0.98
ρ_3 (Kg / m^3)	0.89	0.89	0.88	0.85	0.83
S_0	1.0	1.0	1.0	1.0	1.0
S_1	2.57	2.07	1.67	1.31	1.14
S_2	3.12	2.82	2.51	1.56	1.11
S_3	3.92	3.92	3.65	1.73	1.11
Flow rate (l / h)	428.3	379.3	329.1	243.6	170.9

Chapter 4

MODELLING THE PARTICLE CONDENSATIONAL GROWTH

4.1 Theory of Particle Growth and Evolution

Particle growth could have two reasons: condensation of water vapour on pre-existing particles or the nucleation of molecules forming clusters without the presence of pre-existing particles and additional growth of these clusters. The first is called the heterogeneous nucleation and the second one homogeneous nucleation.

The successful process of the homogeneous nucleation depends mainly on how many and how large molecular clusters are formed at the beginning (Pruppacher $et\ al.$, 1997). It has been found that the saturation is a very important factor for the formation of clusters. When the saturation is greater than 4.5 at 273 K or 3.5 at 293 K, enough molecular clusters can be formed, leading to the onsetting of homogeneous nucleation (Pruppacher $et\ al.$, 1997; Hinds, 1991). This homogeneous nucleation can occur easily in a supersonic nozzle with high Mach numbers (Wegener and Pouring, 1964; Fukuta $et\ al.$, 1976). In nozzles with low Mach numbers, the influence of the homogeneous nucleation was found unlikely to cause any significant effect on the particle growth (Mallina $et\ al.$, 1997).

In this study, we focus on the case of subsonic flow through nozzles. The saturation in the nozzle will not be greater than 3.5. Therefore, the homogeneous nucleation is neglected. The condensation of water vapour on pre-existing particles is our main interest in this work.

4.1.1 Single Particle Growth Equations

For the condensation of water vapour on pre-existing particles, the mass condensation rate of water vapour on the particles can be expressed as

$$\dot{m} = \frac{\mathrm{d}m_p}{\mathrm{d}t}. \tag{4.1}$$

If a particle is in heat balance, then according to Eq. (2.36), the heat release by condensation is equal to the heat convection at the same time:

$$\dot{q}_c = -\dot{q}_m = -L_v \frac{\mathrm{d}m_p}{\mathrm{d}t}. \tag{4.2}$$

In cloud physics, the growth rate of droplets by condensation of water vapour and the rate of the heat release, according to Mason (1962, 1971), can be expressed as

$$\dot{m} = 4\pi r_p D_v(\rho_{v,\infty} - \rho_{v,s}), \tag{4.3}$$

$$\dot{q}_c = 4\pi r_p K_g(T_s - T_\infty). \tag{4.4}$$

Here $\rho_{v,\infty}$ and $\rho_{v,s}$ are densities of water vapour at remote distance from the droplet-particle and at the droplet-particle surface, respectively. They are

$$\rho_{v,\infty} = \frac{e_{v,\infty} M_v}{\mathrm{R}T_\infty}, \tag{4.5}$$

$$\rho_{v,s} = \frac{e_{v,s} M_v}{\mathrm{R}T_s}, \tag{4.6}$$

where M_v is the water vapour molecular weight, R the universal gas constant, $e_{v,\infty}$ the vapour pressure in the air, and $e_{v,s}$ the vapour pressure on the particle surface. The Köhler effect, describing the increase of the equilibrium vapour pressure due to particle curvature (Kelvin effect) and decrease due to salt solution (Pruppacher $et\ al.$, 1997), should be considered for determining the vapour pressure on the particle surface (see chapter 2).

Mason's equations are used quite extensively, and ways to solve this set of equations analytically and numerically are numerous (Wagner, 1982; Barrett and Clement, 1988; Kulmala, 1988; Kulmala $at\ al.$, 1989). By comparing Eqs. (4.3) and (4.4) to Eqs. (2.24) and (2.30) we see that Mason's equations are the only case of

condensational growth of particles in a continuum regime. As being pointed out previously, under standard atmospheric conditions, as shown in Table 2.1, only particles with r_p >0.65 μm are in the continuum regime. So Mason's equations should be corrected for particles smaller than this size in non-continuum regime.

Furthermore Mason's equations were derived from static conditions for a particle without relative motion to the surrounding gas. Under static condition, the mass exchange rate is fully dominated by "free" diffusive exchange processes. If the surrounding gas is moving with respect to the particle, the exchange rate is increased because of the "forced" convection due to the relative velocity between gas and particle. The mass and heat diffusive transfer rates are then usually corrected semiempirically by using the Sherwood (Sh) as the Eq. (2.27) and (2.28) and Nusselt number (Nu) (Renksizbulut, 1983; Huang $et\ al.$, 1990; Chiang $et\ al.$, 1992) as the Eq. (2.33).

By considering two corrections, we can get the extended condensational growth equations

$$\dot{m} = 2\pi r_p D_v \mathrm{Sh}(\rho_{v,\infty} - \rho_{v,s}) f_c(\mathrm{Kn}_c), \tag{4.7}$$

and

$$\dot{q} = 2\pi r_p K_g \mathrm{Nu}(T_s - T_\infty) f_h(\mathrm{Kn}_h). \tag{4.8}$$

$f_c(Kn_c)$ and $f_h(Kn_h)$ in Eqs. (4.7) and (4.8) account for the Knudsen effects, that is the correction for the non-continuum effect. Similar non-continuum corrections were used by various authors (Kulmala, $et\ al.$, 1991; Mallina, $et\ al.$, 1997). Barrett and Clement (1988) once gave a good correction for the growth of cloud droplets. It was however derived from small supersaturation and therefore is suitable for cloud droplet only. It is unsuitable for solving this problem as the supersaturation in the nozzle may be much larger than that in clouds. Here the Loyalka equation (Loyalka, 1983; Loyalka $et\ al.$, 1988) was adopted as this formula gives very good results (Loyalka $et\ al.$, 1988). It can be written as:

$$f_c(\mathrm{Kn}_c) = [1 + \mathrm{Kn}_c(\frac{1.333\Psi_c + 1.0161}{1.333\mathrm{Kn}_c + 1})]^{-1}, \tag{4.9}$$

$$f_h(\mathrm{Kn}_h) = [1 + \mathrm{Kn}_h(\frac{1.9234\Psi_h + 1.3026}{1.9234\mathrm{Kn}_h + 1})]^{-1}, \tag{4.10}$$

where

$$\mathrm{Kn}_c = \frac{2D(\frac{M_v}{2kT_\infty})^{1/2}}{r_p}, \mathrm{Kn}_h = \frac{\frac{4}{5}\frac{K_g T_\infty}{p_\infty}(\frac{M_g}{2kT_\infty})^{1/2}}{r_p}, \tag{4.11}$$

$$\Psi_c = \pi^{1/2}\mathrm{Kn}_c, \Psi_h = \frac{5}{4}\pi^{1/2}\mathrm{Kn}_h. \tag{4.12}$$

k is the Boltzmann constant and M_g is the carrier gas molecular mass (in our case for dry air). For practical reasons, i.e. for considering an arbitrary accommodation, the expressions for $f_c(\mathrm{Kn}_c)$ and $f_h(\mathrm{Kn}_h)$ should be replaced by (Loyalka $et\ al.$, 1988)

$$f_c(\mathrm{Kn}_c)' = \frac{f_c(\mathrm{Kn}_c)}{1 + \frac{1-A_w}{A_w}\Psi_c f_c(\mathrm{Kn}_c)}, \tag{4.13}$$

$$f_h(\mathrm{Kn}_h)' = \frac{f_h(\mathrm{Kn}_h)}{1 + \frac{1-A_t}{A_t}\Psi_h f_h(\mathrm{Kn}_h)}. \tag{4.14}$$

Here A_w is the condensation coefficient and A_t is the thermal accommodation coefficient. With these sets of equations, equations (4.7) and (4.8) can be solved numerically.

4.1.2 Evolution of the Particle Size Distribution

The aerosol growth equation can be expressed as (Brock, 1983),

$$\frac{\partial n(v,t)}{\partial t} + \frac{\partial}{\partial v}(I_v(v,t)n(v,t)) = \Lambda_p(v,t), \tag{4.15}$$

where $n(v,t)$ is the aerosol size distribution function. It is defined so that $n(v,t)dv$ is the number of particle per unit volume, with particle volumes in the range $(v, v+dv)$ at time t. $I_v(\mathrm{d}v/\mathrm{d}t)$ is the condensational growth rate of a particle volume. $\Lambda_p(v,t)$ is a 'source' rate accounting for nucleation, emission and other particle sources as well as sinks.

In this study, we can neglect the particle source term. If we define $I_r = \mathrm{d}r_p/\mathrm{d}t$ as the radius condensational growth rate of a single-particle ($I_v = 4\pi r_p^2 I_r$), then Eq. (4.15) can be written as

$$\frac{\partial n(r_p,t)}{\partial t} + \frac{\partial}{\partial r_p}(I_r(r_p,t)n(r_p,t)) = 0 \tag{4.16}$$

because of the approximation:

$$I_r = \frac{I_m}{4\pi r_p^2 \rho_p}. \tag{4.17}$$

With Eq. (4.7), we can simulate the evolution of the particle size distribution with time. So the size distribution evolution can be obtained along the x-axis or the centre line of the nozzle.

4.2 Initial Equilibrium Assumption

The source of Aitken particles is mainly gas-to-particle conversion and they consist often of water soluble salts, e.g. sulphate or nitrate such as $(NH_4)_2SO_4$ and NH_4NO_3 (Whitby, 1978). The existence of such compositions strongly favours the condensation of water vapour on particles as they greatly reduce the equilibrium vapour pressure on the particle surface (Pruppacher $et\ al.$, 1997). In order to avoid the case that particles grow or evaporate at the beginning before entering the nozzle, they were treated as initially in equilibrium with the ambient air. A particle contains a certain amount of soluble salts, with which the water vapour pressure on the particle surface equilibrates to ambient vapour pressure, so that no condensational growth takes place before the particle enters the nozzle.

Fig. 4.1 shows the soluble salt fraction in particles of various sizes at RH=90%, 70% and 50% calculated under this initial equilibrium assumption. At RH=70%, particles with size r_p $\leq$0.01 μm contain over 60% of soluble mass. This value changes to about 40% for particles with sizes of about 0.1 μm and about 30% for particles larger than 1.0 μm. This result agrees well with recent measurements (Svenningsson $et\ al.$, 1992; Svenningsson $et\ al.$, 1994; Eichel $et\ al.$, 1996) in the atmosphere.

4.3 Model Comparison

To see how large the difference between employing Mason's model equations (4.3), (4.4), and the corrected equations (4.7), (4.8) used in this paper (EUP) is, the two models were numerically compared. Fig. 4.2 and 4.3 show the mass and radius condensation rates calculated from the two models. For particles with sizes $r_p \geq 1.0$ μm, the two models give similar results. For smaller particles however, the two models show a large deviation. The Mason equation largely overestimates the growth rate. The saturation S was found to have no evident effect on this deviation.

The relative velocity between particle and fluid is found to have a noticeable effect on the growth rate, as shown in Fig. 4.5. The growth rate may be 10% higher for particles with radii larger than 1.0 μm at a relative velocity of 50 m/s than for particles without relative motion with respect to ambient air. This effect becomes

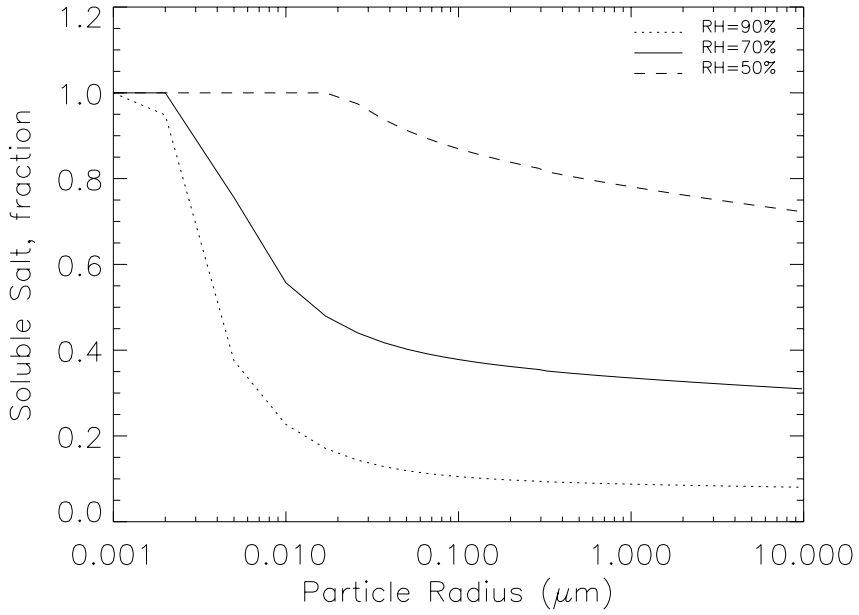

Figure 4.1: Soluble salt fraction in particles in equilibrium with ambient RH=90%, 70%, and 50%

more important for particles with sizes larger than 0.1 μm when the relative velocity reaches up to 200 m/s. As shown in Fig. 4.15, relative velocities larger than 50 m/s exist at the nozzle inlet. So this effect should be taken into account for particles with radius larger than 0.1 μm in this simulation. Fig. 4.4 demonstrates the radius condensational rates at various saturation values.

4.4 Time Required for Particle Growth to Detectable Size

Fig. 4.6, 4.7, 4.8, 4.9, and 4.10 are the results that show the time required for the particle growth to a detectable size of 0.15 μm or 0.30 μm for a laser optical device at various saturations. It is obvious that it takes less time for a particle to grow to a detectable size in high saturations.

As discussed in the above section, the relative velocity has a positive influence on the condensational growth rate. So it can be estimated that it needs a shorter time for particle to grow to the detectable size in a nozzle flow than under a static

condition.

4.5 Solving Methods for Single Particle Growth in Nozzle Flow

If $u_p = 0$, by numerically solving the equations (4.1), (4.2), (4.5), (4.6), (4.7), and (4.8) with Newton roots method, T_s and r_p can be evaluated, and then again using equation (4.7), we can get condensational growth rates for particles with different sizes r_p. Usually the particle velocity depends not only on the flow fields but also on the particle mass. The residence time of particles in the nozzle will be extended by the increase of mass from vapour condensation.

The motion equation (2.16) is obviously a function of r_p and u_p. As r_p is related to T_s, this equation can be expressed as a function of three variables

$$\frac{\mathrm{d}u_p}{\mathrm{d}t} = f_1(r_p, T_s, u_p). \tag{4.18}$$

As

$$\frac{\mathrm{d}m_p}{\mathrm{d}t} = 4\pi {r_p}^2 \rho_p \frac{\mathrm{d}r_p}{\mathrm{d}t}, \tag{4.19}$$

the particle growth equation (4.7) can be expressed as function of r_p, T_s, and u_p too:

$$\frac{\mathrm{d}r_p}{\mathrm{d}t} = f_2(r_p, T_s, u_p). \tag{4.20}$$

In this modelling, it is convenient to express the above differential equation with the x coordinate instead of time t:

$$\frac{\mathrm{d}r_p}{\mathrm{d}t} = \frac{\mathrm{d}r_p}{\mathrm{d}x}\frac{\mathrm{d}x}{\mathrm{d}t} = \frac{\mathrm{d}r_p}{\mathrm{d}x}u_p, \tag{4.21}$$

$$\frac{\mathrm{d}u_p}{\mathrm{d}t} = \frac{\mathrm{d}u_p}{\mathrm{d}x}\frac{\mathrm{d}x}{\mathrm{d}t} = \frac{\mathrm{d}u_p}{\mathrm{d}x}u_p. \tag{4.22}$$

So the growth and movement equations have the form of functions F_1 and F_2:

$$\frac{\mathrm{d}u_p}{\mathrm{d}x} = F_1(r_p, T_s, u_p), \tag{4.23}$$

$$\frac{\mathrm{d}r_p}{\mathrm{d}x} = F_2(r_p, T_s, u_p). \tag{4.24}$$

The flow fields can be obtained by using the CFX-FLOW3D algorithm as described in chapter 3. The effect of condensation on the change of the flow fields can be ignored under the assumption that the particle concentration is very low. The above set of equations can be solved using the forth-order Runge-Kutta integration. In the calculation, equations (4.23) and (4.24) are integrated from the x direction origin (see Fig. 3.1) to the nozzle exit, $i.e.$ the viewing volume of the optical detection device.

4.6 An Example: Particle Growth in the Nozzle of OPC

Optical particle counters (OPC) were developed by Gucker $et\ al.$ (1947a, 1947b), and the detectors have been set to both forward and 90^o viewing (Gucker and Rose, 1954). The detection size of an OPC is limited by the Rayleigh scattering of air molecules, the instrument noise, and the stray light resulting from imperfect optics. For a carefully designed laboratory instrument, the detection size can be as low as 0.15 μm in diameter. For commercial counters, it is usually about 0.3 μm to 0.5 μm in diameter, e.g. the laser particle counter model TSI 3753 (0.3 μm to 3.0 μm) and TSI 3755 (0.5 μm to 5.0 μm). The sensing volume in OPC is built very small in order to reduce the probability of the occurrence of coincidence that is caused by the presence of more than one particle in the sensing volume at the same time (Jaenicke, 1972). The application of a laser beam excellently meets these requirements as the laser offers an inherently well defined parallel beam focused to a very tiny spot. That cannot be achieved with the white light illumination used previously. Umhauer (1983) described an OPC for $in\ situ$ measurements with the sensing volume 100×100×100 μm^3. It was recently reduced to 36×52×35 μm^3 for the measurement of high concentrations up to 10^7 particles per millilitre (Sachweh $et\ al.$, 1998).

Such a small sensing volume demands high aerodynamic focusing of the aerosol beam, which is usually obtained by a nozzle or orifice with inner size about 0.5 mm in diameter. In order to keep the thin stream passing diametrically through the laser beam avoiding partially illuminated particles, the nozzle capillary is usually surrounded by sheath air (Husar, 1974; Allen, 1986). By producing

an accelerating flow at the nozzle outlet, the aerosol flow can be well confined just before being measured. The geometry of a nozzle injector in an OPC (Allen, 1986) is shown in Fig. 4.11. Fig. 4.12 shows the setting of two laser beams and aerosol stream in Aerodynamic Particle Sizer spectrometer (TSI) in which the aerodynamic size of particles are determined according to their 'residence time' in the accelerating stream between two parallel laser beams.

The use of the focusing nozzle can, however, induce a new problem. That is the condensational growth of particles in the nozzle, which will hinder the measurement results from revealing the "real" particle size distribution. Here the rapid condensational growth of aerosol particles in the expanding air stream of the nozzle will be investigated and the influence on measurement results will be estimated.

4.6.1 Single Particle Growth in the Nozzle

The nozzle shape in OPC is similar as in Fig. 3.1. However the main nozzle capillary has the size of 0.5 mm inner diameter and the length of 20 mm. The boundary conditions for pressure at the inlet and outlet were set to 1000 hPa and 700 hPa, respectively. The air temperature and relative humidity (RH) at inlet were assumed to be 288 K and 70 %, respectively. Under these conditions, the flow rate through the nozzle was calculated to be 28.5 ml/s. This is a typical flow rate for many optical particle counters. Fig. 4.13 shows the modelling results of temperature, pressure, and air density along the centre line of the nozzle. The saturation calculated by Eq. (3.20) in the nozzle is shown in Fig. 4.14 with the ambient relative humidity of 70%. Obvious saturation increase to about 3 times of that in the initial ambient air, can be seen in this figure. Fig. 4.15 is the simulation result of flow velocity for air, and for particles with initial radius of 0.1 μm and 1.0 μm. It shows that particles have a lag in response to flow, and the larger a particle, the longer is its 'residence' time in nozzle.

The particle growth was modelled under the assumption that the initial equilibrium condition is RH=70%. Fig. 4.16 shows the growth of various sized particles along the axis of the nozzle. Particles with initial radii smaller than 0.1 μm grow very rapidly in the very short time in which they pass through the nozzle. For a particle with a size of 1.0 μm, the radius growth ratio is about 1.01, but it increases to about 1.11 for the particle with an initial radius of 0.1 μm and 1.23 for

the particle with initial radius of 0.05 μm. The small particles have larger radius condensational growth rates than larger ones.

For a particle with a size of r_m=0.15 μm (r_m is the minimum detectable radius size), which is the typical minimum detectable size of many commercial optical particle sizing instruments such as the laser particle counter TSI model 3753, the condensational growth ratio is found to be 1.07. This means an increase of 7$\%$ in particle size compared to its original size at the end side of the nozzle. If the sensing point is located very close to the nozzle outlet, than the measured size can be 7% larger than the original size. This phenomenon could be termed as 'over-sizing' effect. Besides that, particles with initial radii smaller than r_m can be counted. Particles in the size range between about 7% smaller than r_m to r_m can also grow up to detected. This results in an 'over-counting' of the real particle number in the detectable size range. The 'over-counting' can be higher if the minimum detectable size (r_m) is smaller than 0.15 μm. For an optical sizing instrument with the minimum detectable size r_m=0.0665 μm (diameter 0.133 μm) (Allen, 1986), the 'over-sizing' degree can be as high as 17%.

4.6.2 Over-counting Particles and the Shift of the Particle Size Distribution

As particles in each size bin grow simultaneously, the whole size distribution will therefore evolve and shift to larger sizes at the same time. Based on tropospheric aerosol size distributions given by Jaenicke (1988, 1993) as shown in table 1.1, the evolution of particle size distribution at the end of the nozzle can be modelled by using equation (4.16) for various types of aerosols. Fig. 4.17 shows the particle size distributions at the inlet and outlet of the nozzle for remote continental, polar and urban aerosols. The shifts of the distributions for particles smaller than 1.0 μm in radius are evident, and the smaller the particle, the greater is the shift from the original size distribution. The whole particle size spectrum therefore becomes narrower after the condensational growth.

Table 4.1 and 4.2 list the number of particles larger than the minimum measurement sizes r_m=0.15 μm and r_m=0.075 μm at the inlet and outlet of the nozzle, and the over-counted particle number as well as the over-counting percentage. For particles with remote continental, rural and urban size distributions, the 'over' counted percentages are very high, ranging from 27.4% to 44.5%. For other

Table 4.1: The over-counted effects for various types of aerosol size distributions (the minimum detectable radius r_m is 0.15 μm)

Aerosol type (Jaenicke, 1993)	N (r$\geq r_m$) inlet cm^{-3}	N (r$\geq r_m$) outlet cm^{-3}	N (over-counted) cm^{-3}	Over-counted portion %
polar	2.07	2.57	0.50	24.12
background	69.79	74.49	4.70	6.73
maritime	30.72	34.95	4.23	13.78
remote conti.	89.74	124.36	34.62	38.58
desert dust	139.06	149.03	9.97	7.17
rural	53.01	67.73	14.72	27.76
urban	416.95	531.29	114.34	27.42

types of aerosol size distributions, the ‘over’ counted portion can be over 5.8%. The condensational growth of particles in the nozzle results in ‘over-sizing’ and ‘over-counting’ results in detectable size classes.

The asymmetric property of non-spherical particles and their surface chemistry could also be “distorted” since nozzle aerosol instruments are employed for measuring the shape and chemistry of particles (Allen, 1986). For example, a nozzle “laser ionization mass spectrometer” was recently reported in the measurements of aerosol chemical compositions (Murphy and Thomson, 1995, 1997). Furthermore, it should be also taken into account, how much the density of the particles is changed by accumulating so much water.

4.7 Conclusions of Particle Growth Modelling

The theory of particle growth is described in this chapter. The Mason’s diffusion growth equation was corrected and extended to the application for particles below the continuum region. The influence of the particle acceleration on the condensation process was considered. By the modelling of particle growth in the nozzle and in the inlet of particle sizing instruments, important conclusions can be drawn:

- Mason’s diffusion growth equation should be corrected for particles beyond

Table 4.2: The over-counted effects for various types of aerosol size distributions (the minimum detectable radius r_m is 0.075 μm)

Aerosol type (Jaenicke, 1993)	N (r$\geq r_m$) inlet cm^{-3}	N (r$\geq r_m$) outlet cm^{-3}	N (over-counted) cm^{-3}	Over-counted portion %
polar	9.89	12.37	2.49	25.14
background	108.92	115.26	6.34	5.82
maritime	65.25	69.85	4.60	7.06
remote conti.	902.96	1256.61	353.64	39.16
desert dust	250.25	282.42	32.17	12.85
rural	381.88	540.52	158.64	41.54
urban	2959.22	4277.94	1318.71	44.56

the continuum region. The influence of the particle acceleration in the nozzle air flow on the condensation process should be considered.

- Particles grow faster in an accelerating state than in a stationary state because of the forced convection from the relative movement between the particles and gases.

- Small size particles grow much quicker than large size particles. The whole particle size distribution evolve itself in the nozzle and will become narrower. After a long enough time, all sizes of particles larger than r_k can grow up to a detectable size.

- In the inlet nozzle of OPCs, the condensational growth of particles results in the measured particle sizes larger than their original sizes, which could be termed as “over-sizing” influence. Because particle number concentration is larger in fine size region, more particles therefore will be counted, which could be termed as “over-numbering” influence. The “over-numbering” is especially high (higher than 27.4%) for particles with remote continental, rural and urban mode size distributions. For other types of aerosol size distributions, this effect can be over 5.8% too. The measured whole particle size distributions shift to larger radii because of the particle condensational growths. The analysis results from data obtained by direct measurements with these nozzle aerosol instruments will reveal no actual shape of particle size distribution in the natural atmosphere. The ‘real’ shape should be the

one obtained by “extracting” the condensational “over-sizing” and “over-numbering” influences.

- The asymmetric property for non-spherical particles, the surface chemistry as well as the density of particles could be modified too if nozzle aerosol instruments are used for measuring the particle shapes, aerodynamic sizes, and surface chemistry.

- Concerns should be given in evaluating measurement results as well as in aerosol instrument design. For aerosol instruments other than CNCs, the nozzle length should be as short as possible in order to lessen the effect of condensational growth of particles, and to increase the accuracy of the measurements.

Nozzle technology is widely used today in aerosol applications because its ability to meet the requirement of producing a highly focused and accelerating flow. For example, ‘time-of-flight’ instruments are those that involve measuring the acceleration of aerosol particles in response to the accelerating flow in nozzles. The aerodynamic size of a particle determines its rate of acceleration, with larger particles accelerating more slowly due to increased inertias. During the acceleration, their flight time is sensed and recorded by two parallel laser beams and, by using a calibration curve, converted to an aerodynamic diameter. Recently a new type of ’time-of-flight’ instrument named Aerodynamic Particle Sizer spectrometer (Model APS 3320, 1999, TSI) has been introduced into commercial use for particle size measurement. A nozzle Laser Ionization Mass Spectrometer with ‘time-of-flight’ method to provide a complete mass spectrum from each particle was reported for measurements of particle chemical compositions (Murphy and Thomson, 1995, 1997). While the advantage of the nozzle has been explored, the accompanying ‘side-effect’, that is the condensational growth of aerosol particles caused by the expansion of accelerating air flow in the nozzle, has not attracted much attention. It is fatal if one fully ignores this effect for exact measurement evaluations.

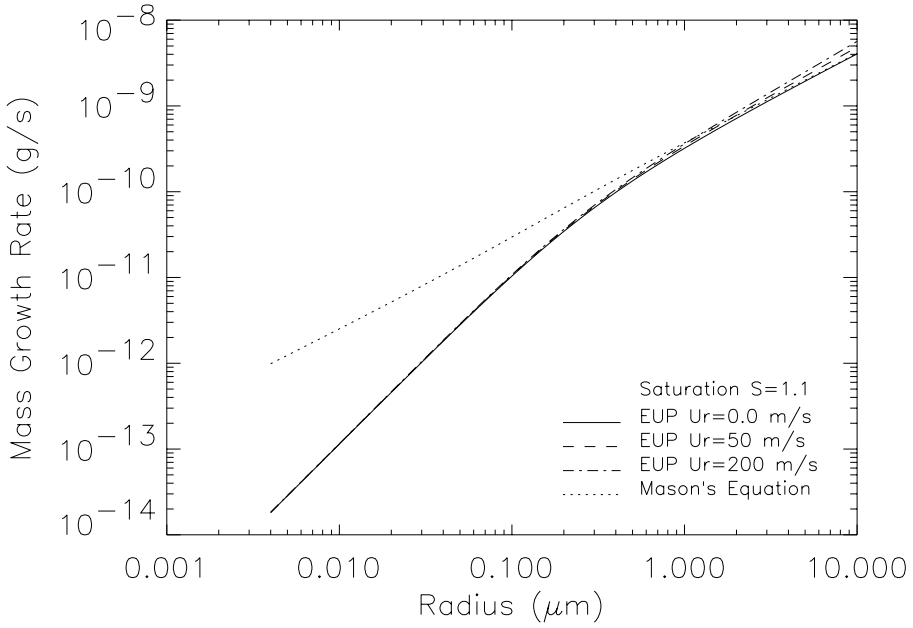

(a)

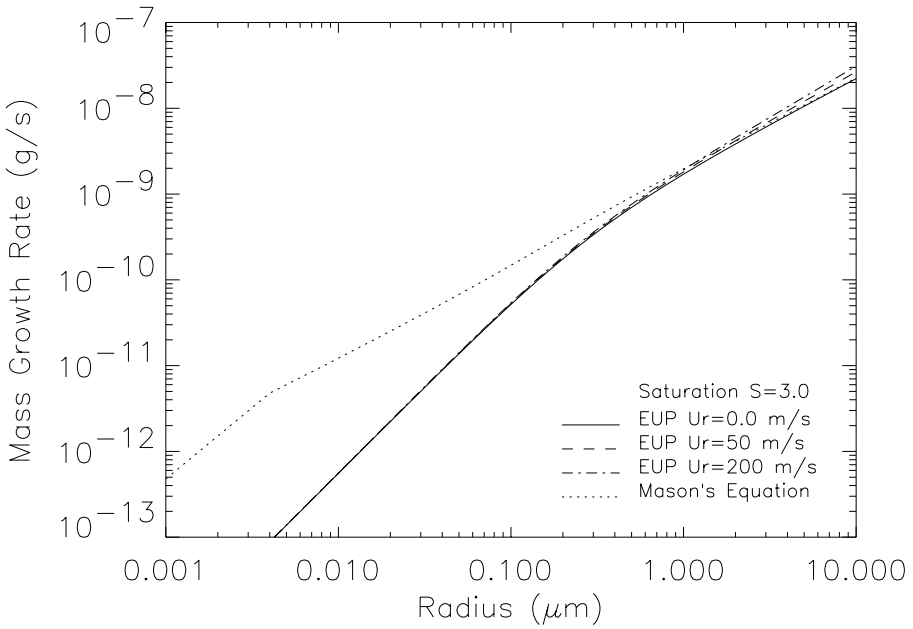

(b)

Figure 4.2: Mass condensational growth rates for Mason's equation, and the equation used in this paper (EUP) with particle to fluid relative velocities U_r=0 m / s, U_r=50 m / s, and U_r=200 m / s (S=1.1 and S=3.0)

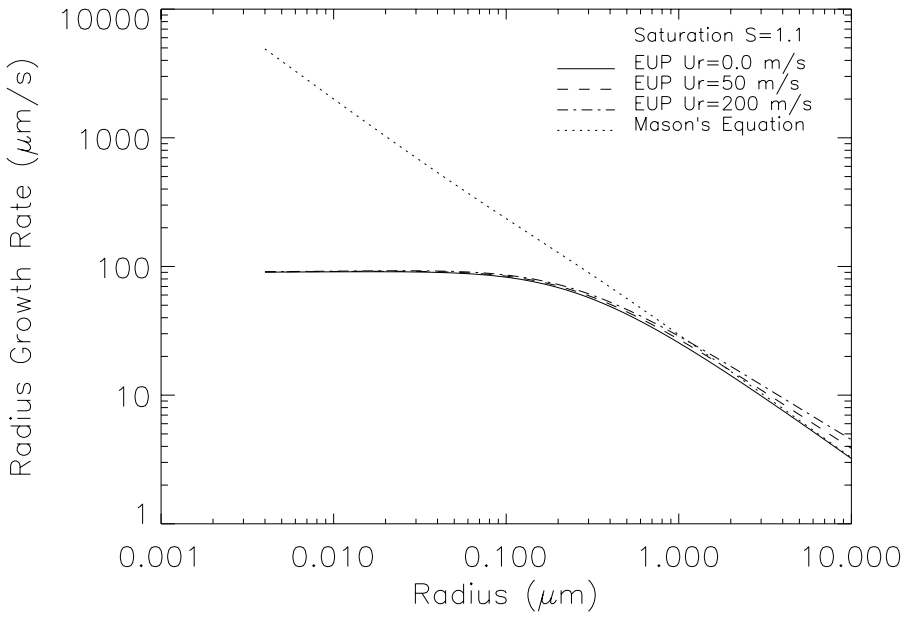

(a)

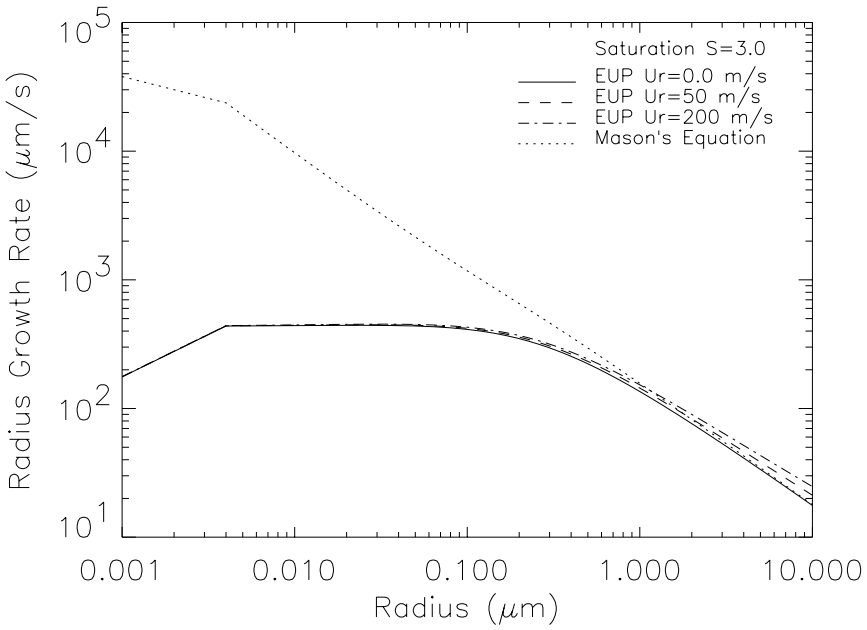

(b)

Figure 4.3: Radius condensational growth rates for Mason's equation, and the equation used in this paper (EUP) with particle to fluid relative velocities U_r=0 m / s, U_r=50 m / s, and U_r=200 m / s (S=1.1 and S=3.0)

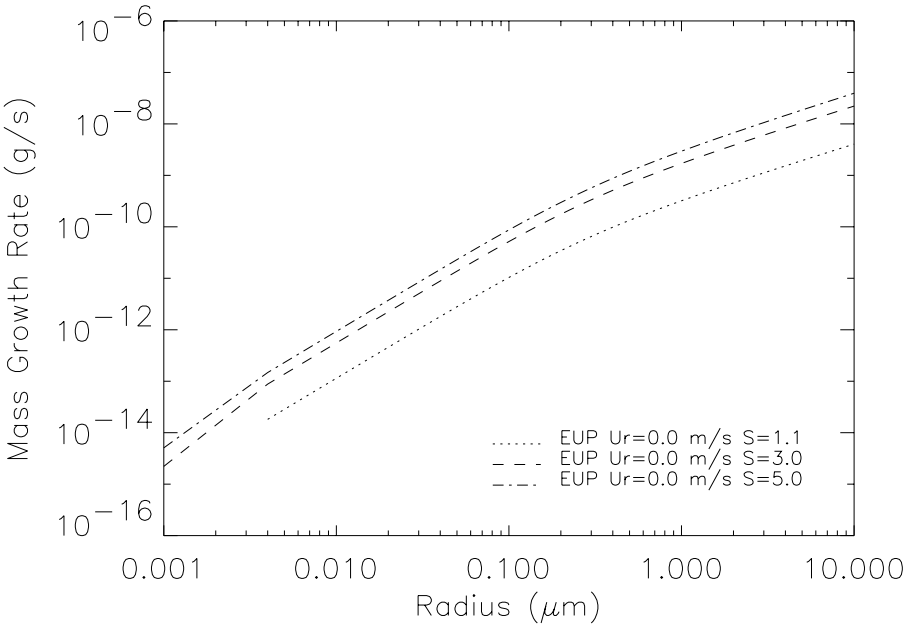

(a)

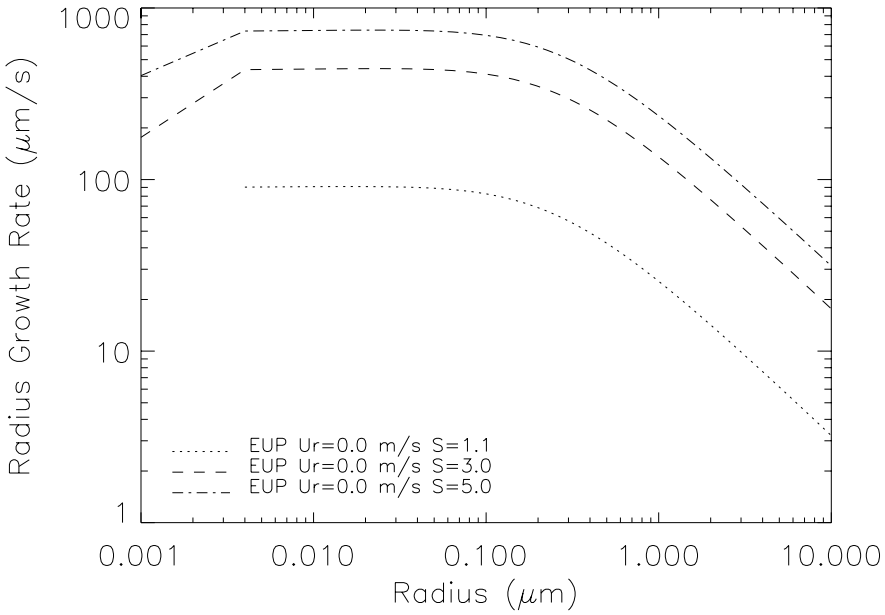

(b)

Figure 4.4: Mass (a) and radius (b) condensational growth rates for the equation used in this paper (EUP) with particle to fluid relative velocities U_r=0 m/s (S=1.1, S=3.0 and S=5.0)

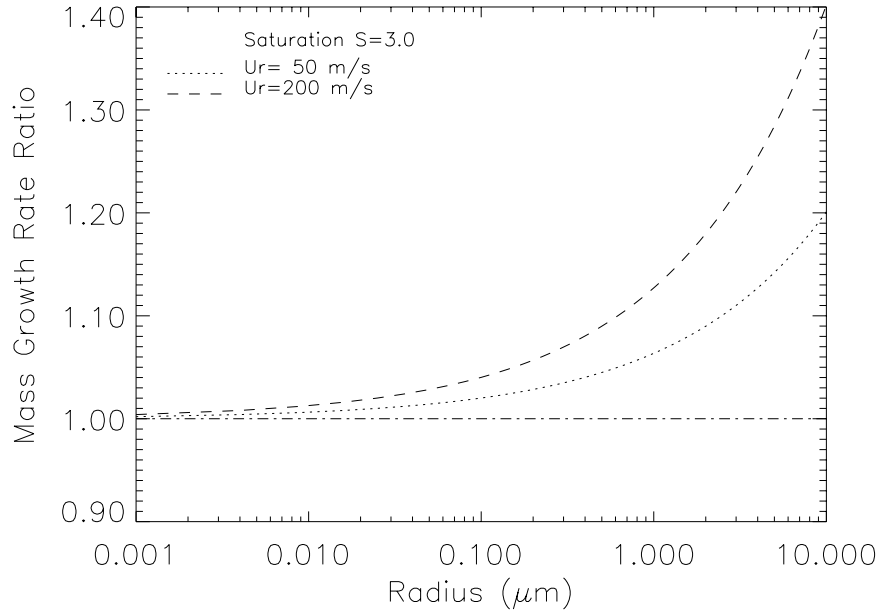

(a)

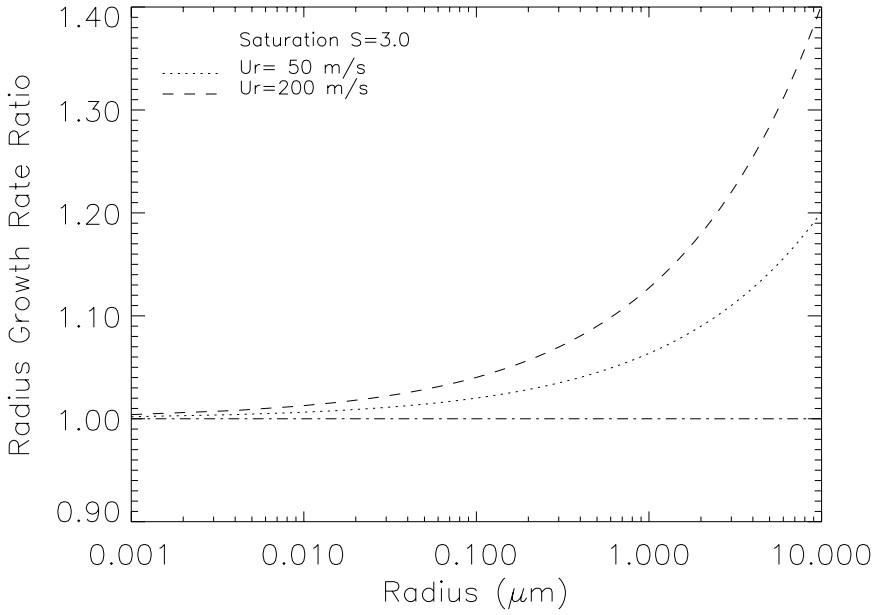

(b)

Figure 4.5: Mass (a) and radius (b) condensational growth ratios for the equation used in this paper (EUP) with particle to fluid relative velocities U_r=50 m/s and U_r=200 m/s vs U_r=0 (S=3.0 only)

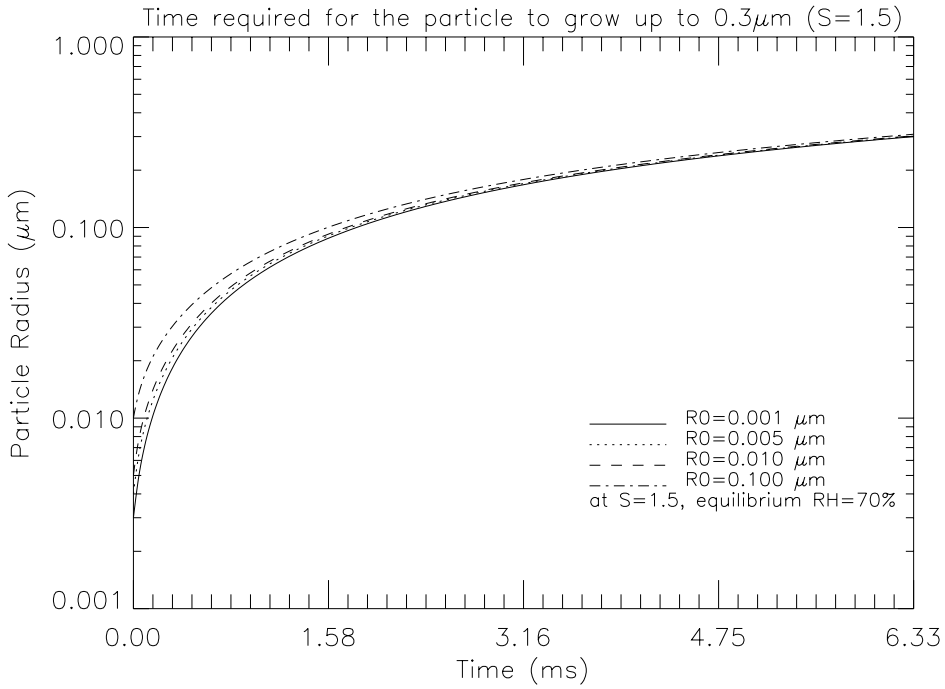

Figure 4.6: Time required for particle growth to detectable size of 0.3 μm at S=1.5

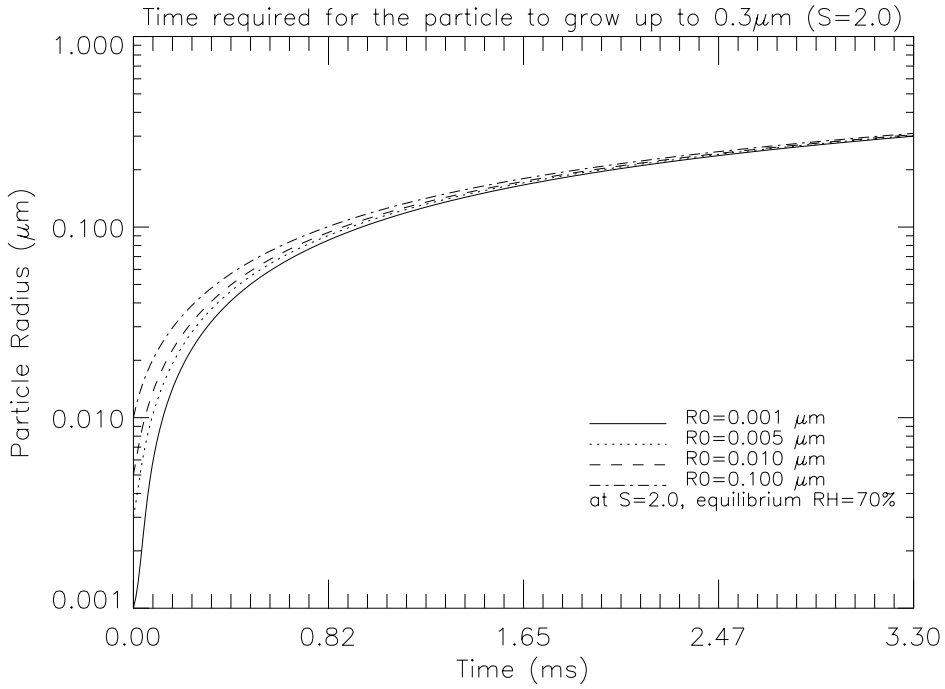

Figure 4.7: Time required for particle growth to detectable size of 0.3 μm at S=2.0

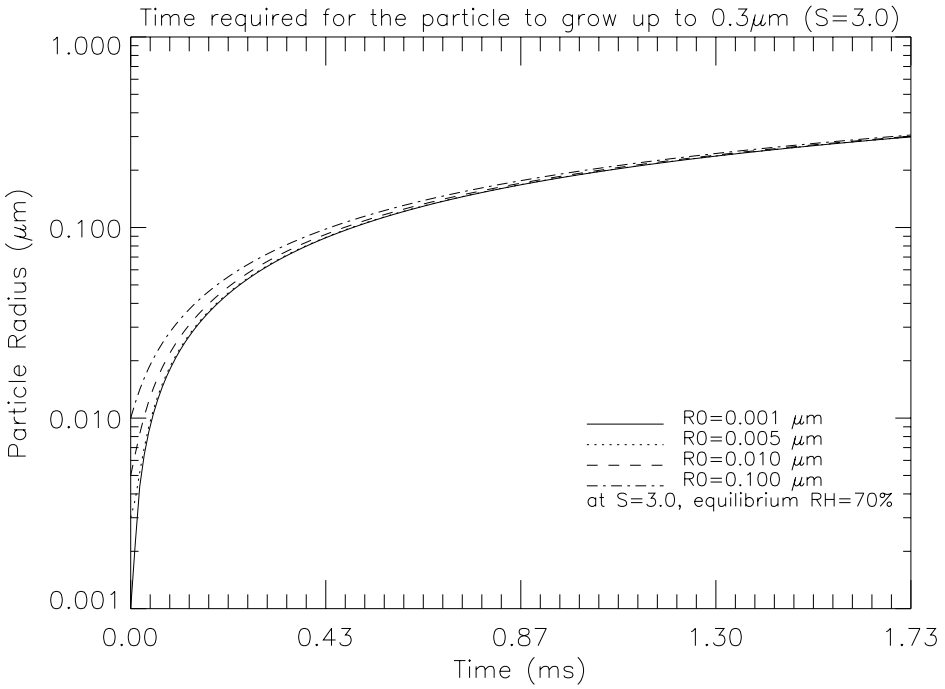

Figure 4.8: Time required for particle growth to detectable size of 0.3 μm at S=3.0

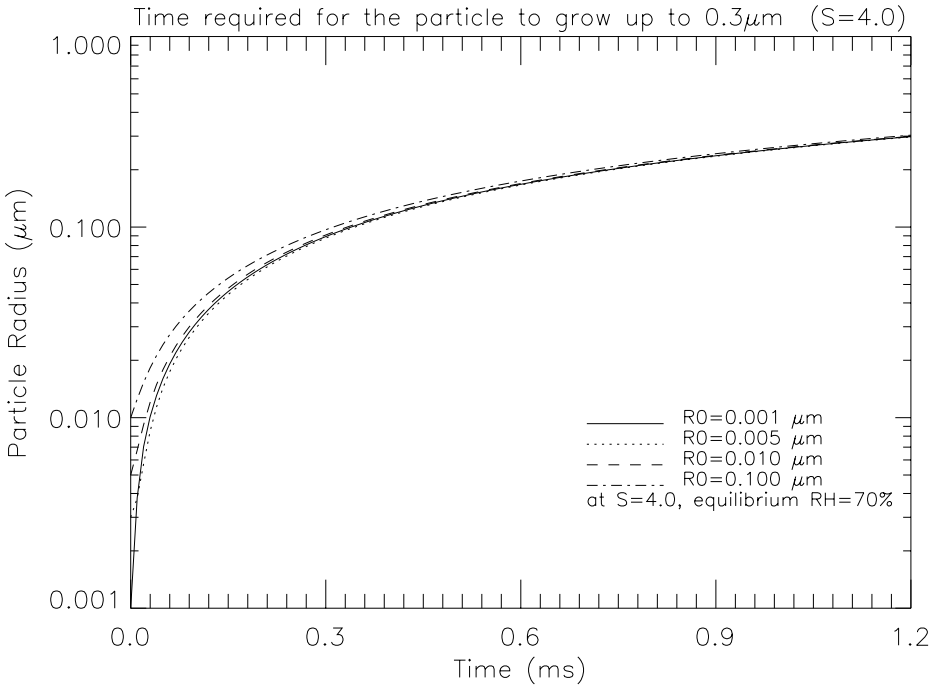

Figure 4.9: Time required for particle growth to detectable size of 0.3 μm at S=4.0

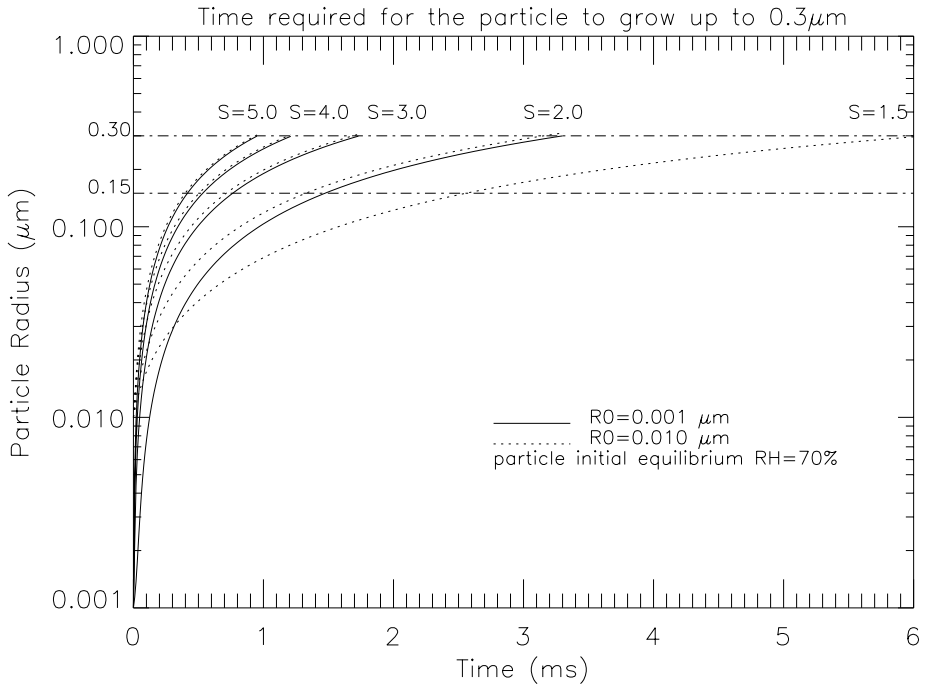

Figure 4.10: Time required for particle growth to detectable sizes of 0.15 μm and 0.3 μm

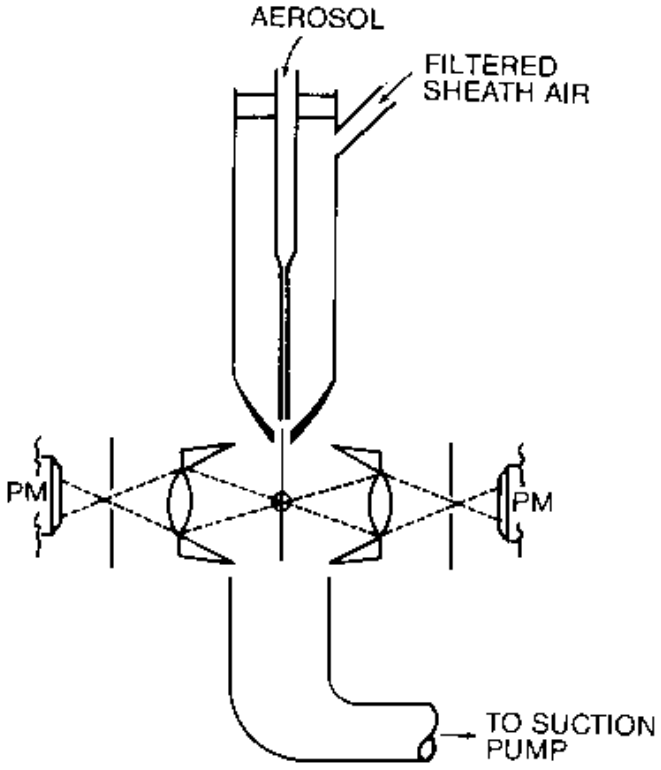

Figure 4.11: Schematic representation of the nozzle injector in an OPC (Allen, 1986)

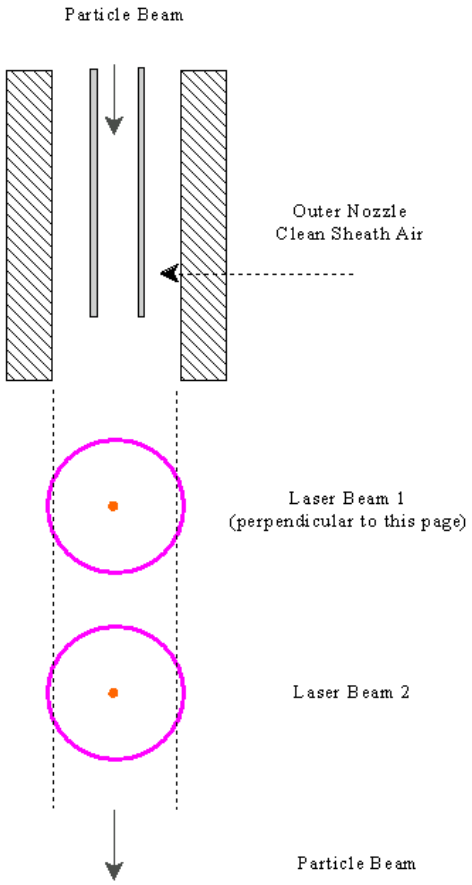

Figure 4.12: Schematic setting of the laser beams and the aerosol stream in APS

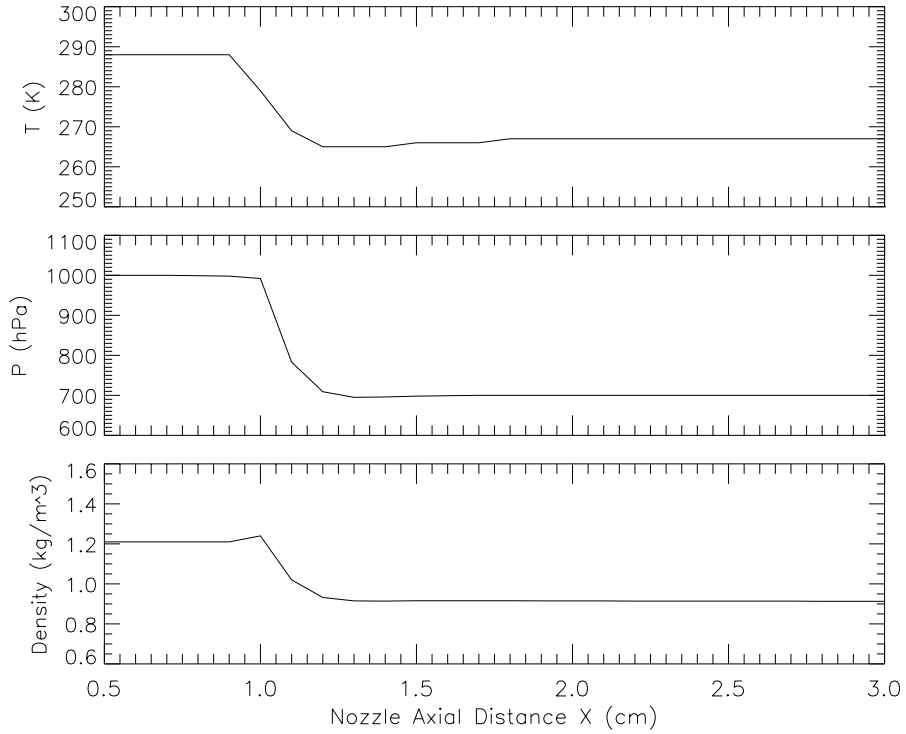

Figure 4.13: Pressure, temperature, and air density along the centre line of the nozzle

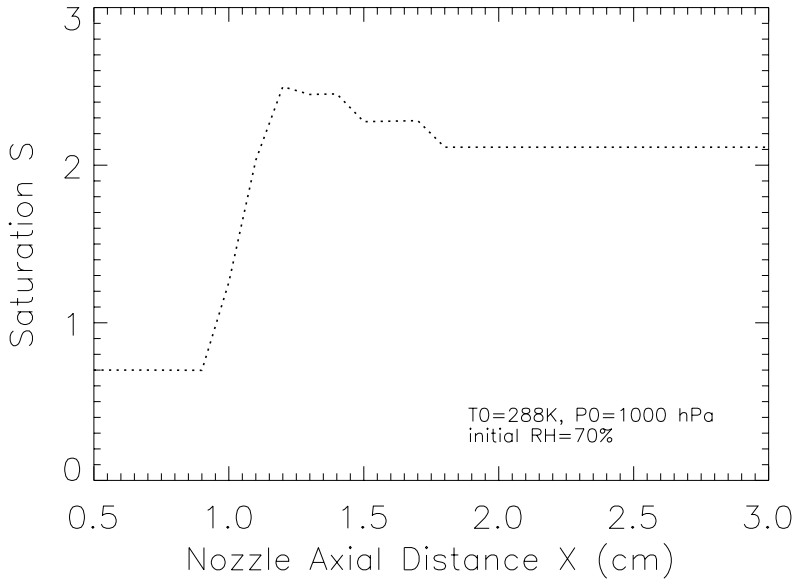

Figure 4.14: Saturation along the centre line of nozzle (the flow rate is 28.5 ml/s, inlet relative humidity is 70%)

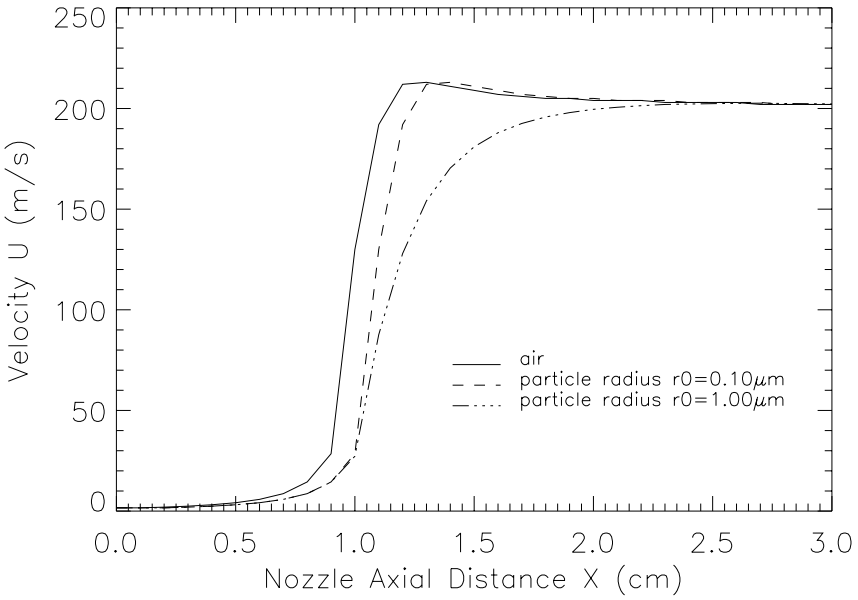

Figure 4.15: Air and particle velocities in the nozzle

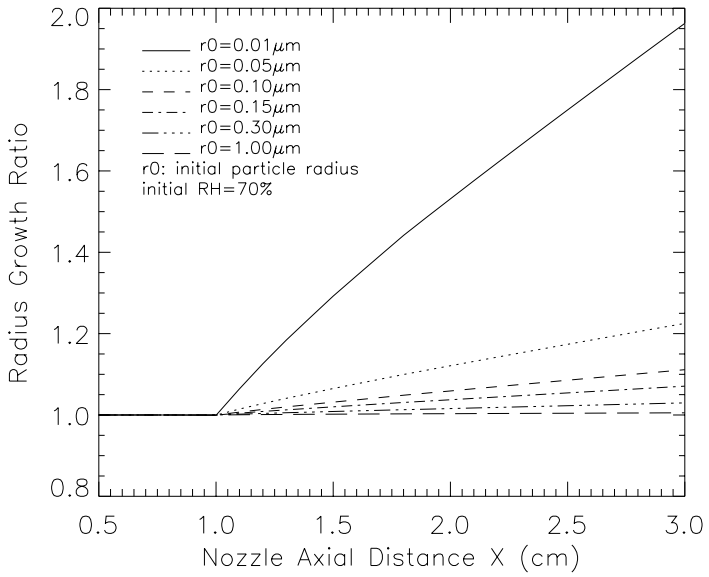

Figure 4.16: Particle radius condensation growth ratio vs horizontal distance along the nozzle

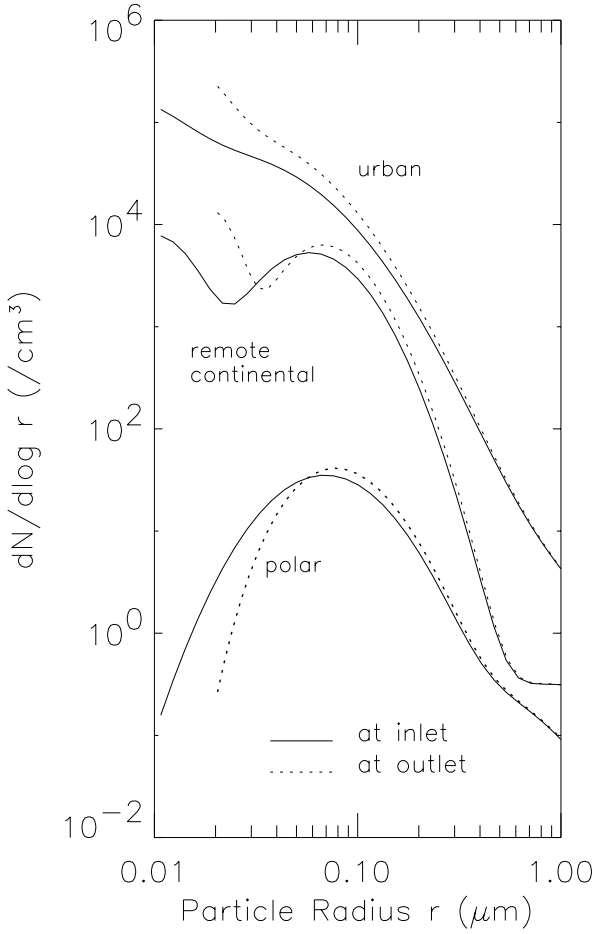

Figure 4.17: The shift of particle size distributions

Chapter 5

EXPERIMENTS WITH NOZZLE-CNC

As shown by flow modelling in Chapter 3, air flow in a nozzle can undergo an adiabatic and isentropic cooling due to its continuous expansion. If air at the nozzle inlet is already saturated with water vapour, then a supersaturation can be achieved. As having been discussed, the cooling degree depends largely on the flow rate through the nozzle — the larger the flow rate, the larger the temperature drop as shown in Fig 3.5. An expected supersaturation can therefore be obtained by just controlling the flow rate (see Fig. 3.6). This method to obtain supersaturation of water vapour has advantages over other methods in that the air flow is cooled isentropically and simultaneously. Besides, the condensation substance is water instead of an organic matters , such as alcohol, used in some commercial condensation nucleus counters (e.g. CNC-TSI Model 3020). Hence the actual number of the atmospheric condensation nuclei can be activated.

By selecting a proper nozzle length, by adjusting the flow rate, and by measuring the number concentration of particles at the end of the nozzle, a nozzle CNC (Nozzle-CNC) for counting atmospheric condensation nuclei can then be constructed. The set-up of this new Nozzle-CNC is shown in Figure 5.1.

5.1 Experiment Description

Figure 5.1 is the schematic diagram of the new CNC with the nozzle technology to create air expansion in this work. Aerosol firstly passes through a regulator [3] by which its flow rate will be controlled and measured. This sample aerosol flow is mixed and diluted with clean air. The clean air comes from the filtration of ambient air by a filter. In order to get 100% water saturated air, the ambient air is warmed and humidified in a water pool with fixed temperatures from 30 ^{o}C to 50 ^{o}C. This pool is large enough so that the air has ample time to become saturated. The aerosol and the clean saturated air mix with each other at the entry of the nozzle. There the temperature and pressure can be measured and the saturation can be calculated.

The condensation nozzle has an internal diameter of 1.0 mm with various lengths from 10 cm to 30 cm depending on the flow rate. The adiabatic expansion causes the initiation of the condensation of water vapour on aerosol particles that are larger than the critical size r_k. These grown particles are counted by electro-optical methods. A laser particle detecting system for detecting particles larger than 0.35 μm in radius is used as the detector. An electrical signal processor and a counting recorder are connected to this laser detecting device for recording the output signals in this experiment. Pressure, temperature and flow rate are also measured at the end of the nozzle.

The aerosol flow rate was measured by a 'soap bubble spirometer' or 'bubble generator flowmeter' (Gilian Gilibrator) in which soap bubble acts as a piston and is displaced with distance proportional to the volume of the aerosol flow. It can precisely measure flow rates in 1 cm^3/min. The temperature at the inlet was measured by thermo-resistance. The optical detecting system processes the mode of single particle counting, by which the optical system produces one signal when a particle passes through the sensing volume. So the number of signals per second reflects the number of particles in the volume of aerosol sample through the nozzle per second. When more than one particle passes through the sensing volume at the same time, the coincidence effect should be considered (Jaenicke, 1972).

Experiment data were formally recorded after at least 30 mins running of the

[3] In aerosol measurements, such regulators should be avoided, because the aerosol might be modified. However, for these first measurements, no great error is introduced.

instruments. It ensures that the saturated air can thermodynamically reach a stable condition before it enters the nozzle. Also the flow field in the nozzle can reach the state of heat balance, that is the balance of heat conduction between the nozzle wall and the flow inside, so that the flow field, especially the saturation in the nozzle keeps stable. The counting value was recorded every 5 minutes by the optical system. Averaged values as well as the standard deviation can then be obtained.

5.2 Experiment Results

Experiments were carried out in room environment. The filtered air was checked and only a very small number of particles (less than 0.1 $/cm^3$) was found. So the produced clean air is satisfactory. As the value of the saturation in the nozzle depends on the flow rate through the nozzle, the total flow rate was fixed in one experiment. The mixing ratio, that is the fraction of the aerosol flow in the total flow rate, was changed. In experiments, procedures were repeated several times by gradually adjusting the mixing ratio of the aerosol flow from a small one (from 0%) to a large one (up to 100%), and then from 100% again to 0%. The results were averaged.

Figures 5.2 is the experiment result, showing the changes of the particle concentration counted by the optical system with the mixing ratio of aerosol in the total flow rate. Calibration against system errors of the instrument including the effect of flow rate (Zhang and Liu, 1990 and 1991; Dreiling, 1994) and other factors such as system noise of optical signals are not considered here.

In order to see the possible influences of the temperature in the water pool, experiments were carried out at pool temperature from 30 ^{o}C to 60 ^{o}C with results shown in Fig. 5.3. No evident effects were found. In fact the increase of the temperature of the water pool can increase the vaporisation of water and therefore shorten the saturation time for air in the pool. It has however no substantial influence on the condensation process in the nozzle. The result in Fig. 5.3 shows that.

With a water pool temperature of 40 ^{o}C, three total flow rates 29.1 l/h, 42.0 l/h, and 126.0 l/h were taken in experiments No.7, No.8, and No.9. Their complete results are listed in Table 5.1, 5.2, and 5.3. The relative humidities (RH) in ambient

air for these three cases were 68%, 93%, and 85%, respectively. The saturations at the nozzle entry were calculated according to the mixing ratio:

$$S_0 = \frac{F_a S_a + F_c S_c}{F_a + F_c}, \tag{5.1}$$

where F_a and F_c are flow rates for aerosol and clean saturated air, respectively; S_a and S_c are their saturations by water vapour. It should be noticed here that the saturation S_a is the value for the temperature at the nozzle entry which was measured by a temperature sensor, rather than for the temperature of the ambient room air. So the ambient RH should be converted. According to the saturation value of the mixing flow at the nozzle entry, its value in the nozzle can be obtained according to Eq. (3.20).

Figure 5.4 and 5.10 as well as 6.11 show the changes of the counting values with the fraction of aerosol flows for these three experiments. Figure 5.5 and 5.11 as well as 6.12 are the corresponding variations of the converted particle concentrations with the fraction of aerosol. From Eq. (5.1) we know, that the change of the aerosol fraction in the total flow rate causes the change of the saturation at the nozzle entry, and finally the change of the saturation in the nozzle. So the number of particles that can be activated response to the saturation changes too. Figures 5.6, 5.12, and 6.13 are results of measured particle concentrations at various saturations in the nozzle. The results are in agreement with the expectation that a larger saturation triggers more particles to activate as particle critical size becomes smaller. The measured number concentration increases unproportionally with the saturation.

5.3 Experiment Analysis

5.3.1 Exponential Relation Between Condensation Nucleus Concentration and S

The measured number concentration (N) of condensation nuclei and saturation (S) in the nozzle are plotted on the double-logarithm coordinate axis, as shown in figures 5.8, 5.9, 5.14, 6.9, 6.16 and 6.17. In this double-logarithm coordinate system, N increases linearly with S. That means there exists an exponential relationship between S and the measured number concentration of condensation

Table 5.1: Results of experiment No. 7 *

F_a (cm^3/s)	Aerosol Fraction (%)	Counting Value (/s)	Concentration measured (N/cm^3)	r_k (Rural) (μm)	r_k (Urban) (μm)	Saturation at entry S_0 (%)	Average S_1 (%)
0.123	1.52	4.36±0.98	35.45±7.97	0.11611	0.13721	99.31	100.30
0.289	3.58	7.96±2.10	27.54±7.27	0.12627	0.14893	98.26	99.24
0.633	7.83	18.38±3.32	29.03±5.24	0.12393	0.14658	96.46	97.42
0.958	11.85	29.45±3.97	30.74±4.14	0.12158	0.14346	94.64	95.59
1.786	22.09	38.95±6.46	21.81±3.62	0.13565	0.15908	90.01	90.91
2.527	31.26	56.60±8.33	22.40±3.30	0.13487	0.15830	85.87	86.73
3.885	48.06	39.23±7.44	10.09±1.92	0.17158	0.19893	78.28	79.06
5.513	68.20	15.84±5.62	2.87±1.02	0.25362	0.27861	69.17	69.86
8.083	100.0	9.82±2.34	1.21±0.29	0.35000	0.35000	54.80	55.35

* Total flow rate at inlet is 29.1 l/h, water pool t=40^{o}C. Ambient air t=26.0^{o}C, RH=68%. Temperature at inlet t_0=29.8 ^{0}C, P_0=1000 hPa. At the outlet of the optical device P=828 hPa, flow rate at outlet=80 l/h. At 21:40 h, Sept. 15, 1999.

nuclei (N). This exponential relationship has the form:

$$N = CS^{\alpha}, \tag{5.2}$$

where α and C are constants. By comparing the fitted lines in Fig. 5.8, 5.14, and 6.16, we find that the value α depends strongly on the total flow rate through the nozzle. It has the value 5.52 at the flow rate of 29.1 l/h, 16.30 at the flow rate of 42.0 l/h, and 19.82 at the flow rate of 126.0 l/h, respectively, as tabulated in Table 5.4. The larger the flow rate, the larger the value α. The reason is that a larger flow rate produces a larger saturation and causes a quicker mass and heat transfer between particles and gases, so particles can grow more quickly.

A similar relationship was once found between supersaturation (S_s) and number concentration for cloud condensation nuclei (CCN) by Twomey (Twomey, 1959):

$$N = CS_s{}^{\alpha} \tag{5.3}$$

In this equation, S_s is expressed as a percentage. For various atmospheric backgrounds, α has different values. It was suggested that α =0.333 and C=310 for CCN in maritime air and α =0.4 and C=600 in continental air (Twomey 1959). They were later suggested to be α =0.5 and C=200 (Hegg and Hobbs, 1992) and α =0.5 and C=600 for these two backgrounds (Twomey and Wojcienchowski,

Table 5.2: Results of experiment No. 8 **

F_a (cm^3/s)	Aerosol Frac. (%)	Counting Value (/s)	Concentration measured (N/cm^3)	r_k (Rural) (μm)	r_k (Urban) (μm)	S_0 (%)	Average S_1 (%)	Counting Region
0.104	0.89	10.86± 3.61	104.42± 34.71	0.04424	0.06065	99.77	102.26	CCN
0.298	2.55	22.06± 6.26	74.03± 21.01	0.05518	0.07158	99.33	101.81	CCN
0.315	2.70	18.12± 3.83	57.52± 12.16	0.06299	0.07939	99.30	101.78	CCN
0.895	7.67	39.09± 4.93	43.67± 5.51	0.07158	0.08799	98.00	100.45	CCN
1.219	10.45	49.32± 4.22	40.46± 3.46	0.07392	0.09111	97.27	99.70	
1.483	12.71	56.04± 4.53	37.79± 3.05	0.07628	0.09346	96.68	99.10	HN
1.742	14.93	65.75± 6.88	37.74± 3.95	0.07627	0.09346	96.10	98.50	HN
1.907	16.35	70.44± 10.93	36.94± 5.73	0.07705	0.09424	95.73	98.12	HN
2.078	17.81	85.59± 12.32	41.19± 5.93	0.07393	0.09033	95.35	97.73	HN
2.533	21.71	89.66± 11.52	35.40± 4.55	0.07862	0.09580	94.33	96.69	HN
2.622	22.47	107.35± 12.30	40.94± 4.69	0.07393	0.09033	94.13	96.50	HN
2.942	25.22	102.20± 5.84	34.74± 1.99	0.07939	0.09580	93.42	95.76	HN
3.147	26.97	103.53± 8.98	32.90± 2.85	0.08096	0.09815	92.96	95.28	HN
4.148	35.55	119.77± 11.14	28.87± 2.69	0.08487	0.10283	90.12	92.37	HN
5.387	46.17	138.70± 15.25	25.75± 2.83	0.08877	0.10674	87.95	90.15	HN
6.182	52.99	107.56± 10.53	17.40± 1.70	0.10283	0.12237	86.17	88.32	HN
7.657	65.63	38.68± 8.23	5.05± 1.07	0.15283	0.17783	82.87	84.94	HN
11.667	100.0	4.76± 1.70	0.41± 0.15	0.35000	0.35000	73.90	75.75	HN

** Total flow rate at inlet is 42.0 l/h, water pool temperature t=40^{o}C. Ambient air t=24.5^{o}C, RH=93%. Temperature at inlet t_0=28.5 ^{o}C, P_0=1001 hPa. At the outlet of the optical device P=679 hPa, flow rate at the outlet 130 l/h. Correction β=9.43 for rural and 43.78 for urban aerosol. At 23:15, Sept. 16, 1999.

1969). The variation of the parameters C and α in various geographical regions results from the variability of aerosol size and chemical composition both spatially and with time, as these two factors determine largely the activation efficiency of aerosol particles in the cloud environment. In this study, measurements were finished at the same place. So these two factors shouldn't cause major variations of α and C in Eq. (5.2). The particle behaviours response to the accelerating flow and the increase of mass and heat transfer in the flow should be the main reasons.

It should be noted that S_s is supersaturation instead of saturation used in Eq. (5.2), and Eq. (5.3) is suitable only for CCN in the atmosphere. In our study, not only CCN can be counted with the "Nozzle-CNC", but also condensation nuclei in other regions (for higher supersaturation) can be measured too.

Table 5.3: Results of experiment No. 9 ***

F_a (cm^3/s)	Aerosol Frac. (%)	Counting Value (/s)	Concentration measured (N/cm^3)	r_k (Rural) (μm)	r_k (Urban) (μ m)	S_0 (%)	Average S_1 (%)	Counting Region
0.102	0.29	4.71±0.63	46.15±6.18	0.04072	0.05322	99.94	112.93	CN
0.136	0.39	6.42±1.87	47.23±13.75	0.03447	0.05323	99.92	112.91	CN
0.228	0.65	9.79±2.14	42.78±9.39	0.04073	0.05948	99.87	112.85	CN
0.375	1.07	16.70±3.19	44.55±8.51	0.04072	0.05947	99.78	112.75	CN
0.923	2.63	34.79±5.98	37.69±6.48	0.04698	0.05948	99.47	112.40	CN
1.589	4.54	56.99±7.67	35.87±4.83	0.04699	0.06572	99.09	111.97	
3.677	10.51	128.40±16.45	34.92±4.47	0.04700	0.06572	97.89	110.61	
5.324	15.21	160.83±28.67	30.21±5.39	0.05322	0.06573	96.94	109.54	CCN-CN
7.855	22.44	206.74±31.26	26.32±3.98	0.05323	0.07198	95.49	107.90	CCN-CN
9.283	26.52	221.39±33.83	23.85±3.64	0.05937	0.07822	94.67	106.98	
11.591	33.12	247.12±29.56	21.32±2.55	0.05948	0.07823	93.34	105.47	CCN
15.487	44.25	245.31±37.31	15.84±2.41	0.07198	0.09073	91.11	102.95	CCN
18.446	52.70	196.81±36.87	10.67±1.20	0.08447	0.10322	89.41	101.03	CCN
20.076	57.36	132.70±21.55	6.61±1.07	0.10322	0.12198	88.47	99.97	
27.395	78.27	56.11±13.88	2.05±0.51	0.14697	0.17198	84.27	95.22	
29.395	83.98	33.69±7.80	1.15±0.27	0.17822	0.20322	83.11	93.92	HN
29.791	85.12	25.27±5.99	0.85±0.20	0.19072	0.22198	82.89	93.67	HN
35.0	100.0	5.27±1.37	0.15±0.04	0.35000	0.35000	79.90	90.29	HN

*** Total flow rate at inlet is 126.0 l/h, water pool temperature t=40^{o}C. Ambient air t=27.1^{o}C, RH=85%. Temperature at inlet t_0=28.2 ^{o}C, P_0=999 hPa. At nozzle outlet P_3=820 hPa, flow rate at outlet 370 l/h. Correction β=25.77 for rural and 119.65 for urban aerosol. At 15:20, Sept. 22, 1999.

5.3.2 Counting Regions

The mixing of the aerosol flow with saturated clean air results in a variation of saturation in the nozzle, as shown in Table 5.1, 5.2, and 5.3. When the aerosol fraction is small, a supersaturation can be produced. In experiment No. 9, particles with radii of about 0.04 μm can be activated. This critical size corresponds to the minimum detectable sizes of some commercial CNCs, such as GE counter with r_k of 0.04 μm. This counting region is in the 'normal' CN region.

A small supersaturation below 5% can also be created in the nozzle. This is the typical necessary supersaturation for CCN as discussed in Chapter 1. Hence the measured number concentration at this small S_s stands for that of CCN. Because of the Kelvin solution effect, the required saturation for a particle to grow to its balance size at this saturation can be smaller than 1. These nuclei that can

Table 5.4: Value value α and correction factor β at three flow rates

Flow Rate (l/h)	Value C	Value α	β (rural)	β (urban)
29.1	35.65	5.52	3.19	14.83
42.0	65.58	16.30	9.43	43.78
126.0	5.21	19.82	25.77	119.65

grow at "subsaturation" are hygroscopic nuclei (HN). In the atmosphere, particle size distribution and their optical absorbing and scattering coefficients are always changing because of the hygroscopic growth of aerosol particles in the changing relative humidities (RH) in the troposphere. This can be found in the parameterisation of regional and global aerosol radiation and climate model (d'Almeida, $et\ al.$, 1991). These HN can be counted in the Nozzle-CNC even when the flow in the nozzle is not fully saturated. Between CN and CCN are the intermediate nuclei (CCN-CN region). The counting regions for CN, CCN-CN, CCN, and HN are marked in Table 5.2 and Table 5.3.

So just by adjusting the fraction of aerosol flow, various nuclei from HN to CCN, to CCN-CN and CN can be counted.

5.4 Conclusions from the Experiment

The nozzle flow can produce fast, nearly adiabatic and isentropic cooling due to the continuous expansion. When the induced flow is saturated with water vapour, then a supersaturation can be created, and the condensation process can be initiated in the nozzle. This is the basis on which the new "Nozzle-CNC" has been constructed. This method of creating cooling differs greatly from other cooling principles such as thermal diffusion in CNC 3020 and mechanical expansion in Sholtz counter.

Through a series of experiments with the "Nozzle-CNC", we can achieve the following conclusions:

① When clean air is 100% saturated, a supersaturation in the nozzle can be

reached. The saturation can be adjusted by just regulating the mixing ratio of the aerosol flow while keeping the same total flow rate through the nozzle.

② The measured number concentration of condensation nuclei changes unproportionally with the fraction of the aerosol sample flow. There exists an exponential relation between the measured nucleus number concentration and saturation S in the nozzle: $N = CS^{\alpha}$. The value of α depends largely on the flow rate through the nozzle, ranging from 5.52 at the flow rate of 29.1 l/h, to 16.30 at the flow rate of 42.0 l/h, and to 19.82 at the flow rate of 126.0 l/h. This equation differs from the relation for atmospheric CCN obtained by Twomey and other researchers.

③ The adjustability of the saturation in the nozzle gives a possibility to extend the counting region with this Nozzle-CNC, from measuring hygroscopic nuclei (HN), to cloud condensation nuclei (CCN), to condensation nuclei (CN) and the intermediate region between CCN and CN (CCN-CN).

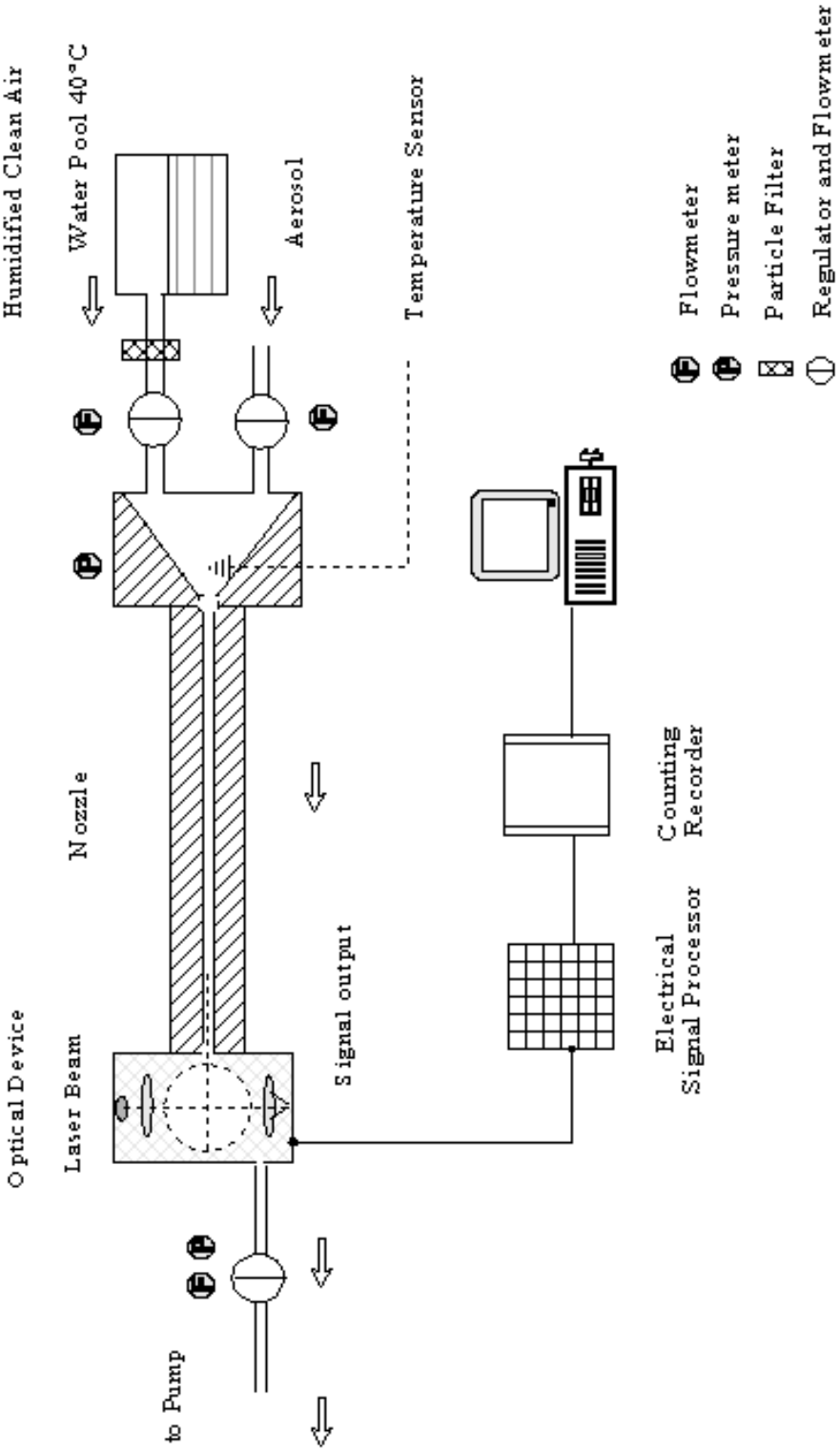

Figure 5.1: Schematic diagram of the Nozzle-CNC

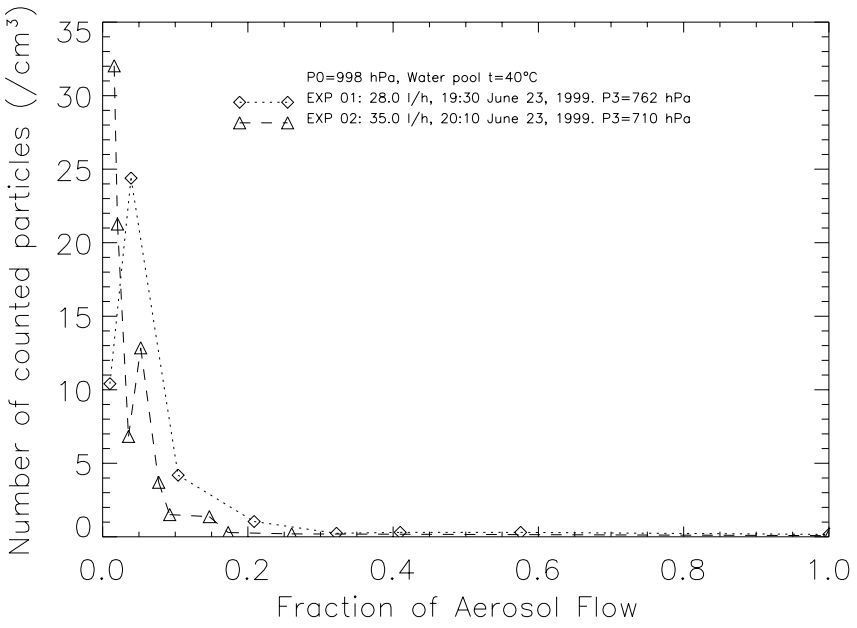

Figure 5.2: Measured particle number concentration of the experiment No. 1 and No. 2 (P_3 here is the pressure at the outlet of the optical device)

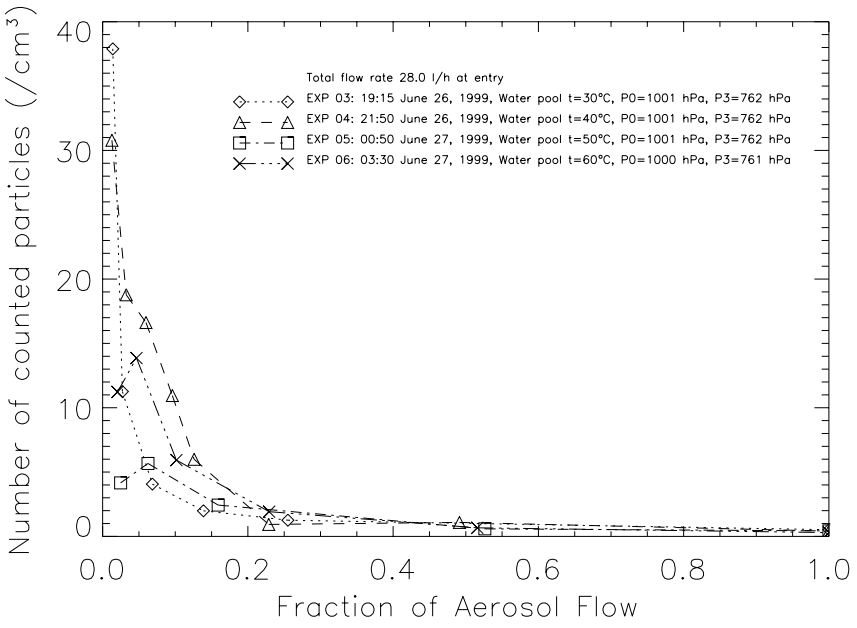

Figure 5.3: Measured particle number concentration of the experiment No. 3, No. 4, No. 5 and No.6 (P_3 here is the pressure at the outlet of the optical device)

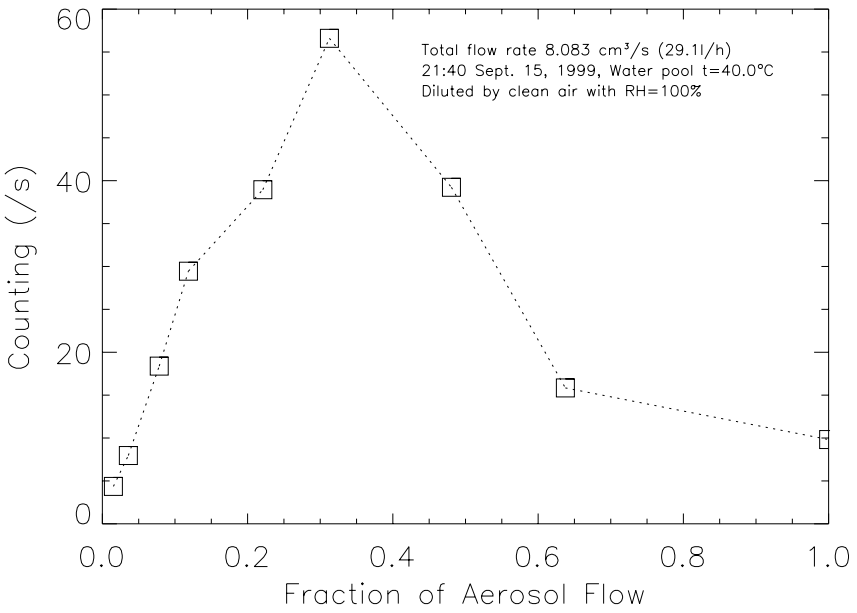

Figure 5.4: Experiment No.7: Change of the counting value with the fraction of aerosol flow (see also Fig. 5.7)

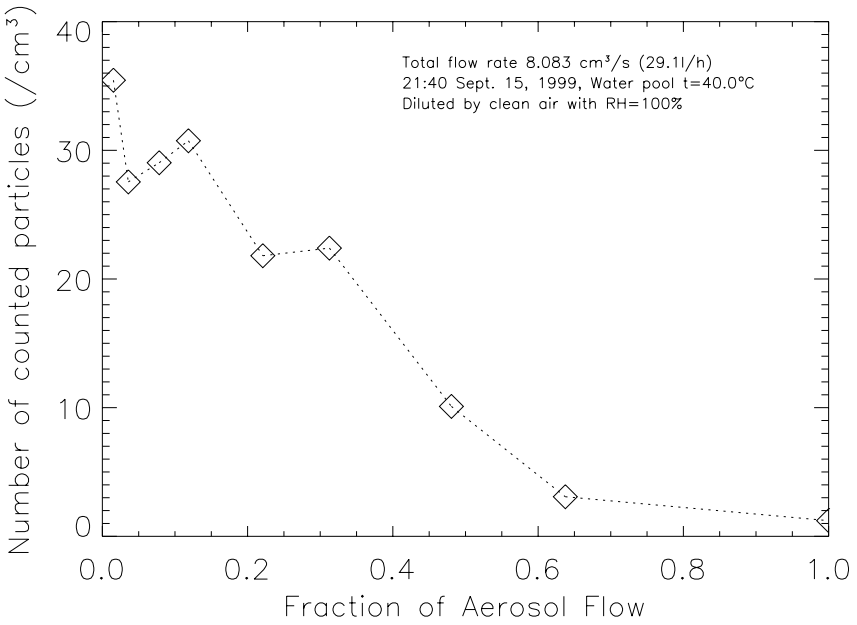

Figure 5.5: Experiment No.7: Change of the direct measured particle number concentration with the fraction of aerosol flow (before correction)

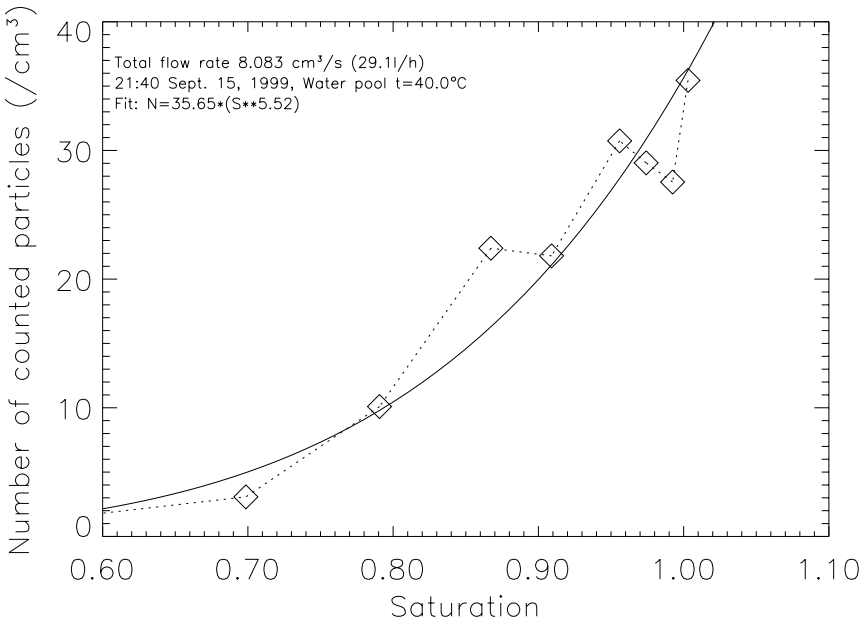

Figure 5.6: Experiment No.7: Change of the direct measured particle number concentration with the saturation in the nozzle (before correction)

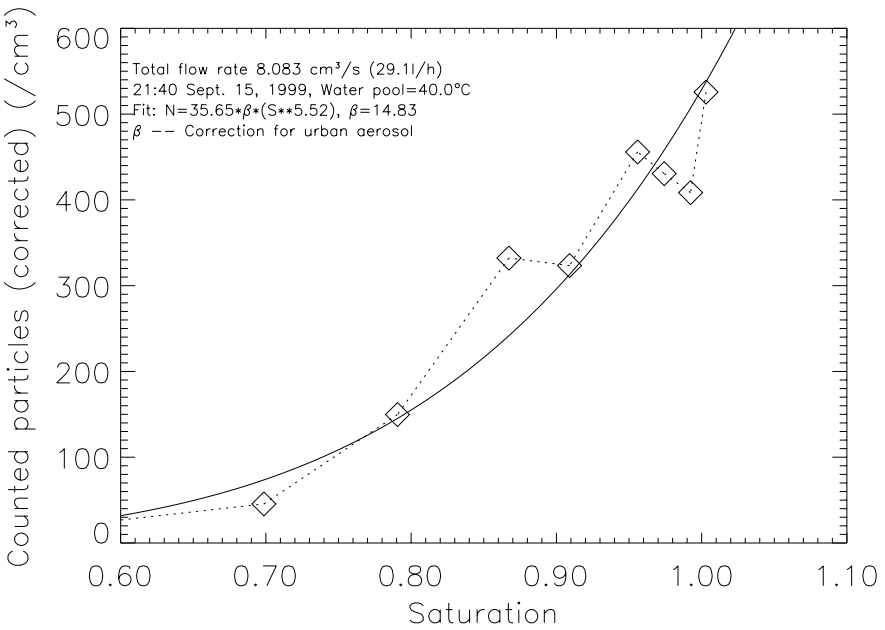

Figure 5.7: Experiment No.7: Change of the direct measured particle number concentration with the saturation in the nozzle (corrected as urban aerosol mode)

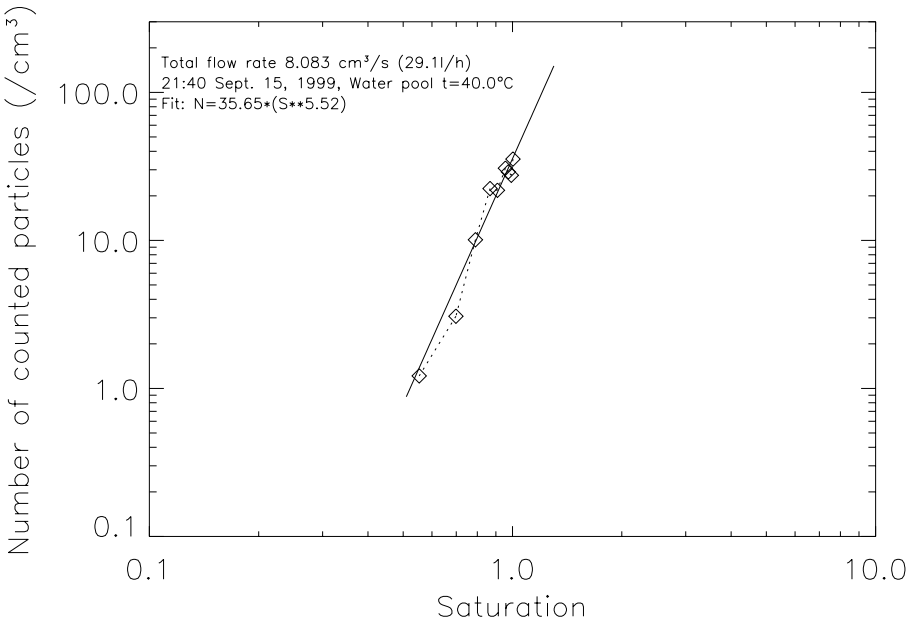

Figure 5.8: Experiment No.7: The fitted relationship between the measured particle number concentration and the saturation in the nozzle (before correction)

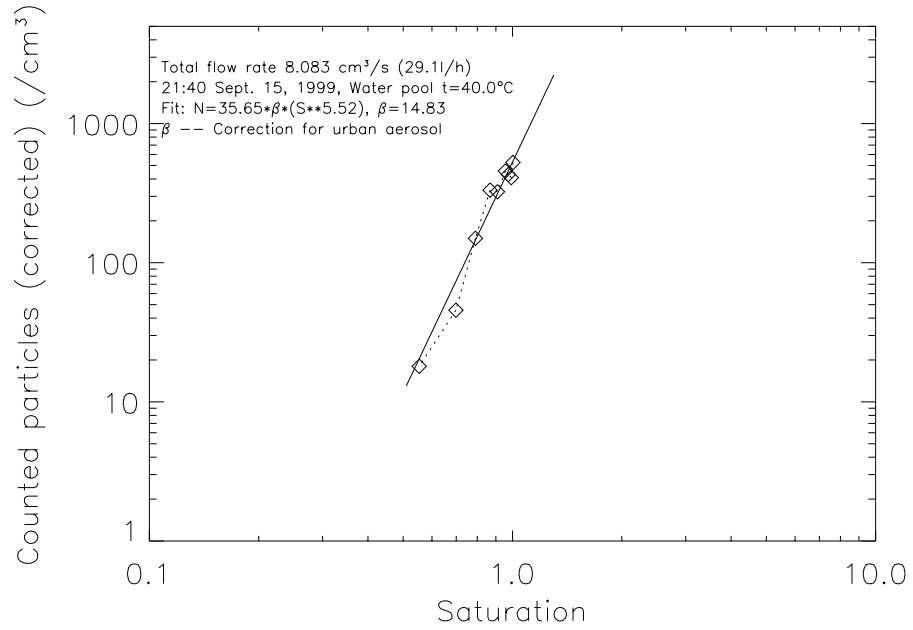

Figure 5.9: Experiment No.7: The fitted relationship between the measured particle number concentration and the saturation in the nozzle (corrected as urban aerosol mode)

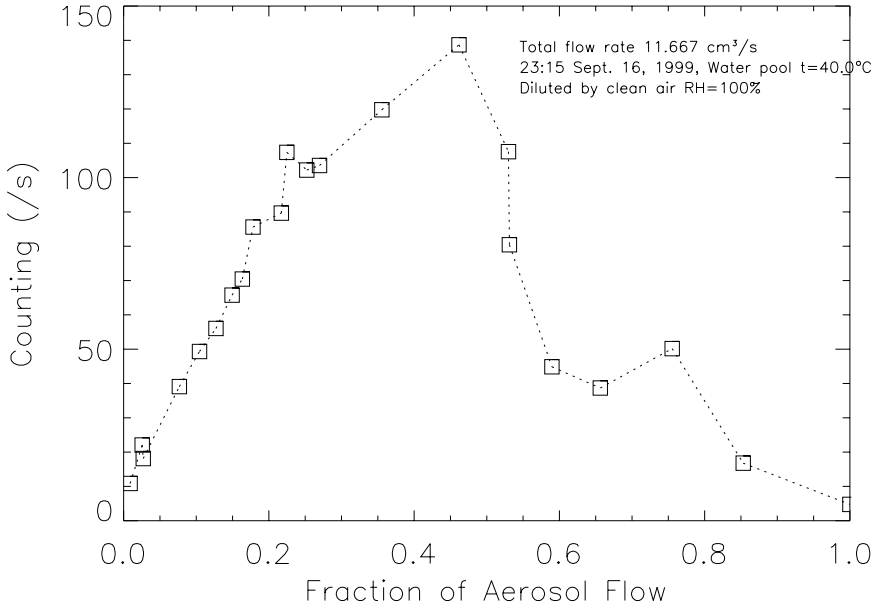

Figure 5.10: Experiment No.8: Change of the counting value with the fraction of aerosol flow

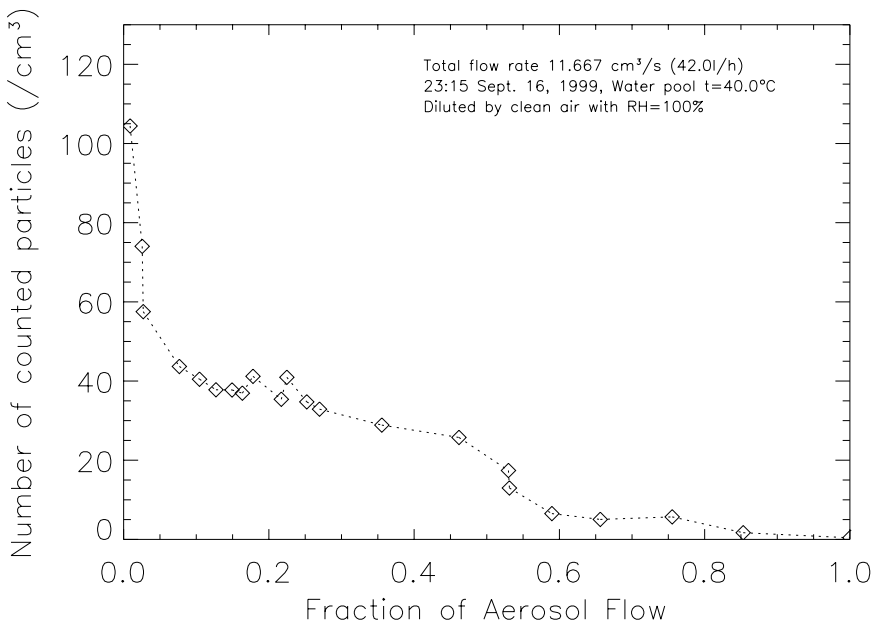

Figure 5.11: Experiment No.8: Change of the direct measured particle number concentration with the fraction of aerosol flow (before correction)

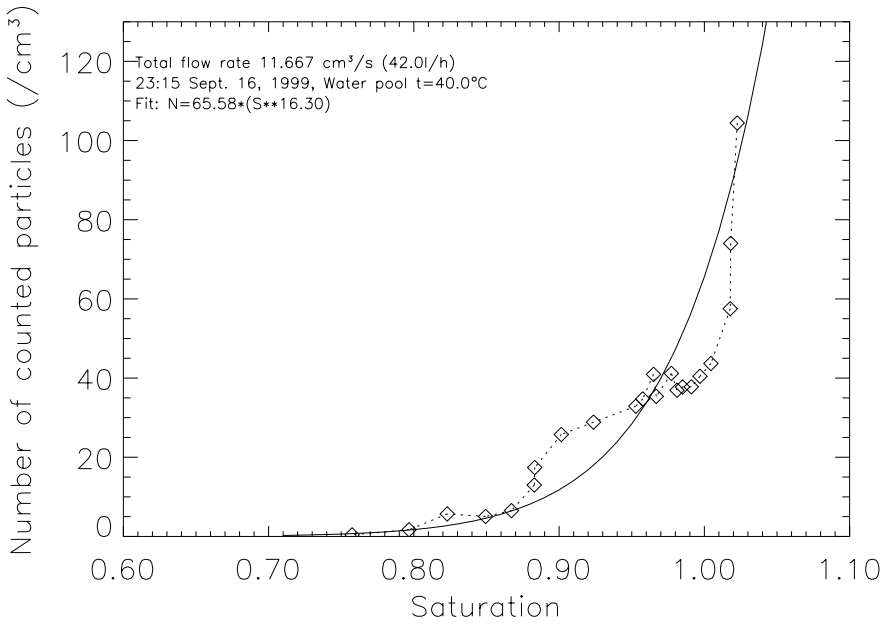

Figure 5.12: Experiment No.8: Change of the direct measured particle number concentration with the saturation in the nozzle (before correction)

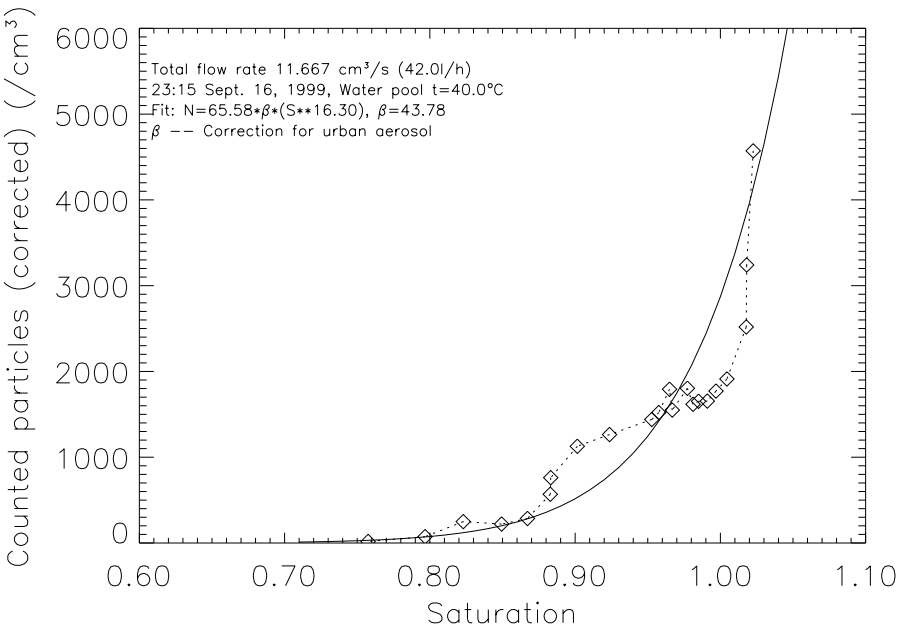

Figure 5.13: Experiment No.8: Change of the direct measured particle number concentration with the saturation in the nozzle (corrected as urban aerosol mode)

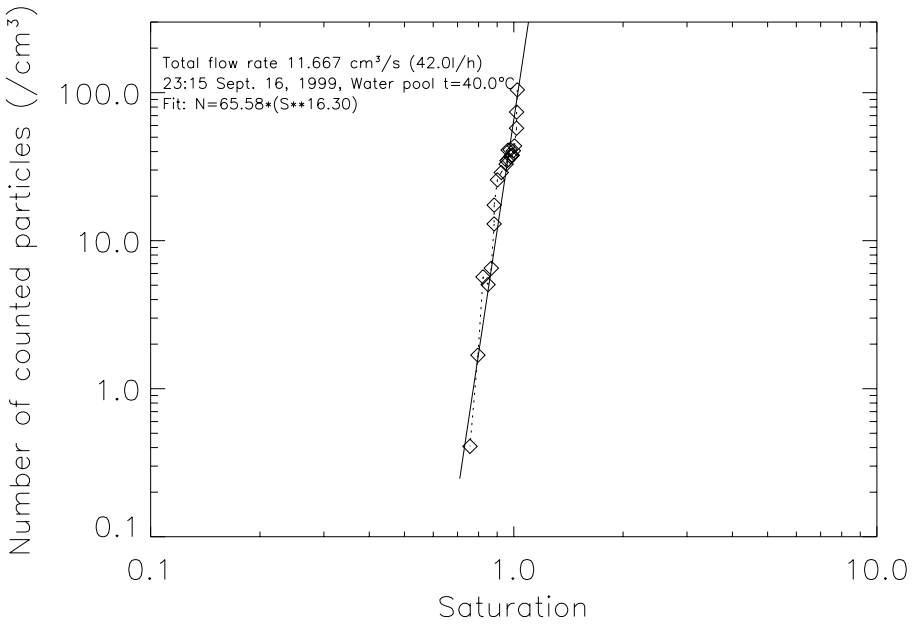

Figure 5.14: Experiment No.8: The fitted relationship between the measured particle number concentration and the saturation in the nozzle (before correction)

Chapter 6

ANALYSIS OF THIS NEW NOZZLE-CNC

6.1 Analysis of this New Nozzle-CNC

6.1.1 System Calibration

The number concentration of aerosol particles can be counted both directly or indirectly. Counting with microscope, photographs or visual single-particle inspection are the direct measuring methods. Measurement with light attenuation and scattering by particle cloud are usually named indirect methods. The indirect counting is widely used today as it can quickly, automatically and continuously record the results and the results can be electrically processed and saved. However, as this method gives relative values, the results are always converted and calibrated before they can show “real” measurement results. The calibration is usually made against the instrument itself, the way of the counting, the instrument noise, the counting environment, and other measurement errors. Effects such as cross-sensitivity and coincidence, that is the measurement of more than one aerosol particle in a sensing volume in a time (Jaenicke, 1972), should then be taken into consideration in optical data post-processing.

The optical laser detecting system in this work can be regarded as a direct measuring method as it directly counts the number of pulses. However it was found that the flow rate through the sensing volume can result in a counting deviation (Zhang and Liu, 1990; Dreiling, 1994). Figure 6.1 shows the counting

results (particle number concentration) by a laser particle counter (LPC Model 3755) at changing flow rates. The instrument is very sensitive to the flow rates especially in the region of small flow rates (smaller than 100 l/h). The reason is that the increase of the velocity decreases the 'residence' time for particles in the illumination in the optical sensing volume. Hence less particles are counted at larger flow rates.

From these reasons, a system calibration is necessary. By assuming that particles have size distributions of urban and rural modes, corrections can be given and results are shown in figures 5.9, 6.7, 6.9, 6.10, 6.17, and 6.18.

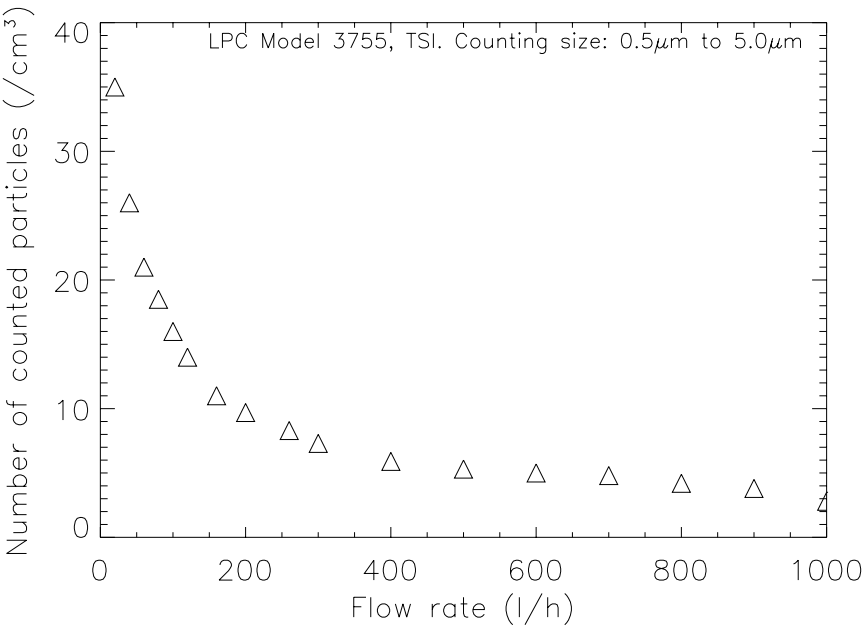

Figure 6.1: Measured particle number concentration with the variation of flow rate through LPC Model 3755 – TSI

6.1.2 Critical Particle Radius

Condensation will be initiated on all particles larger than a minimum size corresponding to that supersaturation. This minimum size is named critical particle size. Mason (1971) once gave a relation to estimate the minimum radius (r_k) for a

droplet in an environment of water vapour with a supersaturation S_s:

$$r_k = \frac{2\gamma}{\rho_w \mathrm{R}_w T \ln S_s}, \tag{6.1}$$

where γ is the surface tension of water, ρ_w the density of liquid water, R_w the gas constant for water vapour, and T is the temperature in Kelvin.

Equation (6.1) is correct only in a certain sense. If particles are hygroscopic, then the solution on the particle surface will act. This reduces the supersaturation required for particle growth for a given size. The required relative humidity for growth can actually be reduced below 100% if the particles are large enough and if the particles contain soluble compounds. The solubility of aerosol particles as discussed in the section 1.3 is not only size-dependent but also source-dependent. Under experimental conditions, the minimum detectable size in fact, depends not only on the supersaturation and physical and chemical properties of aerosol particles, but also on the design of the measuring device.

Table 6.1: Critical particle size vs saturation according to Eq. (6.1)

Critical size r_k (μm)	Saturation (%)
0.001	3.03179
0.002	1.74120
0.004	1.31955
0.01	1.11730
0.02	1.05702
0.04	1.02812
0.10	1.01115
0.20	1.00556
0.40	1.00278
1.0	1.00111
2.0	1.00055
4.0	1.00028

As mentioned in Chapter 1, the size distribution of aerosol particles in a region can be well described by the log-normal distribution mode, that is the overlapping of more than one log-normal distributions. Here the urban and rural modes

for the aerosol distribution (Jaenicke, 1988) as Eq. (1.3) was adopted. The minimum sensitive size to optical system is 0.35 μm in radius. When condensation processes begin, particles that are larger than the critical size will grow. Assuming that all particles larger than the critical size (r_k) can grow to detectable sizes ($\geq$ 0.35 μm), the measurable number concentration of particles $N^c_{r_k}$ according to this distribution mode should be

$$N^c_{r_k} = \int_{r_k}^{\infty} \mathrm{d}N(r) = \int_{r_k}^{\infty} n \mathrm{dlog}\, r. \tag{6.2}$$

The number concentration of particles larger than 0.35 μm in ambient air is

$$N^c_{0.35} = \int_{0.35}^{\infty} \mathrm{d}N(r) = \int_{0.35}^{\infty} n \mathrm{dlog}\, r. \tag{6.3}$$

Here the superscribe "c" indicates the calculated value. In the experiments, we can get the measured particle number concentrations with the optical device without having the condensational growth $N^m_{0.35}$. If the measured nucleus concentration with the Nozzle-CNC is N^m, then we have

$$\frac{N^m_{0.35}}{N^m} = \frac{N^c_{0.35}}{N^c_{r_k}}. \tag{6.4}$$

By the way, the concentration correction factor β can be defined as

$$\beta = \frac{N^c_{0.35}}{N^m_{0.35}}. \tag{6.5}$$

By knowing the measured values of $N^m_{0.35}$ and N^m as well as the calculated $N^c_{0.35}$, according to Eq. (6.4), we can estimate the critical particle radius r_k. The critical particle radii for urban and rural aerosol modes at different S in experiment No. 7, No. 8, and No. 9 are listed in Table 5.1, 5.2, and 5.3.

The Rhine-Main region around Mainz is one of the typical industrial areas in Germany. The aerosol mode in Mainz however should be between the rural aerosol mode and urban aerosol mode (as defined in table 1.1) as Mainz cannot be numbered as a large city with severe air pollution. So the actual critical particle radius in the experiment with this Nozzle-CNC should be between the calculated critical particle sizes for urban aerosol mode and rural aerosol mode as tabulated in Table 5.1, 5.2, and 5.3. As shown in Table 5.3, the minimum detectable size is 0.04 μm.

6.1.3 Counting Range

Usually, the largest number concentration of aerosol particles in a sampled air for an OPC within calibrated coincidence is about 25 cm^{-3}. This limit may be greatly enlarged if the sampled air is diluted by clean air. If the clean air is 100 times as much as the sampled air, then the maximum counting range can be 2500 cm^{-3}. The dilution ratio can be chosen according to particle concentration in the sampled air. It was once reported that with a small sensing dimension $36\times52\times35\ \mu\text{m}^3$ in OPC, a high concentration up to 10^7 particles per millilitre can be measured by dilution (Sachweh $et\ al.$, 1998).

In this experiment, the dilution will produce a variation of saturation in the nozzle (as shown in Chapter 5), and therefore results in the change of counting results. But this problem can be solved if the sampled air is diluted, for example with the use of Aerosol Diluter TSI Model 3302A, before being fed into the mixing chamber with saturated clean air.

6.1.4 Counting Efficiency

The counting efficiency of a condensation nucleus counter depends not only on the physical properties of the aerosol particles in the local air but also on the system set-up of an instrument. There are several factors that should be concerned for the accuracy of the counting efficiency in this experiment.

Diffusion loss

The loss of small particles due to diffusion during the time when aerosol particles through the nozzle system is a problem that may affect the counting efficiency.

In a CNC, the counting efficiency can be greatly reduced resulting from the diffusion loss of particles to the inner walls. Jaenicke (1976) once found the counting efficiency is 88% after 1 min wait, and only 66% after 4 mins wait for the Scholz pocket counter.

The diffusion loss of particles to a wall can be estimated. If we assume that the initial particle concentration is N_0, and the horizontal distance from the wall is x, then the particle concentration $N(x,t)$ at the distance x and time t should satisfy

Fick's second diffusion law:

$$\frac{\mathrm{d}N}{\mathrm{d}t} = D_p \frac{\mathrm{d}^2 N}{\mathrm{d}^2 x}, \qquad N = N_0 \text{ for } t = 0, \text{ and } N = 0 \text{ for } x = 0. \tag{6.6}$$

This equation has the solution

$$N(x,t) = \frac{2N_0}{\sqrt{4\pi D_p t}} \int_0^x \exp\left(\frac{-y^2}{4D_p t}\right) dy, \tag{6.7}$$

where D_p is the diffusion coefficient for particles of size r_p:

$$D_p = \frac{kTC_c}{6\pi\mu_g r_p} \tag{6.8}$$

The diffusion coefficient for various sizes of particles is displayed in Fig. 6.2. According to this solution, the concentration depletion near the wall can be estimated. For the case of particles in a capillary with circular cross-section, the diffusion loss depends strongly on the dimensionless deposition parameter ς. ς is defined as:

$$\varsigma = \frac{4D_p L}{\pi D^2 \overline{U}} = \frac{D_p L}{Q}, \tag{6.9}$$

where Q is the volume flow rate through the capillary, L the length of the capillary, D the diameter of the capillary, and $\overline{U}$ the average velocity of the air flow. The penetration factor N_1/N_0 (N_0 is the concentration at the inlet and N_1 at the outlet), for the case of a laminar flow through the capillary, can be expressed as a function of ς with an accuracy of 1%:

$$\begin{aligned} \frac{N_1}{N_0} =& 1 - 5.50\,\varsigma^{2/3} + 3.77\varsigma && \text{for } \varsigma < 0.007 \\ =& 0.819\exp(-11.5\varsigma) + 0.0975\exp(-70.1\varsigma) \\ &+ 0.0325\exp(-179\varsigma) && \text{for } \varsigma > 0.007. \end{aligned}$$

According to the flow Reynolds numbers given previously, the flow in the nozzle is in fact than a laminar flow but a turbulent flow. Diffusion deposition in turbulent flow is more complicated than in laminar flow. Fuchs (1964) and Davies (1966) studied this problem. The penetration factor N_1/N_0 can be expressed as

$$\frac{N_1}{N_0} = \exp\left(\frac{-4V_{dep}L}{D\overline{U}}\right), \tag{6.10}$$

where V_{dep} is the deposition velocity of particles that can be written as

$$V_{dep} = \frac{D_p}{\delta_d}. \tag{6.11}$$

Here δ_d is the thickness of the diffusion boundary (Fuchs, 1964):

$$\delta_d = \frac{28.5 D D_p^{1/4}}{\mathrm{Re}^{7/8}(\mu_g/\rho_g)^{1/4}}, \tag{6.12}$$

where Re is the fluid Reynolds number.

By assuming the laminar flow, the penetration ratio of particles through the nozzle at three flow rates can be calculated, and the results are shown in Fig. 6.3. Figure 6.4 shows the diffusion losses of particles in a turbulent flow in the nozzle according to Fuchs equation (6.10).

We can see that, for particles with sizes smaller than 0.01 μm, the diffusion loss is very substantial. For particles with the size of 0.01 μm, the diffusion loss is below 5%. For particles with radii of 0.001 μm, more than 70% particles cannot pass through the nozzle in the turbulent flow. In the case of laminar flow, the diffusion losses show an inverse proportion to the flow rates for a given size. This is easy to understand as particles have less 'residence' time in the nozzle at a larger flow rate than at a smaller flow rate. However in turbulence flow, as we can see in Fig. 6.4, the diffusion loss curves at three flow rates almost overlap. The flow rate has very little effect on the result. A large flow rate produces a large fluid Reynolds number and therefore the thickness of the diffusion boundary δ_d (Eq. 6.12) becomes thin, which causes the increase of the deposition velocity (V_{dep}). This just offsets the short 'residence' time influence on the diffusion losses in the nozzle. Therefore the final diffusion losses are almost the same for all turbulent nozzle flows.

For particles larger than 0.03 μm, the diffusion loss is within 1%. This value becomes smaller if the condensational growth was considered into calculation. As the critical particle radius is larger than 0.03 μm for this Nozzle-CNC, the diffusion loss can be fully neglected although the nozzle has only 1 mm of inner diameter.

Electrical effects

A great part of aerosol particles in the atmosphere can carry electrical charges as cosmic rays and radioactive substances can produce both positive and negative ions. This leads to a bipolar charging of aerosol particles. Exposure to gas ions of one sign will produce an unipolar charging. Unipolar charging can also be realised in an electric field. In the presence of an electric field, a charged particle will

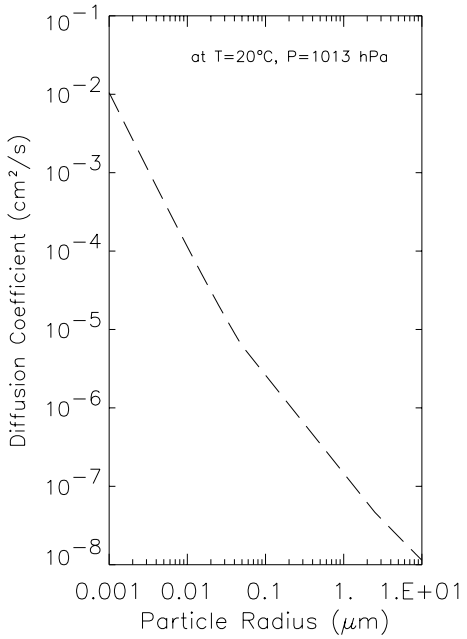

Figure 6.2: Particle diffusion coefficient as function of radius

deviate from its original streamline to or opposite to the direction of the electric field.

In this experiment, static charges will be produced resulting from the friction of the high speed air flow with the inner nozzle wall. In order to avoid inducing the electrical effect, metal nozzle was employed. So the electrical effect on the counting efficiency of this Nozzle-CNC may be neglected. As metal has a good electrical conductivity, charges cannot accumulate on the inner wall as the experiment is going on. In contrary, they will be transported to the outside wall of the nozzle according to the principle of static electrics.

Other factors

The nonisokinetic sampling is an another factor that may affect the counting accuracy of the measurement. Isokinetic sampling refers to withdrawing a sample from a moving aerosol at the same velocity of the moving aerosol, insuring that the collected sample will be representative for the moving aerosol. If the sampling velocity and the aerosol velocity are not the same, there may be a distortion of the flow near the sampler inlet, which will cause particles to move in a curved path

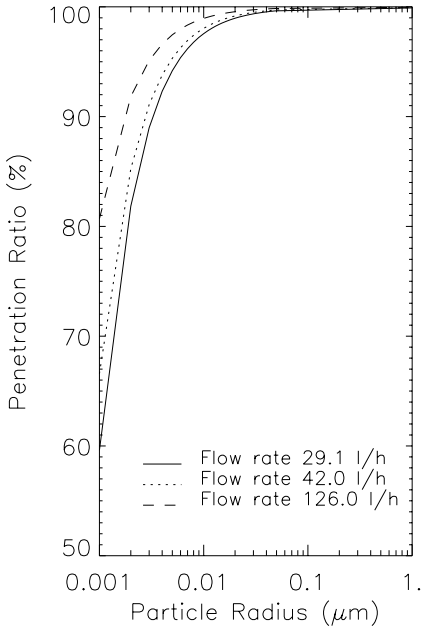

Figure 6.3: Particle penetration ratios through the nozzle in laminar flows at three flow rates (without considering the condensational growth)

following the streamlines of the distorted flow. If the sampling velocity is less than the gas velocity, then some of the ambient flowing gas must pass around the inlet by curving away from the axis of the inlet. Large particles in the flow may not be able to follow the curved path because of inertial motion and will therefore enter the inlet, resulting in a higher concentration of particles in the sample than that is present in the air stream. If the sampling velocity is higher than the air velocity, the larger particles will not be able to follow the curved streamlines and will therefore be excluded from the sample into the inlet. As a result, this will produce a particle concentration smaller than the real concentration. The effect of nonisokinetic sampling can usually be neglected for particles smaller than 1 μm approximately.

In this experiment however, no by-flow was adopted, so the effect of non-isokinetic sampling can be omitted. In addition, there are particle losses due to the turbulence of air in the nozzle. The gravitational effect on particle losses in this experiment can be neglected too as the residence time of particles in the nozzle is quite short and only fine size particles are of our main concern.

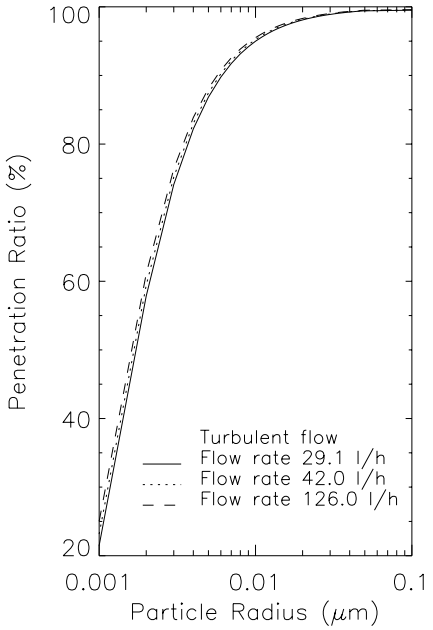

Figure 6.4: Particle penetration ratios through the nozzle in turbulent flows (without considering the condensational growth)

6.2 Advantages and Problems

This new Nozzle-CNC has several advantages compared with other CNCs. The first one is that its condensation substance is water instead of organic compounds such as alcohol, ethanol, glycol and butanol which are used in some commercial CNCs such as TSI CNC Model 3032. So the measured nucleus concentration can better reveal the actual state of the atmospheric condensation nuclei. The second one is that the air flow in the nozzle is cooling adiabatically and isentropically. The condensation process on all particles larger than the critical particle radius can take place at the same time. It avoids the time delay for condensation resulting from the heat conduction to produce a temperature drop in the above mentioned CNC.

One of common problem in CNCs is the condensation of vapour at the inner wall of instrument. It is serious especially for those CNCs with the cooling principle of thermal diffusion, for example in the counters of Rosen (Rosen $et\ al.$, 1974, 1978), Hoppel (Hoppel $et\ al.$, 1979), Bricard (Bricard $et\ al.$, 1976), Sinclair (1975, 1982), Agarwal and Sem (1980), and Keady (Keady $et\ al.$, 1983). As the

temperature at the wall of condensation tube is lower than that in the flow in the tube, vapour condensates on the tube wall. On the contrary, the nozzle cooling produces a lower temperature in the flow than at the nozzle wall, as shown in Fig. 3.7. If we keep the temperature of the flow at the nozzle entrance equal to that of the ambient air, then the temperature of the air flow in the nozzle is always lower than that at the nozzle wall. No condensation of water vapour at the inner wall of nozzle can therefore occur.

Several problems were found in the experiment concerning the efficient and exact counting with this Nozzle-CNC. They are:

❶ Because the saturation in the nozzle is very sensitive to the sample aerosol ratio, the aerosol flow rate should be measured very accurately. The total flow rate must be stable during a measurement.

❷ The changing environmental conditions, such as temperature (T) and relative humidity (RH), will bring about the change of the saturation generated in the nozzle. Therefore to keep this Nozzle-CNC running under stable ambient conditions is very important for exact counting.

❸ The optical system can exactly count single particles under standard conditions indicated by the manufacturer. It should be calibrated against the volume flow rate and the pressure, when it is used at different flow rates and different pressures.

Further investigations on this condensation process in the Nozzle-CNC are still needed.

6.3 Significance of Numerical Optimisation and Experiment

Like often in the studies of many scientific problems, the design of the new Nozzle-CNC is firstly based on theoretical and numerical modelling that provide us with the best optimisation. By combining the results from nozzle flow modelling and particle growth modelling, a condensation nucleus counter was then constructed. This counter can be applied for measuring atmospheric condensation nuclei and for studying the formation of cloud droplets and cloud physics.

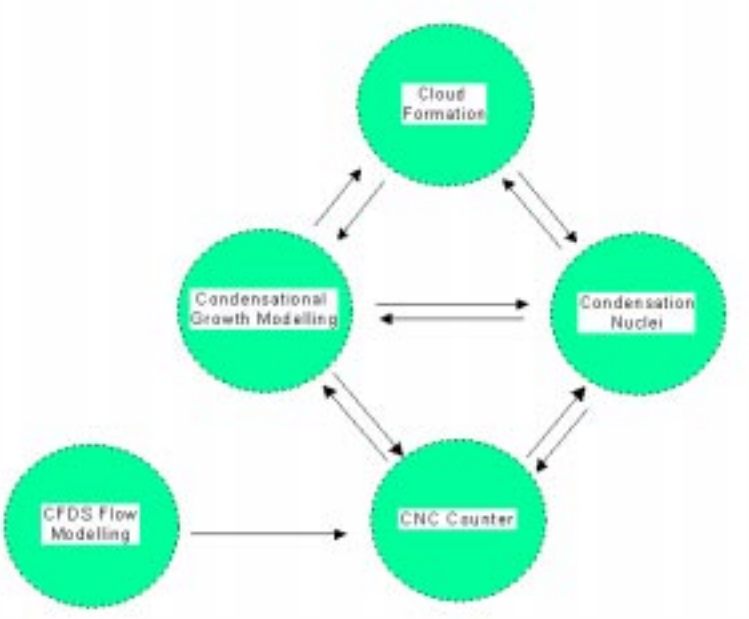

Figure 6.5: Relationship between experiment and theoretical modelling

The significant relationships between the modelling, experiment and studying of the reality of the atmospheric condensation nuclei or cloud physics can be described as in Fig. 6.5.

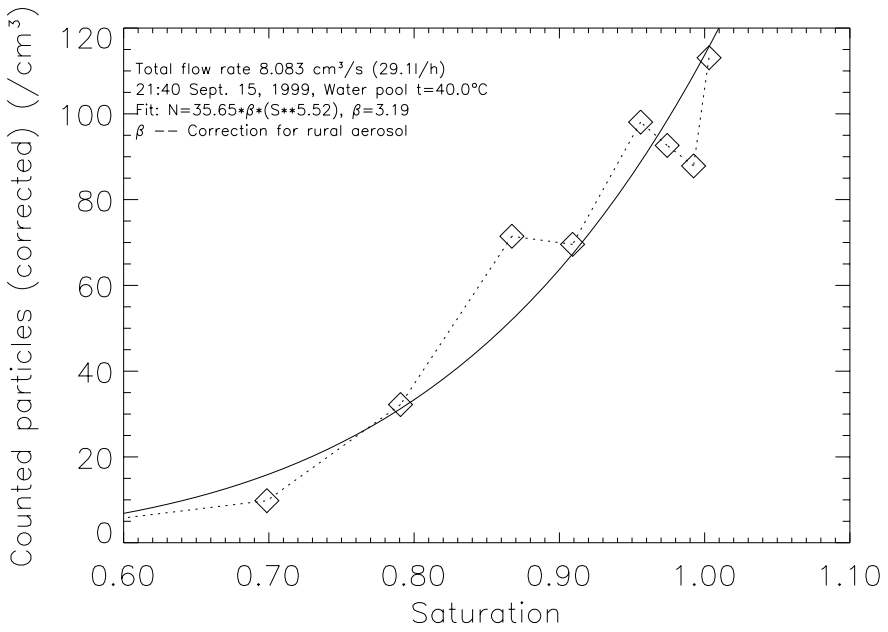

Figure 6.6: Experiment No.7: The fitted relationship between the measured particle number concentration and the saturation in the nozzle (corrected as rural aerosol mode)

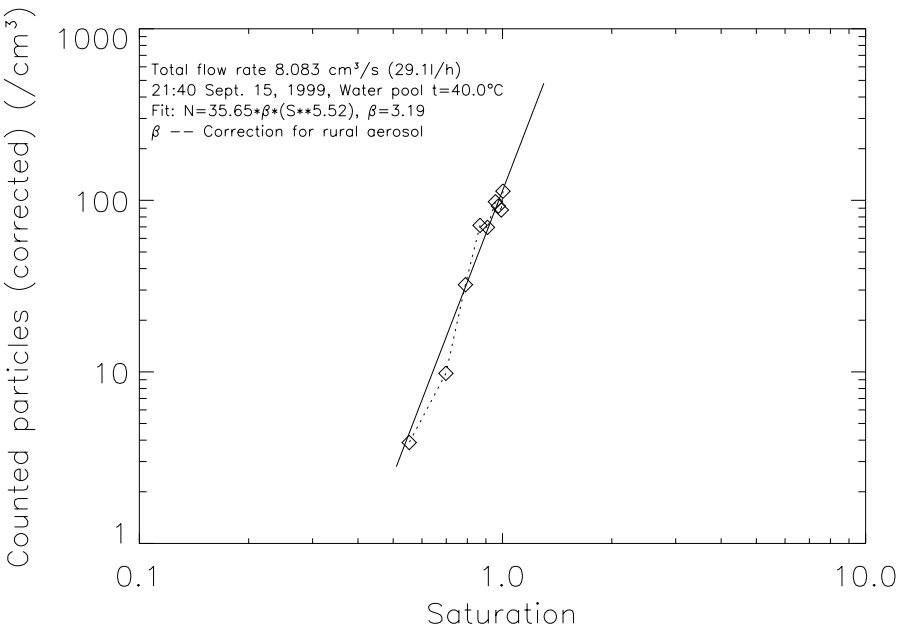

Figure 6.7: Experiment No.7: The fitted relationship between the measured particle number concentration and the saturation in the nozzle (corrected as rural aerosol mode)

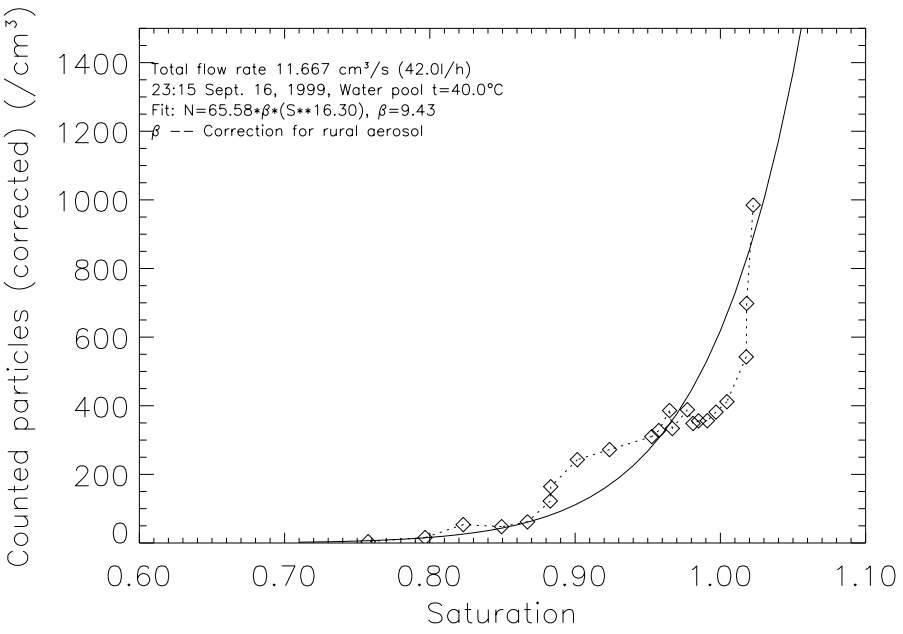

Figure 6.8: Experiment No.8: The fitted relationship between the measured particle number concentration and the saturation in the nozzle (corrected as rural aerosol mode)

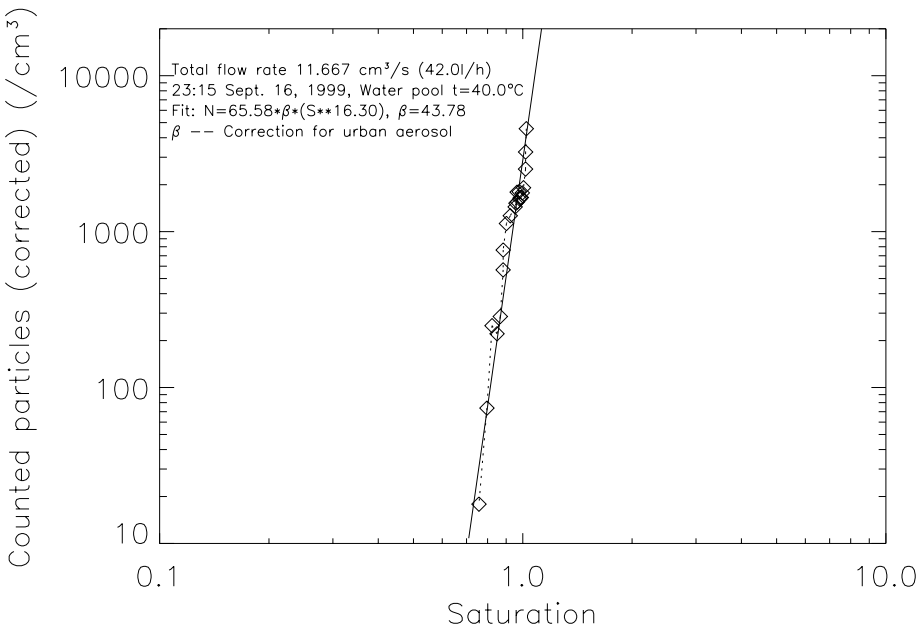

Figure 6.9: Experiment No.8: The fitted relationship between the measured particle number concentration and the saturation in the nozzle (corrected as urban aerosol mode)

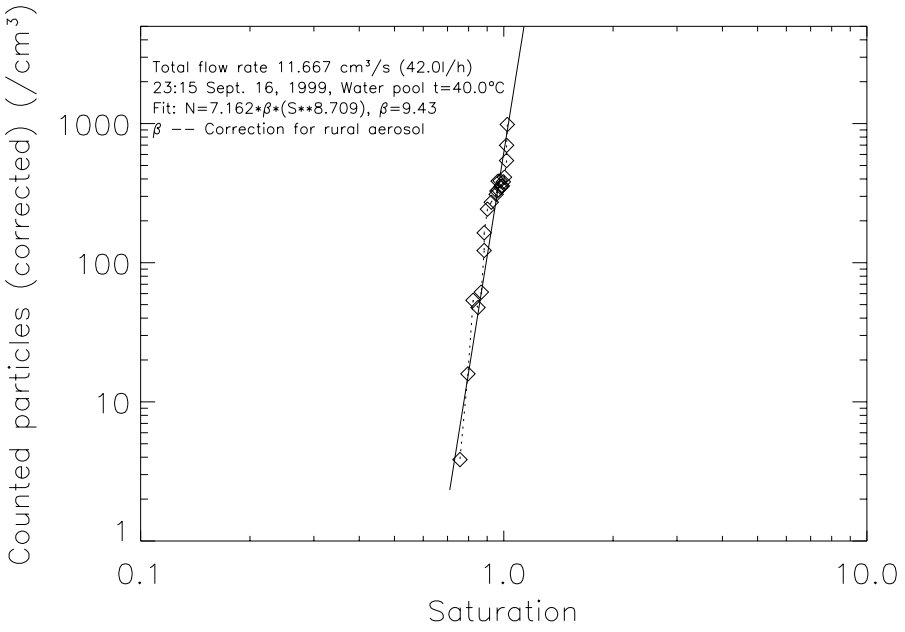

Figure 6.10: Experiment No.8: The fitted relationship between the measured particle number concentration and the saturation in the nozzle (corrected as rural aerosol mode)

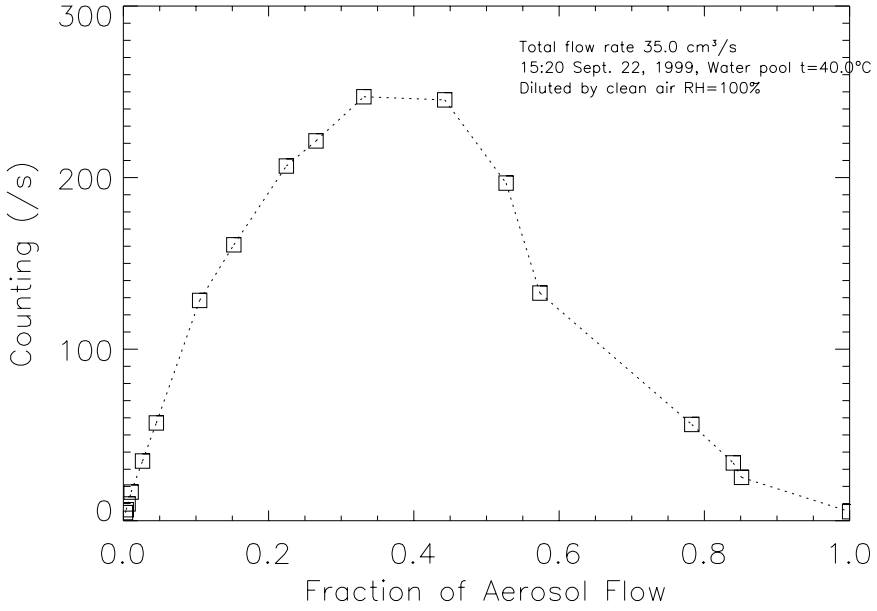

Figure 6.11: Experiment No.9: Change of the counting value with the fraction of aerosol flow

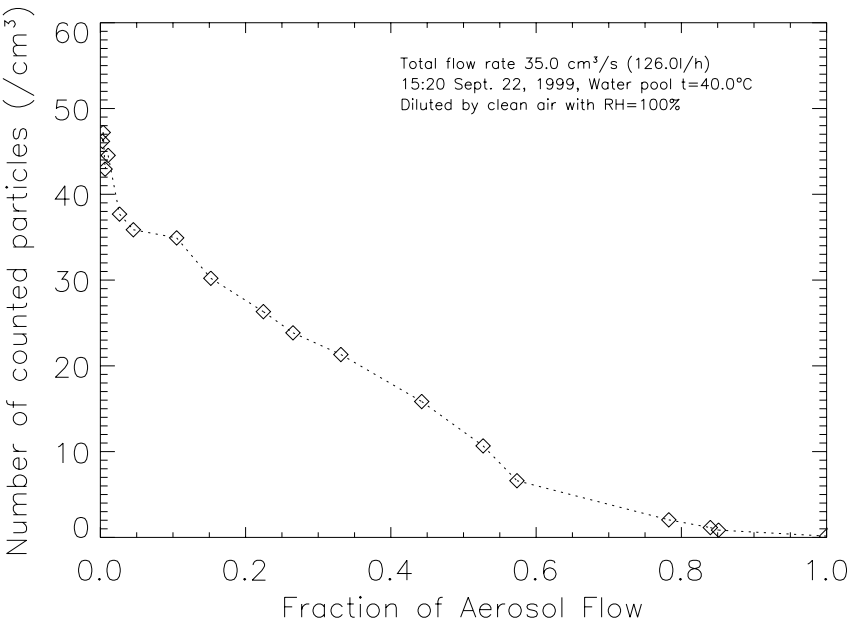

Figure 6.12: Experiment No.9: Change of the direct measured particle number concentration with the fraction of aerosol flow (before correction)

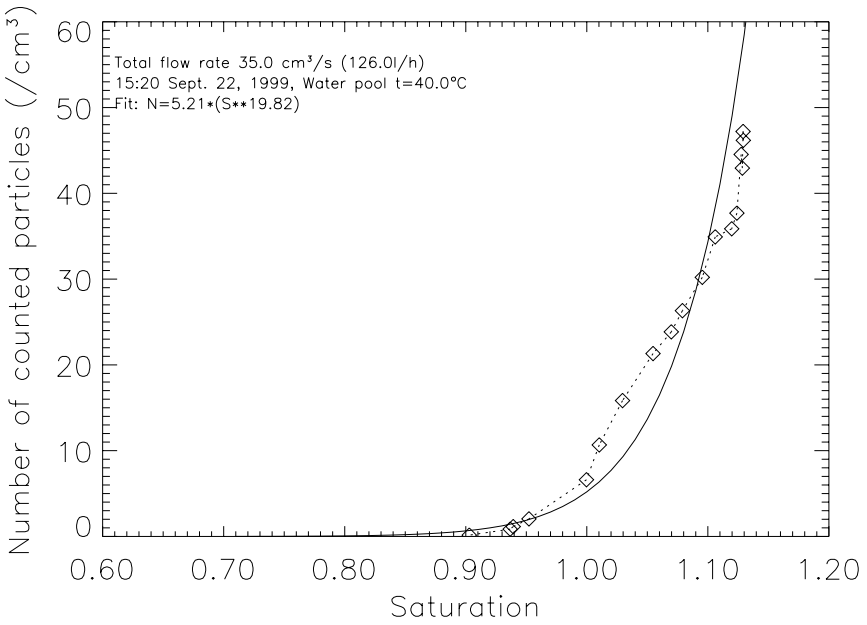

Figure 6.13: Experiment No.9: Change of the direct measured particle number concentration with the saturation in the nozzle (before correction)

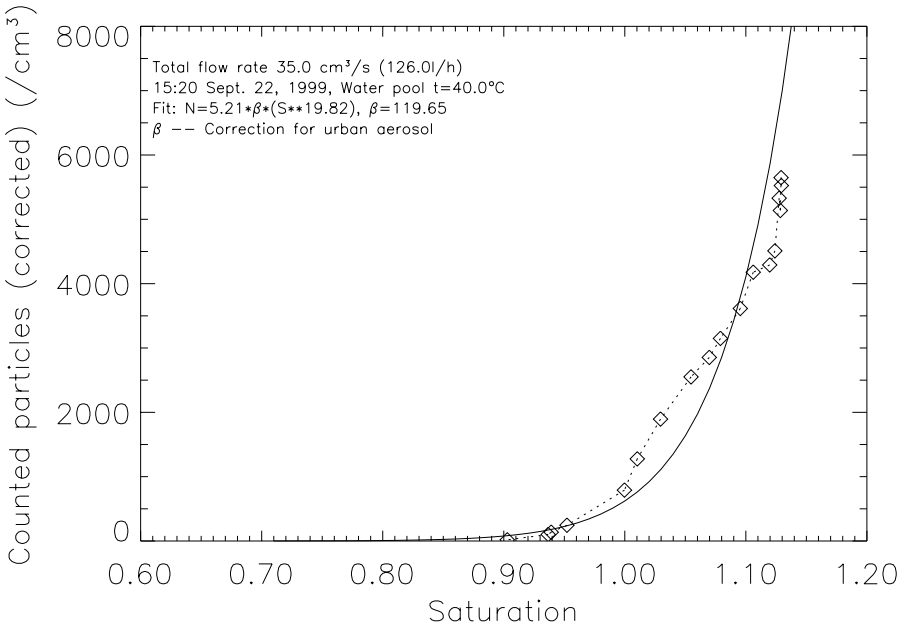

Figure 6.14: Experiment No.9: Change of the direct measured particle number concentration with the saturation in the nozzle (corrected as urban aerosol mode)

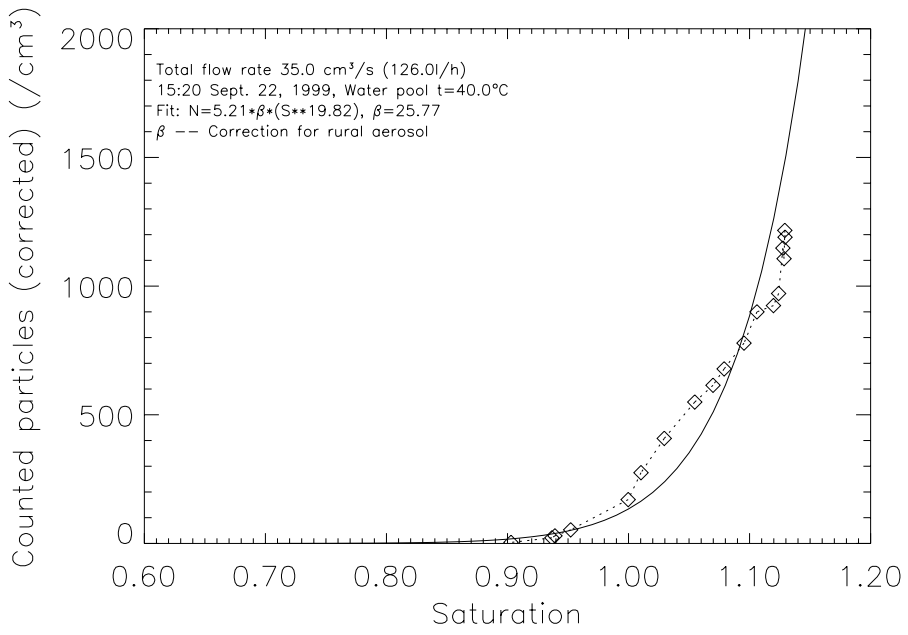

Figure 6.15: Experiment No.9: Change of the direct measured particle number concentration with the saturation in the nozzle (corrected as rural aerosol mode)

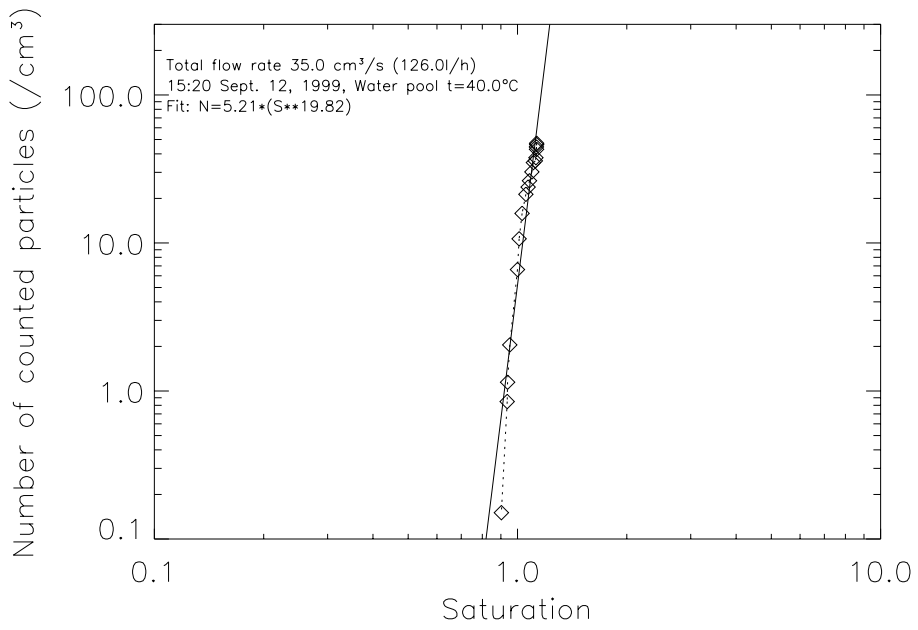

Figure 6.16: Experiment No.9: The fitted relationship between the measured particle number concentration and the saturation in the nozzle (before correction)

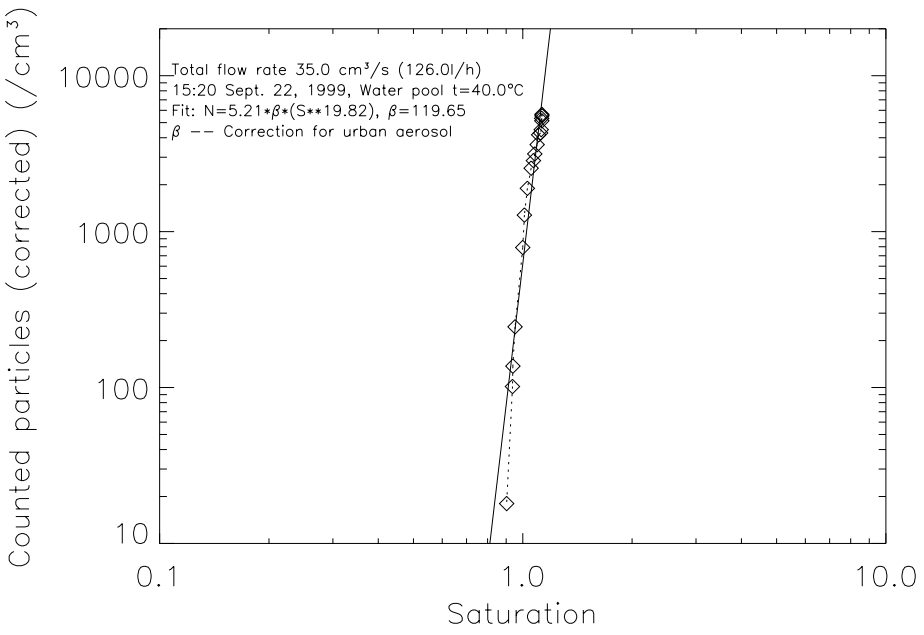

Figure 6.17: Experiment No.9: The fitted relationship between the measured particle number concentration and the saturation in the nozzle (corrected as urban aerosol mode)

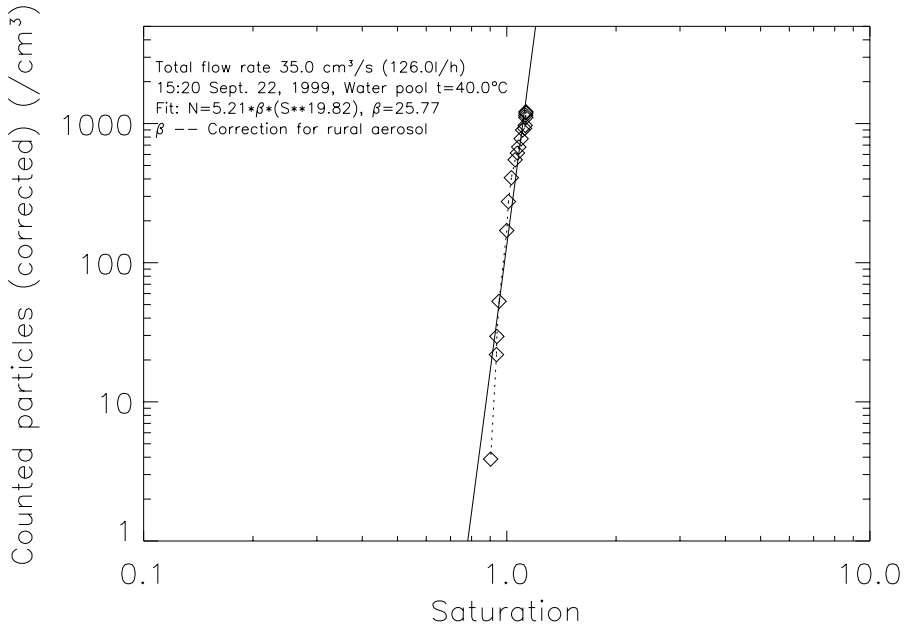

Figure 6.18: Experiment No.9: The fitted relationship between the measured particle number concentration and the saturation in the nozzle (corrected as rural aerosol mode)

Chapter 7

SUMMARY AND RECOMMENDATION

The aim of this work is to investigate the heterogeneous nucleation of aerosol particles in the subsonic nozzle flow and based on the optimisation of theoretical modelling results, to construct a new Nozzle-CNC that can remedy some drawbacks of currently commercially used CNCs.

Theoretical and numerical modelling of the particle condensational growth in the flow field of a capillary nozzle that was modelled by CFX-FLOW3D were first introduced. The results provide the well estimated anchorage for the afterwards experimental design – the Nozzle-CNC. With this Nozzle-CNC new aspects of the atmospheric condensation nuclei can be investigated, which is helpful for us to understand basic behaviours of these nuclei in the formation of cloud droplets and their indirect climate effects. The interactive relationships among the flow modelling, the particle growth modelling, CNC counter and the studying of the condensation nuclei in the atmosphere can be exactly displayed in Fig. 6.5.

In cloud physics, particle droplets are always regarded to be in stationary state because there are no or very small relative movements between particle droplets and ambient carrier gases. Therefore the responses of particles to the air flow are always neglected. In the aerosol application areas such as in the aerosol measurements, high-speed accelerating aerosol beams are widely utilised. The expanding property of high-speed air flow and the fast mass and heat transfer between particles and air medium in this environment favourite particle growth from the condensation of water vapour. As supersonic and transonic nozzles produce strong

cooling which may cause homogeneous nucleation, a subsonic 'standard' nozzle (capillary nozzle) was adopted here because the condensation on pre-existing particles is our main concern.

Firstly, the air flow in the nozzle with an inner diameter of 1.0 mm was modelled to be a steady, compressible and heat-conducting flow with the computational program CFX-FLOW3D. The nozzle was divided into 20×150 grids in the modelling. As the fluid Reynolds number in the main nozzle part is larger than 2000, the flow was treated as a turbulent one in the calculation. The results show that an adiabatic and isentropic cooling in the nozzle can occur, and as the consequence, a supersaturation can be created. The cooling degree depends mainly on the flow rates through the nozzle. The heat conduction between the nozzle wall and the inside air flow can increase the air temperature near the nozzle wall, but has small influence on the flow near the centreline of the nozzle. For the same boundary conditions at both sides of the nozzle, there is a larger temperature drop in a short nozzle than in a long nozzle.

Secondly, a particle condensational growth model in air stream was developed. An extended Mason's diffusion growth equations with size correction for particles beyond the continuum regime and with the correction for a certain particle Reynolds number in an accelerating state were given. The growth modelling results show:

- Supersaturation created in the nozzle can result in the condensation of water vapour on aerosol particles larger than a critical particle size (r_k), and these particles will grow.

- Particles grow faster in an accelerating state than in a stationary state because of the forced convection from the relative movement between the particles and gases.

- Small size particles grow much quicker than large size particles. The whole particle size distribution evolve itself in the nozzle and will become narrower. After a long enough time, all sizes of particles larger than r_k can grow up to the detectable size.

As nozzle designs are widely used for producing accelerating and focused aerosol beams in aerosol instruments like OPC and APS, particle condensational

growth in the aerosol nozzle instrument was studied with this model and the influences on measurement results were estimated. The results can be summarised as:

- Particles with initial radii smaller than 1.0 μm can grow rapidly in the very short 'residence' time in the inlet nozzle of particle sizing instruments (with example OPC). For a particle with the size of r=0.15 μm that is the normal minimum detectable size of OPC, the condensational growth ratio can be as high as 1.07. The measured particle size may be 7% larger than its original size at the end of the nozzle, which results in "over-sizing" influence. Because particle number concentration is larger in fine size region, more particles therefore will be counted, which can be termed as "over-numbering" influence. The "over-numbering" is especially high (higher than 27.4%) for particles with remote continental, rural and urban mode size distributions. For other types of aerosol modes, this effect can be over 5.8% too.

- The measured whole particle size distributions shift to larger radii because of the particle condensational growths. The analysis results from data obtained from direct measurements with these nozzle aerosol instruments will reveal no 'pure' shape of particle size distribution in the actual atmosphere. The 'real' shape should be the one obtained by "extracting" the condensational "over-sizing" and "over-numbering" influences.

- The asymmetric property for non-spherical particles, the surface chemistry as well as the density of the particles could be modified too if nozzle aerosol instruments are used for measuring the particle shapes, aerodynamic sizes, and surface chemistry.

- Concerns should be given in evaluating measurement results as well as in aerosol instrument designs. For aerosol instruments other than CNCs, the nozzle length should be as short as possible in order to lessen the effect of the condensational growth of particles, and to increase the accuracy of the measurements.

Thirdly, according to the rapid growth of particles in the nozzle, a new Nozzle-CNC was built. Under various experimental conditions such as flow rate, ambient temperature, and the fraction of aerosol in the total flow, experiments with this Nozzle-CNC were carried out. The results show:

- The measured nucleus number concentration changes unproportionally with the fraction of the aerosol sample flow in the total flow.
- There exists an exponential function between the measured number concentration and the saturation S in the nozzle as $N = CS^{\alpha}$. The value of α depends largely on the flow rate through the nozzle, ranging from 5.52 for the flow rate of 29.1 l/h, to 16.30 for the flow rate of 42.0 l/h, and to 19.82 for the flow rate of 126.0 l/h. This function differs from the relation for CCN obtained by Twomey and other researchers.
- The Nozzle-CNC can have a wide counting region by just adjusting flow rate. It can count nuclei including hygroscopic nuclei (HN), cloud condensation nuclei (CCN), and traditionally measured atmospheric condensation nuclei (CN). The minimum detectable size of this Nozzle-CNC is 0.04 μm.

Further improvement work on this Nozzle-CNC is recommended in the followings aspects:

① The saturation in the nozzle is very sensitive to the sample aerosol ratio, so the aerosol flow rate should be measured with great accuracy.

② Changing environmental conditions, such as temperature (T) and relative humidity (RH) will cause the changes of the saturation generated in the nozzle, which gives the variation of the measurement results. It is therefore suggested that these conditions be kept stable in the measurement.

③ For determining the counting efficiency of this Nozzle-CNC, it would be better if it can be calibrated by uniform and monodisperse aerosol generated by the method as described by Berglund and Liu (1973).

In comparison with other CNCs, this Nozzle-CNC has several advantages such as no condensation delay as particles larger than the critical size grow simultaneously, low diffusion losses of particles, little water condensation at the inner wall of the instrument, and adjustable saturation — therefore the wide counting region, as well as no calibration compared to non-water condensation substances. With further work for improving and standardising measurement runnings, this Nozzle-CNC may have a brilliant prospect in the field observations.

Appendix A

APPENDIX

A.1 Appendix A1: CFX-FLOW3D Modelling Programme

```
/*********************************************************/
/* AIR FLOW PASSING THROUGH A NOZZLE                     */
/* FOR MODELLING THE GROWTH OF AEROSOL IN FLOW           */
/* DEC.12, 1998, MAINZ                                   */
/* TO USE DOUBLE PRECISION                               */
/*********************************************************/

>>CFXF3D
  >>SET LIMITS
    TOTAL REAL WORK SPACE 2500000
  >>OPTIONS
    TWO DIMENSIONS
    BODY FITTED GRID
    CYLINDRICAL COORDINATES
    AXIS INCLUDED
    TURBULENT FLOW
    HEAT TRANSFER
    COMPRESSIBLE FLOW
    STEADY STATE
    USE DATABASE
    END

>>MODEL TOPOLOGY
  #CALC
    NI=30+120;
    NJ=25;
    NK=1;
    ENTRY_T=273.15+28.5;
    WALL_T=273.15+24.5;
  #ENDCALC
  >>CREATE BLOCK
```

```
    BLOCK NAME 'BLOCK'
    BLOCK DIMENSIONS #NI #NJ #NK
    END
  >>CREATE PATCH
    PATCH NAME 'AXIS'
    PATCH TYPE 'SYMMETRY PLANE'
    BLOCK NAME 'BLOCK'
    LOW J
    END
/* ..............................==> TO CHANGE GRID VALUES ........ */
  >>CREATE PATCH
    PATCH NAME 'IN1'
    PATCH TYPE 'PRESSURE BOUNDARY'
    PATCH LOCATION 1 1 1 #NJ 1 #NK
    BLOCK NAME 'BLOCK'
    LOW I
    END

  >>CREATE PATCH
    PATCH NAME 'OUT1'
    PATCH TYPE 'PRESSURE BOUNDARY'
    BLOCK NAME 'BLOCK'
    PATCH LOCATION #NI #NI 1 5 1 #NK
    HIGH I
    END

  >>CREATE PATCH
    PATCH NAME 'WALLOUT'
    BLOCK NAME 'BLOCK'
    PATCH TYPE 'WALL'
    PATCH LOCATION 31 #NI 5 5 1 1
    HIGH J

  >>CREATE PATCH
    PATCH NAME 'SOLID1'
    PATCH TYPE 'SOLID'
    PATCH LOCATION 12 #NI #NJ #NJ 1 1
    BLOCK NAME 'BLOCK'
    END

  >>CREATE PATCH
    PATCH NAME 'SOLID1'
    PATCH TYPE 'SOLID'
    PATCH LOCATION 13 #NI 24 24 1 1
    BLOCK NAME 'BLOCK'
    END

  >>CREATE PATCH
    PATCH NAME 'SOLID1'
    PATCH TYPE 'SOLID'
    PATCH LOCATION 14 #NI 23 23 1 1
    BLOCK NAME 'BLOCK'
    END

  >>CREATE PATCH
```

```
  PATCH NAME 'SOLID1'
  PATCH TYPE 'SOLID'
  PATCH LOCATION 15 #NI 22 22 1 1
  BLOCK NAME 'BLOCK'
  END


>>CREATE PATCH
  PATCH NAME 'SOLID1'
  PATCH TYPE 'SOLID'
  PATCH LOCATION 16 #NI 21 21 1 1
  BLOCK NAME 'BLOCK'
  END

>>CREATE PATCH
  PATCH NAME 'SOLID1'
  PATCH TYPE 'SOLID'
  PATCH LOCATION 17 #NI 20 20 1 1
  BLOCK NAME 'BLOCK'
  END

>>CREATE PATCH
  PATCH NAME 'SOLID1'
  PATCH TYPE 'SOLID'
  PATCH LOCATION 18 #NI 19 19 1 1
  BLOCK NAME 'BLOCK'
  END

>>CREATE PATCH
  PATCH NAME 'SOLID1'
  PATCH TYPE 'SOLID'
  PATCH LOCATION 19 #NI 18 18 1 1
  BLOCK NAME 'BLOCK'
  END

>>CREATE PATCH
  PATCH NAME 'SOLID1'
  PATCH TYPE 'SOLID'
  PATCH LOCATION 20 #NI 17 17 1 1
  BLOCK NAME 'BLOCK'
  END
>>CREATE PATCH
  PATCH NAME 'SOLID1'
  PATCH TYPE 'SOLID'
  PATCH LOCATION 21 #NI 16 16 1 1
  BLOCK NAME 'BLOCK'
  END
>>CREATE PATCH
  PATCH NAME 'SOLID1'
  PATCH TYPE 'SOLID'
  PATCH LOCATION 22 #NI 15 15 1 1
  BLOCK NAME 'BLOCK'
  END
>>CREATE PATCH
  PATCH NAME 'SOLID1'
```

```
  PATCH TYPE 'SOLID'
  PATCH LOCATION 23 #NI 14 14 1 1
  BLOCK NAME 'BLOCK'
  END
>>CREATE PATCH
  PATCH NAME 'SOLID1'
  PATCH TYPE 'SOLID'
  PATCH LOCATION 24 #NI 13 13 1 1
  BLOCK NAME 'BLOCK'
  END
>>CREATE PATCH
  PATCH NAME 'SOLID1'
  PATCH TYPE 'SOLID'
  PATCH LOCATION 25 #NI 12 12 1 1
  BLOCK NAME 'BLOCK'
  END
>>CREATE PATCH
  PATCH NAME 'SOLID1'
  PATCH TYPE 'SOLID'
  PATCH LOCATION 26 #NI 11 11 1 1
  BLOCK NAME 'BLOCK'
  END
>>CREATE PATCH
  PATCH NAME 'SOLID1'
  PATCH TYPE 'SOLID'
  PATCH LOCATION 27 #NI 10 10 1 1
  BLOCK NAME 'BLOCK'
  END
>>CREATE PATCH
  PATCH NAME 'SOLID1'
  PATCH TYPE 'SOLID'
  PATCH LOCATION 28 #NI 9 9 1 1
  BLOCK NAME 'BLOCK'
  END
>>CREATE PATCH
  PATCH NAME 'SOLID1'
  PATCH TYPE 'SOLID'
  PATCH LOCATION 29 #NI 8 8 1 1
  BLOCK NAME 'BLOCK'
  END

>>CREATE PATCH
  PATCH NAME 'SOLID1'
  PATCH TYPE 'SOLID'
  PATCH LOCATION 30 #NI 7 7 1 1
  BLOCK NAME 'BLOCK'
  END

>>CREATE PATCH
  PATCH NAME 'SOLID1'
  PATCH TYPE 'SOLID'
  PATCH LOCATION 31 #NI 6 6 1 1
  BLOCK NAME 'BLOCK'
  END
```

```
 /* ........................................... */

 >>MODEL DATA
   >>AMBIENT VARIABLES
     U VELOCITY 0.0
     V VELOCITY 0.0
     PRESSURE 1.013E+05
     TEMPERATURE #WALL_T
   >>MATERIALS DATABASE
     >>SOURCE OF DATA
       PCP
     >>FLUID DATA
       FLUID 'AIR'
       MATERIAL TEMPERATURE 2.9800E+02
       MATERIAL PHASE 'GAS'
  >>TITLE
     PROBLEM TITLE 'CNC-CONIC NOZZLE FLOW MODELLING (TWO PRESSURE BOUNDARIES)'
     END

   >>DIFFERENCING SCHEME
       ALL EQUATIONS 'UPWIND'
       PRESSURE 'UPWIND'
       DENSITY 'UPWIND'
       END

   >>PHYSICAL PROPERTIES
     >>STANDARD FLUID
        FLUID 'AIR'
        STANDARD FLUID REFERENCE TEMPERATURE 2.9800E+02
     >>COMPRESSIBILITY PARAMETERS
       HIGH MACH NUMBER SIMPLE ALGORITHM
/*       WEAKLY COMPRESSIBLE    (only for U<100m/s)  */
       FULLY COMPRESSIBLE
       UNIVERSAL GAS CONSTANT 8314.0
       FLUID MOLECULAR WEIGHT 28.8
       REFERENCE PRESSURE 0.0
       MINIMUM REAL PRESSURE 0.3E+05
       MINIMUM TEMPERATURE 250.0
       END
     >>HEAT TRANSFER PARAMETERS
       ENTHALPY REFERENCE TEMPERATURE 273.0
       END
     >>TURBULENCE PARAMETERS
       >>TURBULENCE MODEL
         TURBULENCE MODEL 'LOW REYNOLDS NUMBER K-EPSILON'

 /*    >>TRANSIENT PARAMETERS
       >>ADAPTIVE TIME STEPPING
         NUMBER OF TIME STEPS 2
         INITIAL TIME STEP 1.0E-3
         MINIMUM TIME STEP 1.0E-4
         MAXIMUM TIME STEP 1.0E-2
         MULTIPLY TIME STEP BY 2.0
         DIVIDE TIME STEP BY 2.0
         END                 */
```

```
  >>RHIE CHOW SWITCH
      HARMONIC AVERAGING OF COEFFICIENTS

  >>WALL TREATMENTS
    WALL PROFILE 'QUADRATIC'
    NO SLIP

>>SOLVER DATA
  >>PROGRAM CONTROL
    MAXIMUM NUMBER OF ITERATIONS 10000
    MINIMUM NUMBER OF ITERATIONS 50
    OUTPUT MONITOR POINT 60 3 1
    OUTPUT MONITOR BLOCK 'BLOCK'
    MASS SOURCE TOLERANCE 1.0E-15
    END
  >>FALSE TIMESTEPS                    /*  <1.0E-05   */
    U 1.0E-06
    V 1.0E-06

  >>EQUATION SOLVERS
    ENTHALPY 'STONE'
    PRESSURE 'STONE'
    END
  >>UNDER RELAXATION FACTORS
    U VELOCITY 0.2
    V VELOCITY 0.2
    PRESSURE 0.2
    ENTHALPY 0.2
    DENSITY 0.2
    TEMPERATURE 0.2
    VISCOSITY 0.2

>>CREATE GRID
  >>SIMPLE GRID
    BLOCK NAME 'BLOCK'
    X START 0.0
    DX  30*0.001 120*0.001
    Y START 0.0
    DY 5*0.0001 20*0.000235
    Z START 0.0
    DZ 0.1

>>MODEL BOUNDARY CONDITIONS
  >>SET VARIABLES
    PATCH NAME 'IN1'
    PRESSURE    1.00E+05
    TEMPERATURE #ENTRY_T
    END
  >>SET VARIABLES
    PATCH NAME 'OUT1'
    PRESSURE    0.679E+05
  >>WALL BOUNDARY CONDITIONS
    PATCH NAME 'WALLOUT'
    TEMPERATURE #WALL_T
    END
```

```
>>OUTPUT OPTIONS
  >>PRINT OPTIONS
    >>WHAT
/*      GEOMETRIC INFORMATION */
      U
      TEMPERATURE
      PRESSURE
      DENSITY
      END
    >>WHERE
      J PLANES 0 1 2 3 4 5
      END
    >>WHEN
/*      INITIAL GUESS  */
      END
>>STOP
```

A.2 Appendix A2: Error Estimation

Measurement or calculation error for a quantity can be estimated according to Gauss law (Taylor, 1988).

$$\Delta y = \pm\sqrt{\left(\frac{\partial y}{\partial x_1}\right)^2 {\Delta x_1}^2 + \left(\frac{\partial y}{\partial x_2}\right)^2 {\Delta x_2}^2 + \left(\frac{\partial y}{\partial x_3}\right)^2 {\Delta x_3}^2} \tag{A.1}$$

where x_1, x_2, and x_3 are dependent variables of y.

Error Estimation for Particle Concentration

Particle number concentration is calculated by

$$N = \frac{N^c(F_t, p)}{F_a} \tag{A.2}$$

where N^c is the counting value by the optical system, and F_a is the flow rate of aerosol. The counting value N^c changes with the total flow rate F_t through the nozzle and the pressure at the inlet of the optical system. So the error estimation of particle concentration can be written as

$$\Delta N = \pm\sqrt{\left(\frac{N^c}{{F_a}^2}\right)^2 {\Delta F_a}^2 + \left(\frac{1}{F_a}\right)^2 \Delta {N^c}^2} \tag{A.3}$$

and

$$\Delta N^c = \frac{\partial N^c}{\partial F_t}\Delta F_t + \frac{\partial N^c}{\partial p}\Delta p \tag{A.4}$$

Error Estimation for Saturation

The saturation at the nozzle entrance is calculated by

$$S_0 = \frac{F_a S_a + F_c S_c}{F_a + F_c} \tag{A.5}$$

In the nozzle its value will be

$$S_1 = S_0 \cdot \frac{e(T_1)}{E(T_1)} = S_0 \cdot \frac{E(T_0)}{E(T_1)} \tag{A.6}$$

So

$$\Delta S_1 = \pm\sqrt{\left(\frac{E(T_0)}{E(T_1)}\right)^2 {\Delta S_0}^2 + \left(\frac{S_0}{E(T_1)}\right)^2 \left(\frac{\partial E(T_0)}{\partial T_0}\Delta T_0\right)^2 + \left(\frac{S_0 E(T_0)}{E^2(T_1)}\right)^2 \left(\frac{\partial E(T_1)}{\partial T_1}\Delta T_1\right)^2} \tag{A.7}$$

where T_0 and T_1 are the temperatures at the nozzle entry and in the nozzle, respectively.

A.3 Appendix A3: APS 3320

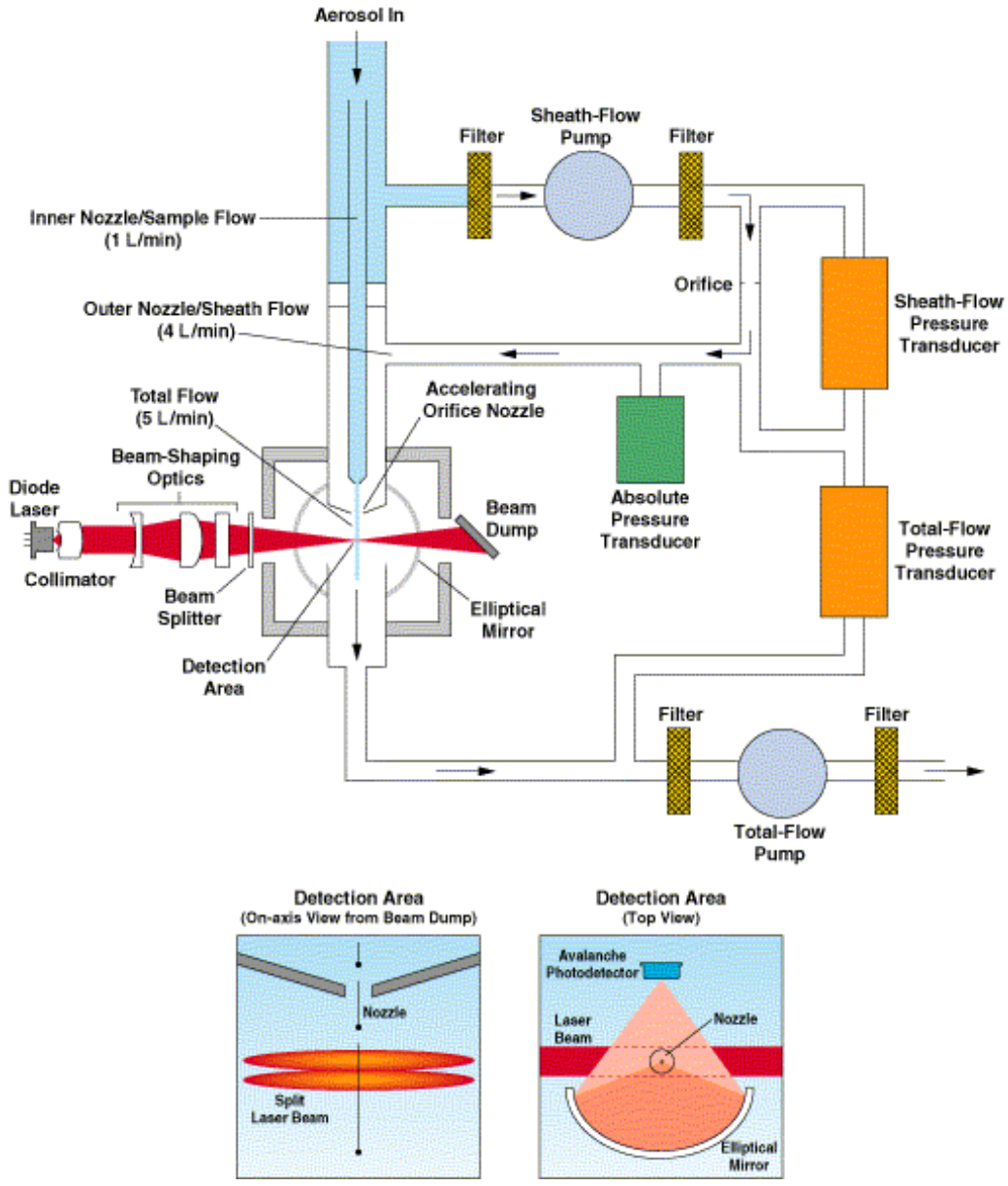

Figure A.1: Schematic Diagram of Aerodynamic Particle Sizer spectrometer – APS Model 3320 TSI

Bibliography

AEA (1997) *CFX-4.2 Flow3D* . CFX International, AEA Technology, UK.

Agarwal, J. K., and Sem, G. J. (1980) Continuous flow single-particle-counting condensation nucleus counter. *J. Aerosol Sci.* **11**, 343.

Aitken, J. (1888) On the number of dust particles in the atmosphere. In: *Collected Scientific Papers of John Aitken. C. G. Knott (ed.), the Royal Society of Edinburg, 1923*. 187-206.

Aitken, J. (1889) On improvements in the apparatus for counting the dust particles in the atmosphere. In: *Collected Scientific Papers of John Aitken. C. G. Knott (ed.), the Royal Society of Edinburg, 1923*. 343-357.

Aitken, J. (1891) On a simple pocket dust counter. *Proc. Roy. Soc.* **18**, London.

Allen, J. (1986) Size and shape measurement of individual aerosol particles by asymmetric laser light scattering. In: *Physical and Chemical Characterisation of Individual Airborne Particles (ed. by K. R. Spurny)*, pp.101-114, John Wiley & Sons.

Barrett, J. C. and Clement, C. F. (1988) Growth rates for liquid drops. *J. Aerosol Sci.* **19**, 223-242.

Berglund, R. N. and Liu, B. Y. H. (1973) Generation of monodisperse aerosol standards. *Environ. Sci. Tech.* **7**(2), 147-153.

Bird, R. B., Stewart, W. E., and Lightfoot, E. N. (1960) *Transport Phenomena*. Wiley, New York.

Bricard, J., Delatre, P., Madelaine, G., and Pourprix, M. (1976) Detection of ultra-fine particles by means of a continuous flux condensation nuclei counter. In: *Fine Particles*, Liu, B. Y. H. (ed). Academic Press Inc., New York, 565-580.

Brock, J. R. (1983) New aspects of aerosol growth processes. *Aerosol Sci. Technol.* **2**, 109-120.

Charlson R., Swartz S., Hales J., Cess R., Coakely J., Hansen J., and Hofmann D., 1992, Climate forcing by anthropogenic aerosols. *Science*, **255**, 423-430.

Chiang, C. H., Raju, M. S., and Sirignano, W. A. (1992) Numerical analysis of convecting, vaporizing fuel droplet with variable properties. *Int. J. Heat Mass Transfer* **35**, 1307-1324.

Courant, R., and Friedrichs, K. O. (1963) Supersonic flow and shock waves. *Pure and Applied Mathematics* **1**, 377-396.

Cunningham, E. (1910) On the velocity of steady fall of spherical particles through fluid medium. *Proc. R. Soc.* **A83**, 357-365.

d'Almeida, G.A., Koepke P., Shettle E.P. (1991) *Atmospheric Aerosols: global climatology and radiative characteristics*. A. Deepark Publishing.

Dahneke, B. and Padliya, D. (1977) Nozzle-inlet design for aerosol beam instruments. In: *Rarefied Gas Dynamics*, Vol. II, edited by Potter, J.J., AIAA, New York.

Davies, C. N. (1966) Deposition from moving aerosols. In: *Aerosol Science*, edited by C. N. Davies. Academic Press, London.

Dreiling, V. and Friederich, B. (1997) Spatial distribution of the arctic haze aerosol size distribution in western and eastern Arctic. *Atmos. Res.* **44**, 133-152.

Dreiling, V. (1994) *Bestimmung von Aerosolgrößenverteilungen in Raum und Zeit aus integralen Parametern*. Dissertation, University of Mainz.

Duce, R. A., Unni, C. K., Ray, B. J., Prospero, J. M. and Merrill, J. T. (1980) Long-range atmospheric transport of soil dust from Asia to the tropical north Pacific: temporal variability. *Science* **209**, 1522-1524.

Eichel, C., Kraemer M., Schuetz L., and Wurzler S. (1996) The water-soluble fraction of atmospheric aerosol particles and its influence on cloud microphysics. *J. of Geophys. Res.* **101**, 29,499-29,510.

Fuchs, N. A. (1964) *The Mechanics of Aerosols*. Pergamon Press.

Fukuta, N. and Paik, Y. (1976) A supersonic expansion method of ice nuclei generation for weather modification. *J. Appl. Meteor*. **15**, 996-1003

Gruber, S., Matthias-Maser, S., and Jaenicke, R. (1998) Vertical Distribution of Biological Aerosol Particles above the North Sea. *J. Aerosol Sci.*. **29**, S771-S772.

Gucker, F. T., Jr., O'Konski, C. T., Pickard, H. B. and Pitts, J. N., Jr. (1947) A photoelectronic counter for colloidal particles. *J. Am. Chem. Soc.* **69**, 2422-2431.

Gucker, F. T. Jr., Pickard, H. B., and O'Konski, C. T. (1947) A photoelectronic instrument for comparing concentrations of very dilute aerosols and measuring very low light intensities. *J. Am. Chem. Soc.* **69**, 429-438.

Gucker, F. T. Jr., and Rose, D. C. (1954) A photoelectronic instrument for counting and sizing aerosol particles. *Br. J. Appl. Phys.* **3**, 138-143.

Hegg, D. A. and Hobbs, P. V. (1992) Cloud condensation nuclei in the marine atmosphere: a review. In: *Nucleation and Atmospheric Aerosols*, Edited by Fukuta N. and Wagner P. E., Deepak Publishing, Hampton, VA. pp. 181-192.

Heyder, J. (1986) Single-particle deposition in human airways. In: *Physical and Chemical Characterisation of Individual Airborne Particles (ed. by K. R. Spurny)*, pp.72-85, John Wiley & Sons.

Hinds, W. C. (1991) *Aerosol Technology: properties, behaviour, and measurement of airborne particles*. 2nd ed. John Wiley & Sons, Inc.

Hofmann, D., and Solomon, S. (1989) Ozone depletion through heterogeneous chemistry following the eruption of the El Chichon Volcano. *J. Geophys. Res.*, **94**, 5029-5041.

Hoppel, W. A., Twomey, S., and Wojciechowski, T. A. (1979) A segmented thermal diffusion chamber for continuous measurements of CN. *J. Aerosol Sci.* **10**, 369.

Huang, L. -J. and Ayyaswamy, P. S. (1990) Evaporation of a moving liquid droplet: solutions for intermediate Reynolds numbers. *Int. Commun. Heat Mass Transfer* **17**, 27-38.

Hughmark, G. A. (1967) Mass and heat transfer from rigid spheres. *Am. Inst. Chem. Engng J.* **13**, 6.

Husar, R. B. (1974) Recent developments in $in\ situ$ size spectrum measurement of submicron aerosol. In: *Instrumentation for Monitoring Air Quality*. A.S.T.M.S.T.P. 555, American Society for Testing Materials. Philadelphia.

Iwasaka Y., Yamato M, Imasu R. and Ono A. (1988) Transport of Asian dust (KOSA) particles: importance of weak KOSA events on the geochemical cycle of soil particles. *Tellus*. **40B**, 494-503.

Jaenicke, R. (1972) The optical particle counter: cross-sensitivity and coincidence. *J. Aerosol Sci.* **3**, 95-111.

Jaenicke, R. and Kanter H. J. (1976) Direct condensation nuclei counter with automatic photographic recording, and general problems of "absolute" counters. *J. Appl. Metero.* **15**, No. 6, 620-632.

Jaenicke, R. (1988) Aerosol physics and chemistry. In: *Landolt-Börnstein, Zahlenwerte und Funktionen aus Naturwissenschaft und Technik. Fischer, G. (ed.)*. Neue Serie, Band Meteorologie 4b, Springer Berlin. pp391-457.

Jaenicke, R. (1993) Tropospheric aerosols. In: *Aerosol-Cloud-Climate Interactions (ed. by P.V. Hobbs)*, Academic Press, Inc.

John, W., Wall, S. M., Ondo, J. L. and Winklmayr, W. (1990) Modes in the size distribution of atmospheric inorganic aerosol. *Atmos. Environ.*, **24A**, 2349-2359.

Johnston, P. V., McKenzie, R. L., Keys, J. G., and Matthews, A. W. (1992) Observations of depleted stratospheric NO_2 following the Pinatubo volcanic eruption. *Geophys. Res. Lett.*, **19**, 211-213.

Junge, C. (1963) *Air Chemistry and Radioactivity*. New York, Academic Press, 382 pp.

Junge, C. and McLaren E. (1971) Relationship of cloud nuclei spectra to aerosol size distribution and composition. *J. Atmos. Sci.* **28**, 382-390.

Kanter, H. J. (1970) Bau und Eichung eines automatischen Kondensationskernzählers mit fotografischer Registrierung. Diplomarbeit, University of Mainz.

Kanter, H. J. and Junge, C. E. (1971) A new automatic condensation nuclei counter for low particle concentrations. *Supl. Vol. Proc. 7th Int. Conf. Condens. and Ice Nuclei*. Prague and Vienna, Sept. 1969. Academia, Prague, 205-212.

Kassner, J. L.,Jr., Carstens, J. C., Vietti, M. A., Biermann, A. H., Yue, P. C. P., Allen, L. B., Eastburn, M. A., Hoffman, D. D., Noble, H. A., and Packwood, D. L. (1968) Expansion cloud chamber technique for absolute Aitken nuclei counting. *J. Rech. Atmos.* **3**, 45-51.

Kassner, J. L., Jr., Carstens, J. C., Allen, L. B. (1968) The myth concerning the condensation nucleus counters. *J. Rech. Atmos.* **3**, 25-31.

Keady, P. B., Quant, F. R., and Sem, G. J. (1986) *Proc. Inst. Environ. Sci.* **445**.

Kulmala, M. (1988) Condensation in the continuum regime: integration of the mass flux. In: *Reports series in aerosol science 8*. 2-5, Finnish Association for Aerosol Research.

Kulmala, M., Majerowicz, A. and Wagner, P. E. (1989) Condensational growth at large vapour concentration: limits of applicability of the Mason equation. *J. Aerosol Sci.* **20**, 1023-1026.

Kulmala, M., and Vesala, T. (1991) Condensation in the continuum regime. *J. Aerosol Sci.* **22**, 337-346.

Kulmala, M. and Vesala, T. (1995) Mass transfer from a drop - II. Theoretical analysis of temperature dependent mass flux correlation. *Int. J. Heat Mass Transfer* **38**, 1705-1708.

Launder, B. E., and Sharma, B. T. (1974) Application of the energy dissipation model of turbulence to the calculation of flow near a spinning disc. *Lett. Heat Mass Transfer* **1**, 131-138.

Liu, B. Y. H., Pui, D. Y. H., Mc Kenzie, R. L., Agarwal, J. K., Jaenicke, R., Pohl, F. G., Preining, O., Reischl, G., Szymanski, W., and Wagner, P. E. (1975) *Aerosol Sci.* **13**, 429.

Liu, B. Y. H. and Kim, C. (1977) On the counting efficiency of condensation nuclei counter. *Atmos. Environ.* **11**, 1097-1100.

Loyalka, S. K. (1982) Condensation on a spherical droplet – II. *J. Colloid Interface Sci.* **87**, 216.

Loyalka, S. K. (1983) Mechanics of aerosols in nuclear reactor safety: a review. *Prog. Nucl. Energy* **12**, 1-11.

Loyalka, S. K. and Park, J. W. (1988) Aerosol growth by condensation: a generalization of Mason's formula. *J. Colloid Interface Sci.* **125**, 712-716.

Loyalka, S. K., Hamoodi, S. A., and Tompson, R. V. (1989) Isothermal condensation on a plane surface. *Phys. Fluids A* **1**, 384.

Loyalka, S. K., Hamoodi, S. A., and Tompson, R. V. (1989) Isothermal condensation on a spherical particle. *Phys. Fluids A* **1**, 358.

Mason, B. J. (1962) *Clouds, Rain and Rainmaking*. The University Press, Cambridge.

Mason, B. J. (1971) *The Physics of Clouds*. Clarendon Press, 2nd ed.

Mallina, R. V., Wexler, A. S. and Johnston, M. V. (1997) Particle growth in high-speed particle beam inlets. *J. Aerosol Sci.* **28**, 2, 223-238.

Miller, S. W., and Bodhaine, B. A. (1982) Supersaturation and expansion ratios in condensation nuclei counter: an historical perspective. *J. Aerosol Sci.* **13**, 481-490.

Mills, M. J., Langford, A. O., O'Leary, T. J., Arpag, K., Miller, H. L., Proffitt, M. H., Sanders, R. W., and Solomon, S. (1993) On the relationship between stratospheric aerosols and nitrogen dioxide. *Geophys. Res. Lett.*, **20**, 1187-1190.

Murphy, C. H. (1984) *Handbook of particle sampling and analysis methods*.

Murphy, D. M., and Thomson, D. S. (1995) Laser ionization mass spectroscopy of single aerosol particles. *Aerosol Sci. Technol.*, **22**, 237-249.

Murphy, D. M., and Thomson, D. S. (1997) Chemical composition of single aerosol particles at Idaho Hill: Negative ion measurements. *J. Geophys. Res.*, **102**, 6353-6368.

Nolan, P. J., and Pollak, L. W. (1946) *Proc. R. Ir. Acad.* 51, A:9.

Park, J. W., and Loyalka, S. K. (1988) Kinetic theory of gelation: numerical simulation and comparison with analytical results. *J. Colloid Interface Sci.* **125**, 2, 615-618.

Podzimek, J., Carstens, J. C. and Yue, P. C. (1982) Comparison of several Aitken nuclei counters. *Atmos. Environ.* **16**, No.1.

Pollak, L. W. (1952) A condensation nuclei counter with photographic recording. *Geofis. Pura Appl.* **22**.

Pollak, L. W. and Metnieks, A. L. (1959) New calibration of photo-electric nucles counter. *Geofis. Pura Appl.* **43**, 285-301.

Prather, M. J. (1992) Catastrophic loss of stratospheric ozone in dense volcanic clouds. *J. Geophys. Res.*, **97**, 10187-10191.

Pruppacher, H. R. and Klett, J. D. (1997) *Microphysics of Clouds and Precipitation*. Second Revised and Enlarged Edition, pp. 167-190. Kluwer Academic Publishers.

Rahn, K. A. (1981) The Arctic air-sampling network in 1980. *Atmos. Envir.* 15, 1349-1352.

Rahn, K. A., Borys, R. D. and Shaw, G. E. (1981) Asian desert dust over Alaska: Anatomy of an Arctic haze episode. *Geo. Soc. American*. Paper 186.

Renksizbulut, M. and Yuen, M. C. (1983) Numerical study of droplet evaporation in a high-temperature stream. *J. Heat Transfer.* **105**, 389-397.

Rosen, J. M., Pinnick, R. G., and Hall, R. (1974) Recent measurements of condensation nuclei in the stratosphere. *Proc. Third Conf. CIAP*. 298-302, NTIS: DOT-TSC-OST-74-15. DOT, Washington, D.C.

Rosen, J. M., Hofmann, D. J., and Kaselau, K. H. (1978) Vertical profiles of condensation nuclei. *J. Appl. Meteorol.* **17**, 1737.

Sachweh, B., Umhauer, H., Ebert, F., Buettner, H. and Friehmelt, R. (1998) $In\ situ$ optical particle counter with improved coincidence error correction for number concentrations up to 10^7 particles cm^{-3}. *J. Aerosol Sci.* **29**, 9, 1075-1086.

Schmidt, J. L., Kassner, J. L. Jr., and Podzimek, J. (1982) The university of Missouri-Rolla, absolute Aitken nucleus counter. *J. Aerosol Sci.* **13**, 373.

Scholz, J. (1932) Vereinfachter Bau eines Kernzählers. *Meteor. Z.* **49**, 381-388.

Seinfeld, J. H. (1986) *Atmospheric Chemistry and Physics of Air Pollution*. Wiley, New York.

Sinclair, D., and Hoopes, G. S. (1975) A continuous flow condensation nucleus counter. *Aerosol Sci.* **6**, 1-7.

Sinclair, D., (1982) Particle size sensitivity of condensation nucleus counter. *Atmos. Environ.* **16**, 955-958.

Sprengard-Eichel, C. (1998) *Die wasserlösliche Fraktion atmosphärischer Aerosolpartikel: Anteil und Zusammensetzung im Radiusbereich 0.2 bis 2.0 μm*. Dissertation, University of Mainz.

Spurny, K. R. (1986) *Physical and chemical characterisation of individual airborn particles*. Wiley, New York.

Svenningsson, I. B., Hansson, H. C., Wiedensohler A., Ogren, J. A., Noone K. J., and Hallberg, A. (1992) Hygroscopic growth of aerosol particles in the Po Valley. *Tellus* **44B**, 556-569.

Svenningsson, I. B., Hansson, H. C., Wiedensohler A., Noone K. J., Ogren, J. A., Hallberg, A., and Colvile, R. (1994) Hygroscopic growth of aerosol particles and its influence on nucleation scavenging in cloud: Experimental results from Kleiner Feldberg. *J. Atmos. Chem.* **19**, 129-152.

Taylor, J. R. (1988) *Fehleranalyse*. VCH Verlagsgesellschaft mbH, Weinheim.

TSI (1988) Instruction manual: Model 3020 condensation particle counter. TSI incorporated, St. Paul, USA.

Twomey, S. (1959) The nuclei of natural clouds formation. Part II: The supersaturation in natural clouds and the variation of cloud droplet concentration. *Geofis. Pura Appl.* **43**, 243-249.

Twomey, S. (1963) Measurements of natural cloud nuclei. *J. Rech. Atmos.* **1**, 101-104.

Twomey, S. and Wojciechowski, T. (1969) Observations of the geographical variation of cloud nuclei. *J. Atmos. Sci.* **26**, 684-688.

Umhauer, H. (1983) Particle size distribution analysis by scattered light measurements using an optically defined measuring volume. *J. Aerosol Sci.* **14**, 765-770.

Verzar, F. (1953) Kondensationskernzähler mit automatischer Registrierung. *Arch. Meteor. Geophys. Bioklim.* **A5**, 372-376.

Wagner, P. (1974) Untersuchung des Tröpfchenwachstums in einer schnellen Expansionsnebelkammer. Ph.D. Dissertation, Universität Wien.

Wagner, P. E. (1982) Aerosol growth by condensation. In: *Aerosol Microphysics II* (ed. by W.H. Marlow), pp. 129-178, Springer-Verlag, Berlin.

Wegener, P. P. and Pouring, A. A. (1964) Experiments on condensation of water vapour by homogeneous nucleation in nozzles. *Physics of Fluids.* **7**, 352-356.

Whitby, K. T. (1978) The physical characteristics of sulfur aerosols. *Atmos. Environ.* **12**, 135-159.

Willeke, K. and Liu, B. Y. H. (1976) Single particle optical counter: principle and application. In: *Fine Particles: Aerosol Generation, Measurement, Sampling, and Analysis* (ed. by B. Y. H. Liu), pp. 698-712, Academic Press, New York.

Willer, S. W. and Bodhaine, B. A. (1982) Supersaturation and expansion ratios in condensation nuclei counters: an historical perspective. *J. Aerosol Sci.* **13**, No. 6.

Williams, M. M. R. and Loyalka, S. K. (1991) *Aerosol Science Theory and Practice - with special applications to the nuclear industry*. Pergamon Press.

Yang, J. L., Jaenicke, R., Dreiling, V. and Peter, Th. (1999) The condensational growth of aerosol particle and its effect in aerosol measurements. *J. Aerosol Sci.* **30**, S69-S70.

Zhang, Z. Q. and Liu, B. Y. H. (1990) Dependence of the performance of TSI 3020 condensation nuclei counter on pressure, flow rate, and temperature. *Aerosol Sci. Tech.* **13**, 483-504.

Zhang, Z. Q. and Liu, B. Y. H. (1991) Performance of TSI 3760 condensation nuclei counter at reduced pressures and flow rates. *Aerosol Sci. Tech.* **15**, 228-238.

ACKNOWLEDGEMENT

This work was conducted in the Institute for Physics of Atmosphere, University of Mainz. I would like to thank all people in this institute without whom this work would have been impossible.

Dr. Volker Dreiling is the first one to whom a lot of thanks should be given. He gave me many technical helps as well as useful advices from his many years' working experience in aerosol technology and measurements.

Great thanks are given to Dr. Thomas Peter of Max-Planck Institute for Chemistry in Mainz who financially supported this work. The same thanks are addressed to Dr. Hans-F. Graf of Max-Planck Institute for Meteorology in Hamburg.

I would like to express sincere thanks, to Mrs. Graf-Gries and Mrs. Hennig who made me feel welcome from the very first day, and gave me a lot of practical assistances; to my office mates Ms. Sabine Gruber and Mr. Andreas Thomas, who created a pleasant atmosphere for work and their kindly helps in the past three years. Ms. Sabine Gruber also looked over the whole manuscript and gave a number of corrections as well as valuable suggestions; to Prof. Dr. G. Zimmerman and Dr. S. Mitra for their good suggestions and kindly concerns for this work; to Mr. B. Friederich and Mr. Kaltenbach as well as the mechanical workshop of the institute for their technical support; and to Dr. Stefan Borrmann who provided me with the modelling software of CFX-FLOW3D.

Of course, the most important person to whom I want to express my greatest gratitudes is my supervisor professor Dr. Ruprecht Jaenicke. He is the strongest supporter for this work and the source of creation. Without his massive supports and valuable encouragements on all sides, I could not finish this work.

Special thanks are also expressed to Prof. Mingxing Wang of the Institute of Atmospheric Physics of the Chinese Academy of Sciences in Beijing for his special supports and many concerns. This PhD work is also jointly supported by the Max-Planck Gesellschaft and the Chinese Academy of Sciences.

I greatly appreciate the understanding and supports from my family during my PhD work. Ms. Helena Huebner, Ms. Yun Zhang, Family Yabo Zhu and Hong Gao, Ms. Wanxiao Sun $etc.$ gave me a good remembrance during my staying in Mainz.

Ich versichere, die vorliegende Arbeit selbständig und nur unter Verwendung der angegebenen Quellen angefertigt zu haben.

Lebenslauf

Name:	Yang, Jianliang
Geburtsdatum:	22.07.1965
Geschlecht:	Männlich
Geburtsort:	Wujin, Provinz Jiangsu, VR China
Staatsangehörigkeit:	Chinesisch
Anschrift:	Schillstr. 90, 55131 Mainz

Werdegang:

02.1972—07.1977	Grundschule in Wujin
09.1977—07.1983	Gymnasium in Wujin, Abschluß mit Abitur
09.1983—07.1987	Studium an der Universität Nanjing, abgeschlossen mit dem “Bakkalaureus der Wissenschaften” im Sommer 1987
09.1987—07.1988	Aufbaustudium an der Chinesischen Akademie der Wissenschaften in Beijing
09.1988—07.1990	Magisterarbeit am Institut der Atmosphärischen Physik der Chinesischen Akademie der Wissenschaften in Beijing, abgeschlossen mit dem “Magister der Wissenschaften” im Sommer 1990
07.1990 –04.1991 und 02.1992–04.1994	Wissenschaftlicher Mitarbeiter am Institut der Atmosphärischen Physik der Chinesischen Akademie der Wissenschaften in Beijing
05.1991 - 1.1992	Wissenschaftlicher Mitarbeiter am Institut für Physik der Atmosphäre in der Universität Mainz
05.1994–06.1995	Beamter an der Staatlichen Agentur für Umweltschutz in Beijing
21.04.1995	Geburt des Sohnes Atong
06.1996–09. 1996	Deutschkurs am Goethe–Institut in Mannheim
01.10.1996	Beginn der Doktorarbeit am Institut für Physik der Atmosphäre in der Universität Mainz
08.12.1997	Zugelassen als Doktorand am Fachbereich Physik der Universität Mainz
26.11.1999	Fertigstellung der Dissertation

“There are more things in heaven and earth, Horatio,
than are dreamt of in one’s philosophy.”

—— W. Shakespeare

(Hamlet, Act I, Scene 5)